

# Analysis of mitotic phosphoproteomes using SILAC based mass spectrometry

Focus on the site-specific phosphorylation dynamics of  
kinases through different mitotic stages.

Dissertation

zur Erlangung des Doktorgrades der Naturwissenschaften der Fakultät für

Biologie der Ludwig-Maximilians-Universität München

Vorgelegt von

**Kalyana Chakravarthi Dulla**

Martinsried /München, 2010

**Datum der mündlichen Prüfung: 25.10.2010**

**Erstgutachter:** Prof. Dr. Erich A. Nigg

**Zweitgutachter:** Prof. Dr. Harry K. MacWilliams

Hiermit erkläre ich, dass ich die vorliegende Dissertation selbständig und ohne unerlaubte Hilfe angefertigt habe. Sämtliche Experimente wurden von mir selbst durchgeführt, soweit nicht explizit auf Dritte verwiesen wird. Ich habe weder an anderer Stelle versucht eine Dissertation oder Teile einer solchen einzureichen bzw. einer Prüfungskommission vorzulegen, noch eine Doktorprüfung zu absolvieren.

Kalyana Chakravarthi Dulla

München, den 31.05.2010

## Table of Contents

Summary .....	7
1.0 Introduction.....	8
1.1 Cell cycle.....	8
1.2 Mitosis.....	8
1.2.1 Spindle assembly checkpoint .....	10
1.2.2 The molecular mechanism of the SAC.....	10
1.3 Regulation of kinases by phosphorylation .....	12
1.4 Mass spectrometry in biology .....	13
1.5 Mass spectrometric instrumentation .....	14
1.5.1 Ion source.....	14
1.5.2 Mass analyzers .....	15
1.5.2.1 Linear quadrupole ion trap .....	16
1.5.2.2 The electrostatic trap or orbitrap.....	19
1.5.3 Detectors .....	20
1.6 Methods for quantitation.....	20
1.7 Phosphoproteomics.....	22
1.8 Bioinformatic tools for the analysis of mass spectrometry data .....	23
1.8.1 Gene ontology .....	23
1.8.2 Pathway analysis .....	24
1.8.3 Interaction networks .....	25
2.0 Results (Part 1): Phosphorylation dynamics of protein kinases across mitosis.....	26
2.1 Introduction .....	26
2.2 Experimental strategy .....	26

2.3 Large scale synchronization of HeLa cells in different mitotic stages .....	27
2.4 Identification of proteins and phosphorylation sites.....	32
2.5 Mitotic dynamics of kinase phosphorylation sites .....	34
2.6 Network analysis .....	41
2.7 MAPK pathways are activated during late mitosis .....	43
2.8 Changes made during mitotic entry are restored at the end of mitosis.....	45
2.9 Regulation of non-kinases in mitosis.....	46
3.0 Results (Part 2): Characterization of function of BubR1 and Bub1 kinase phosphorylation..	50
3.1 Introduction .....	50
3.2 Identification of BubR1 phosphorylation sites in mitosis.....	51
3.3 Cdk1 phosphorylates S543, S670, and S1043 <i>in-vitro</i> .....	54
3.4 BubR1-5A mutant expressing cells exhibit severe congression defects.....	55
3.5 Bub1 phosphorylation in mitosis.....	58
3.6 Increasing the sequence coverage of Bub1 by using multiple proteases .....	59
3.7 Identification of auto-phosphorylation sites on Bub1 .....	60
3.8 Identification of phosphorylation on Bub1 interactors .....	64
4.0 Discussion.....	65
4.1 Small-molecule kinase inhibitor based enrichment of the kinome .....	65
4.2 HeLa cell synchronization.....	66
4.3 Identification of protein kinases .....	67
4.4 Global view of mitotic kinome.....	68
4.5 Regulation of BubR1 function by phosphorylation.....	69
4.6 Regulation of SAC and chromosome congression by different motifs of BubR1 .....	70
4.7 Autophosphorylation and substrates of Bub1 kinase.....	70
4.8 Advances in MS instrumentation and data analysis tools make large scale proteomic studies possible.....	72

5.0 Experimental procedures:.....	74
5.1 Antibodies .....	74
5.2 Cell Culture, SILAC labeling and synchronization.....	74
5.3 Immunofluorescence staining of cells .....	75
5.4 Kinase enrichment .....	75
5.5 In-gel protein digestion .....	75
5.6 In-solution protein digestion .....	76
5.7 Strong-cation exchange (SCX).....	77
5.8 Phosphopeptide enrichment and desalting .....	77
5.9 Nano-LC-MS/MS Analysis.....	77
5.10 Data processing and analysis.....	78
5.11 Interaction networks and functional clustering .....	79
5.12 Cell lysis and co-immunoprecipitation .....	79
5.13 Kinase assay .....	80
5.14 Peptide array synthesis and spots blotting .....	81
6.0 Appendix.....	82
6.1 PPI network for proteins with upregulated phosphorylation sites.....	82
6.2 PPI network for proteins with downregulated phosphorylation sites.....	83
6.3 Supporting data available at tranche.....	84
Abbreviations.....	85
References .....	87
Acknowledgements.....	102
Publications .....	103
Curriculum Vitae .....	104

## Summary

Mitosis is a key step in the cell cycle process which is strongly regulated by reversible phosphorylation. In our study we used proteomic tools to understand the regulatory mechanisms of mitosis by studying phospho-regulation of kinases. We wanted to compare different stages of cell cycle progression with main focus on mitotic stages in terms of site-specific kinase phosphorylation i.e. identification of phosphorylation sites on kinases and their relative dynamics during mitotic progression. We have done both large scale kinome studies using kinase enrichment as well as targeted studies focusing on single kinases (BubR1, Bub1).

We first standardized methods for large scale synchronization of cells in different stages of the cell cycle. Using large scale kinome study to compare three mitotic states, i.e., prometaphase, metaphase and telophase, we generated a resource of information about phosphorylation dynamics for more than 900 kinase phosphorylation sites from 206 kinases. Around 25% of the kinase phosphorylation sites were found to be modulated by at least 50% during mitotic progression. Further network analysis of jointly regulated kinase groups suggested that cyclin-dependent kinase and mitogen-activated kinase centered interaction networks are coordinately down- and upregulated in late mitosis, respectively. MAP kinase activation is separately verified by western blot analysis. Importantly, being a global study our data provided a global view of the mitotic phospho-regulation of the kinome; and moreover identified attractive candidates for future studies of phosphorylation-based mitotic signaling apart from covering the already known events.

Both BubR1 and Bub1 kinases were identified in the above study though the sequence coverage obtained was limited. We have chosen these kinases for detailed study due to their essential role in mitosis. We mapped phosphorylation sites on BubR1 and searched for the upstream kinase phosphorylating these residues. We demonstrated that BubR1 is phosphorylated by Cdk1 and that phosphorylation is required for BubR1 chromosome congression function. Since it is already established that Bub1 has kinase activity, we tried to identify the autophosphorylation sites on Bub1 and detected 15 sites that are autophosphorylated *in-vitro*.

## **1.0 Introduction**

### **1.1 Cell cycle**

Cell division is one of the fundamental processes required for survival and the continuation of life [1]. During cell division, the parent cell divides into two daughter cells capable of undergoing further divisions. The underlining goal of cell division is the faithful replication followed by equal segregation of genetic material. Eukaryotic cells are highly compartmentalized. Importantly, the nucleus, a double membrane compartment encapsulates the genetic material that is organized into chromatin, long supercoiled DNA structures in complex with a large variety of proteins, notably histones. Eukaryotic cell division proceeds through a number of discrete steps. First, cells prepare for cell division by interpreting various intra and extra-cellular signals. The decision to undergo cell division is a point of no return and cells remain committed for division or trigger apoptosis otherwise. Subsequently, the genetic material is replicated, followed by the equal distribution of cell contents to nascent daughter cells, and finally the physical separation of the daughter cells. Erroneous cell division is costly for organisms. Errors in the replication of genetic material compromise the integrity of the genome. Errors in chromosome segregation and physical separation lead to aneuploidy and polyploidy, fostering cell death and cancer. Fidelity of each step is guarded by multiple redundant pathways, ensuring the robustness of the whole process. These highly orchestrated series of events are collectively termed 'cell cycle' (Figure 1).

### **1.2 Mitosis**

Mitosis is the most spectacular part of the cell cycle during which genetic material is equally divided between the two daughter cells. Mitosis consists of 5 stages, i.e., prophase, prometaphase, metaphase, anaphase and telophase (Figure 1). Cytokinesis, the physical separation of the daughter cells, follows mitosis. Mitosis together with cytokinesis is called M-phase. During prophase, the nuclear membrane breaks down and chromatin starts to condense into chromosomes. By prometaphase, condensed chromosomes are formed and centrosomes start emanating microtubules. In metaphase, all chromosomes are captured by the microtubules and brought to the center of the cell. Following this, chromosomes are moved to the opposite ends (anaphase). In the last stage (telophase) most of the changes that were initiated in the beginning of mitosis are reverted back to the initial state i.e. formation of



nuclear envelope, decondensation of the chromosomes etc. Mitosis is under tight regulation since chromosome segregation errors may result in cancer or cell death [1]. Interestingly, little or no protein synthesis takes place in mitosis and most of the mitotic events are regulated by protein phosphorylation and protein degradation[1].

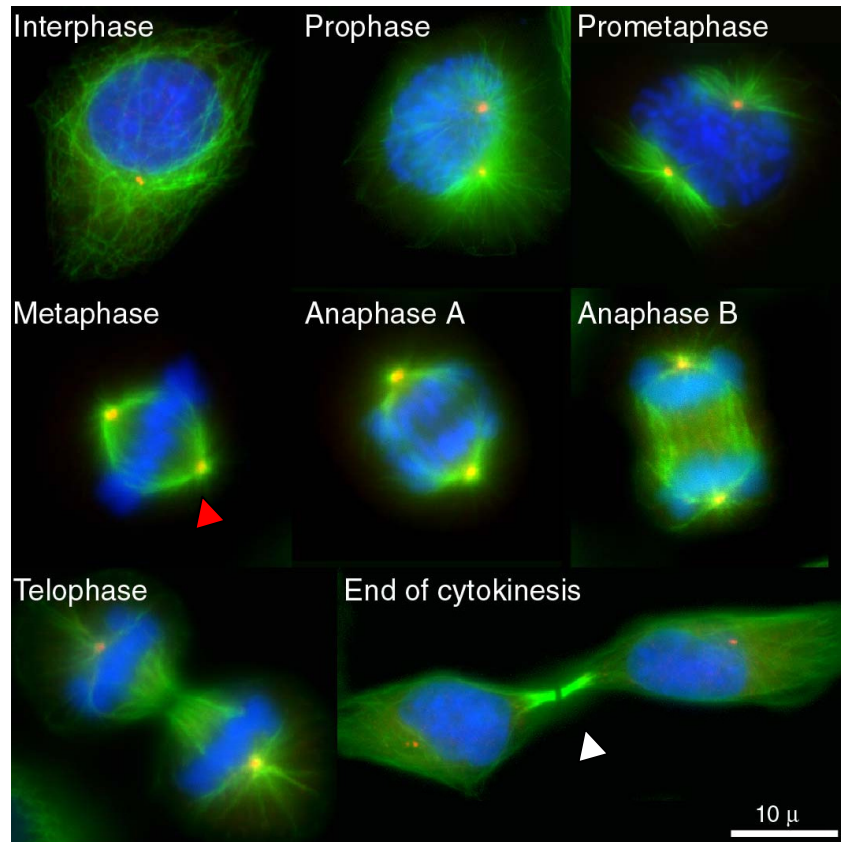


**Figure 1. Eukaryotic cell cycle with emphasis on mitotic stages.**

Representative pictures from different mitotic states are shown. Chromatin/chromosomes are stained with DAPI (Blue) whereas centrosomes and microtubules are stained by antibody coupled to alexa red (Red) and FITC (Green) respectively. The red arrow marks a mitotic spindle; and the white arrow points at a midbody.

### **1.2.1 Spindle assembly checkpoint**

Physically, the segregation of sister chromatids into the two daughter cells is carried out by the mitotic spindle, a highly dynamic microtubule-based structure. Since proper bipolar attachment of chromosomes to spindle microtubules is essential for the correct segregation of chromosomes, this critical step is monitored by a signaling pathway, known as the spindle assembly checkpoint (SAC) [2]. The SAC is a ubiquitous safety mechanism that evolved in eukaryotes to avoid chromosomal segregation errors. It remains active and halts mitotic progression until the two sister kinetochores are bound to microtubules emanating from opposite poles, resulting in bi orientation (amphitelic attachment) (Figure 2). Elegant studies have shown that even single unattached kinetochores keep the SAC active and block the onset of anaphase [3]. In some cases, both kinetochores of a sister chromatic pair may be captured by microtubules emanating from the same centrosome, i.e. syntelic attachments, resulting in loss of tension between the kinetochores. Such mismatches also activate the SAC, giving the cells time to correct the mismatches. Thus, the SAC monitors both unattached kinetochores and tension between the kinetochores. In mitotic HeLa cells, for example, SAC activity is turned on by adding either nocodazole which destabilizes the microtubules leading to attachment defects, or taxol which stabilises the microtubules, leading to tension defects. However, not all kinetochore–microtubule attachment defects are detected by the SAC. Each kinetochore has binding sites for around 20-25 microtubules. Therefore, a kinetochore may bind to microtubules from opposite poles (merotelic attachments). Merotelic attachments generate both tension and chromosome bi-orientation and hence are not detected by the SAC [4], thus leading to aneuploidy. However, both syntelic and merotelic attachments are corrected by Aurora B kinase mediated pathways[2].

### **1.2.2 The molecular mechanism of the SAC**

After DNA replication, sister DNA molecules/chromatids are held together by cohesion rings (Figure 2a). Removal of cohesin rings is thus mandatory for the separation of the sister chromatids. Cohesin rings are cleaved by separase, a caspase like protease which is kept inactive by a protein called securin [5]. The anaphase promoting complex/cyclosome (APC/C) is an E3 ubiquitin ligase that marks target proteins for degradation by the 26S proteasome. Prior to anaphase, securin is ubiquitinated by the APC/C, thus initiating its degradation. This leads to separase activation and cleavage of cohesion rings separating the sister chromatids. The APC/C also initiates the degradation of Cyclin B. leading to the

inactivation of Cdk1 prior to anaphase. Cdc20 is a co-factor of APC/C, which is required for its activity. The SAC negatively regulates the ability of Cdc20 to activate the APC/C [6; 7], preventing polyubiquitylation of two of its key substrates, cyclin B and securin, thereby preventing their destruction by the 26S proteasome.

SAC components are required for metaphase arrest in response to defects in bi-orientation. The mitotic checkpoint complex (MCC) is a main component of the SAC, which contains several proteins, i.e., Mad2, BubR1 and Bub3, as well as Cdc20. The MCC inactivates the APC/C preventing the degradation of securin and cyclin B. Besides the MCC, other important SAC components include Mad1 as well as the kinases Bub1, TTK(MPS1) and Aurora B. These proteins are required for amplification of the SAC signal and regulate the rate of MCC formation [2]. Additional proteins such as ROD, ZW10 and ZWILCH (RZZ complex), MAP Kinases, Cdk1, Nek2, Plk1, CENP-E and dynein also play important roles [2].

Kinetochores are the main sites of SAC activity and assembly of SAC components [8]. During prometaphase, Cdc20 and most of the other SAC proteins accumulate at the kinetochores. The MCC accumulates in mitosis and associates with the APC/C. Within the MCC, both Mad2 and BubR1 bind Cdc20 directly. The interaction of BubR1 with Cdc20 requires all SAC proteins, whereas only Mad1 and MPS1 are required for Mad2–Cdc20 binding [6; 9; 10]. Purified human MCC is a potent inhibitor of APC/C; compared with recombinant Mad2, MCC with all its components is 3,000-fold more effective [11]. BubR1 has a distinct binding site on Cdc20 from Mad2 and, together, Mad2 and BubR1 have a synergistic effect on APC/C inhibition [2].

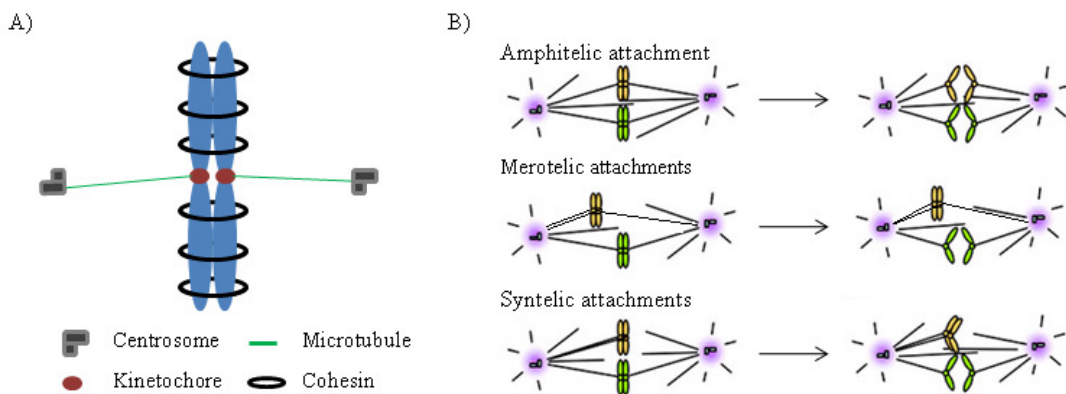


**Figure 2: Different types of kinetochore-microtubule attachments and their consequences in anaphase.**

A) Schematic representation of sister chromatids with amphitelic attachment. B) When the two sister kinetochores are bound to microtubules coming from opposite poles (Amphitelic attachment), tension is generated between the kinetochores, silencing the SAC, and the sister chromatids are pulled in opposite directions leading to normal chromosomal segregation. In cases where both the sister kinetochores are bound to microtubule coming from the same pole (Syntelic attachment) or where a kinetochore is bound to microtubules from opposite poles rather than to just one pole (Merotelic attachment), chromosomal segregation errors may occur. Figure adopted from <http://www.bch.msu.edu/faculty/kuo/histoneH3mitoticprogression.jpg>.

### **1.3 Regulation of kinase by phosphorylation**

Reversible phosphorylation is a ubiquitous posttranslational protein modification, which is involved in the regulation of almost all biological processes [12; 13; 14]. In humans, 518 protein kinases (PKs) have been identified in the genome; these phosphorylate the majority of cellular proteins and increase the diversity of the proteome by several fold [15]. Addition of a phosphate group to a protein can alter its structural, catalytical, and functional properties; hence kinases require tight regulation to avoid unspecific phosphorylation which can be deleterious to cells [16; 17; 18]. As a result, cells employ a variety of mechanisms to ensure proper regulation of kinase activities [19]. Importantly, most kinases are also in turn regulated through auto-phosphorylation and phosphorylation by other kinases, thus generating complex phosphorylation networks. In particular, phosphorylation on activation segments is a common mechanism to modulate kinase activities [20; 21; 22], but additional phosphorylation sites are also frequently required for fine tuning of kinase activities [23]. Some kinases contain phosphopeptide binding domains which recognize pre-phosphorylated sites on other kinases, resulting in processive phosphorylation and/or targeting of kinases to distinct cellular locations [24; 25; 26; 27]. Since such priming phosphorylation events depend on the activities of the priming kinases, these motifs act as conditional docking sites and restrict the interaction with docking kinases to a particular point in time and physiological state. In addition, phosphorylation sites may act through combinatorial mechanisms or through crosstalk with other posttranslational modifications (PTMs) [28; 29], thus further increasing the complexity of kinase regulatory networks.

Regulation of kinases is of particular interest in mitosis as most of the mitotic events are regulated by reversible protein phosphorylation [1]. Cyclin-dependent kinase 1 (Cdk1), an

evolutionarily conserved master mitotic kinase, is activated prior to mitosis and initiates most of the mitotic events. Cdk1 works in close association with other essential mitotic kinases such as Plk1, Aurora A and Aurora B for the regulation of mitotic progression [1; 30; 31; 32; 33]. Plk1 and Aurora kinases dynamically localize to different subcellular locations to perform multiple functions during mitosis and are phosphorylated at several conserved sites. Although little is known about the precise roles of these phosphorylation sites, emerging data indicate that they are involved in regulating localization-specific functions [5; 34]. Further, the kinases Bub1, BubR1, TTK (Mps1), and kinases of the Nek family play important roles in maintaining the fidelity and robustness of mitosis [1]. Recently, a genome-wide RNA mediated interference screen identified M-phase phenotypes for many kinases which have not previously been implicated in cell cycle functions, indicating that additional kinases have important mitotic functions [35].

#### **1.4 Mass Spectrometry in biology**

Any instrument capable of measuring mass-to-charge ratio ( $m/z$ ) of charged particles is called a mass spectrometer. Two particles with the same  $m/z$  move similarly in space and time when subjected to the same electric and magnetic fields. In other words, the motion of a charged particle under the influence of electromagnetic fields is unique and depends only on  $m/z$ . Mass Spectrometry (MS) makes use of this principle to measure the  $m/z$  values of molecules. In MS the analytes are ionized to generate charged molecules and then the  $m/z$  of those molecules is measured. In general a mass spectrometer is composed of three principle components- an ion source, mass analyzer and a detector. Depending on the choice and configuration of these components, MS instrument are available in different forms with different capabilities.

In 1912, the first MS instrument was constructed by J.J.Thomson, which was used to identify the isotopes of various elements. When the accuracy of the measurement is sufficient, it is possible to identify that ion by matching the measured  $m/z$  value to the values in a library (Identification). Fragmenting the molecule and measuring the  $m/z$  values of those fragments (MS/MS spectra) helps in elucidating the chemical structures of molecules, such as peptides (Primary structure identification). Fragmentation can be achieved by collision with inert gas molecules (collision induced dissociation, CID), electron capturing (electron capture disassociation, ECD) or by electron transfer (electron transfer dissociation, ETD). CID, the

most commonly used dissociation technique, produces b- and y- type peptide fragment ions and this is often sufficient to determine the peptide sequence. However, in case of PTMs, such as phosphorylation, CID preferentially cleaves the weakly bound PTM from the peptide, resulting in little fragmentation of the peptide backbone and making the identification of peptide sequence and/or the location of the modification difficult. Alternatively, ETD induces fragmentation of the peptide backbone in a sequence independent manner, keeping the PTM intact and produces primarily c- and z-type fragment ions. Further, the intensity of the peptide in two or more samples can be compared from MS spectra (SILAC) or MS/MS spectra (iTRAQ) to estimate the relative abundance (Quantitation).

Mass spectrometers are rapid and robust; current instruments measure around 1-50 mass spectra per second under typical workflows. Moreover, the sensitivity is in the attomolar range for peptides and they can be configured easily in high throughput workflows. These features of MS instruments changed the way in which biological molecules such as proteins, lipids and carbohydrates are analyzed. It paved path to fields like proteomics. MS become an invaluable tool for the identification of proteins, protein-protein interactions, post-translational modifications and protein quantitation. Especially in recent years, tremendous advances in terms of instrument performance, methods efficiency, and computational power shifted the focus from small-scale projects to large-scale proteomic studies, allowing the study of the dynamics of proteomes in different cell types, under various stimuli, or under diverse experimental conditions.

## **1.5 Mass spectrometric instrumentation**

### **1.5.1 Ion source**

Ion sources generates ions from the analytes, which are channeled to the mass analyzer. A variety of ionization techniques are available for mass spectrometry. Based on the physical state of the analyte, ion sources are classified in to three types, viz. gas, liquid and solid-state. Only liquid- and solid- phase ion sources are used for peptides as peptides are thermally unstable and do not have sufficient vapor pressure[36].

In solid-state ion sources, such as matrix-assisted laser desorption/ionization (MALDI), the analyte is mixed with a matrix (commonly used matrixes are 3,5-dimethoxy-4-

hydroxycinnamic acid,  $\alpha$ -cyano-4-hydroxycinnamic acid and 2,5-dihydroxybenzoic acid)[37; 38]. When the solvent is evaporated the analyte will co-crystallize with the matrix. These crystals are then irradiated by a laser, which ionizes the matrix molecules. The matrix then transfers its charge to the analyte molecules generating analyte ions. Further, apart from aiding the ionization of analyte molecules, the matrix also protects them from the disruptive energy of the laser.

Electrospray ionization (ESI) is the best example for a liquid-phase ion source. This technique was introduced by John Bennett Fenn [39], for which he was awarded the Nobel Prize in 2002. In this method, the analyte is dissolved and passed through a narrow capillary tube at flow rates of 0.05-200  $\mu\text{L min}^{-1}$ . An electric potential (1-7 kV) is applied between the tip of the capillary and the opening of the mass spectrometer, which are typically separated by 0.3-3 cm. This induces charge accumulation at the tip of the capillary tube on the liquid drop that breaks the drop into highly charged smaller droplets. These droplets pass through a heated capillary which is at the opening of the MS instrument, where the solvent is evaporated leaving analyte ions. An inert gas like nitrogen is injected coaxially at low flow rates to limit the spatial dispersion of the spray.

ESI has some characteristic features. Most importantly, it is able to generate multiply charged ions provided the molecules are large enough. Since the mass spectrometer measures only the  $m/z$  values and for a given instrument the measuring range is limited, multiply charged ions make analysis of large molecules such as proteins possible. ESI-trap instruments can measure  $m/z$  values between 50-2000. So proteins/peptides which are out of this range cannot be analyzed in their singly charged ionic states. However, for a protein of 20,000 kDa, for instance, the  $m/z$  value of a typical  $20^+$  charge state is  $\sim 1,000$  and falls within the range of the instrument. Another feature of ESI is that the number of ions generated is proportional to the concentration of the analyte and does not depend on the absolute amount. Further, the number of ions generated is sensitive to the solvent used and the electrolyte concentration in the solvent. One more advantage of the ESI source is that it can be seamlessly coupled to HPLC systems[36].

### **1.5.2 Mass analyzers**

Mass analyzers separate the ions that are generated by the ion source, according to their  $m/z$ . As there are many ion sources, different mass analyzers are also available, each

with specific advantages and disadvantages. All mass analyzers make use of static or dynamic electric and/or magnetic fields but differ in the way these fields are applied. They are broadly divided into two classes; first, scanning analyzers which transmit ions in a stepwise manner based on the  $m/z$  value, e.g., quadrupole and ion-trap mass analyzers. Second, simultaneous analyzers which transmit all the ions in one step, e.g., time of flight (TOF) and Orbitrap analyzers. It is possible to combine different types of mass analyzers in a single MS instrument. This offers versatility and better performance. Before opting for a mass analyzer there are at least five important features which have to be considered, i.e. measuring range, speed of analysis, transmission efficiency, mass accuracy and resolution.

### **1.5.2.1 Linear quadrupole ion trap**

An ion trap is a device which traps ions in two or three dimensional space using direct current (DC) and radio frequency (RF) oscillating alternate current (AC) electric fields. The first generation of ion traps, the 3D ion trap was invented by Wolfgang Paul who was later awarded the Nobel Prize [40]. Linear quadrupole ion traps or 2D ion traps are second generation ion traps, which have improved features compared to 3D ion traps. The linear ion trap can function both as a storage device of ions for a period of time and as a mass analyzer. Linear ion trap is exemplified by the LTQ XL mass spectrometer from Thermo Electron Corporation, the instrument that is used in this study.

The LTQ linear trap is made up of two pairs of orthogonally positioned hyperbolic rods, which are cut into three sections. The central section is about three times larger (37 mm) than the two end sections. The side rods in the central section contain a slit along the z-axis through which ions can be ejected from the trap and the two detectors are placed facing the slits.



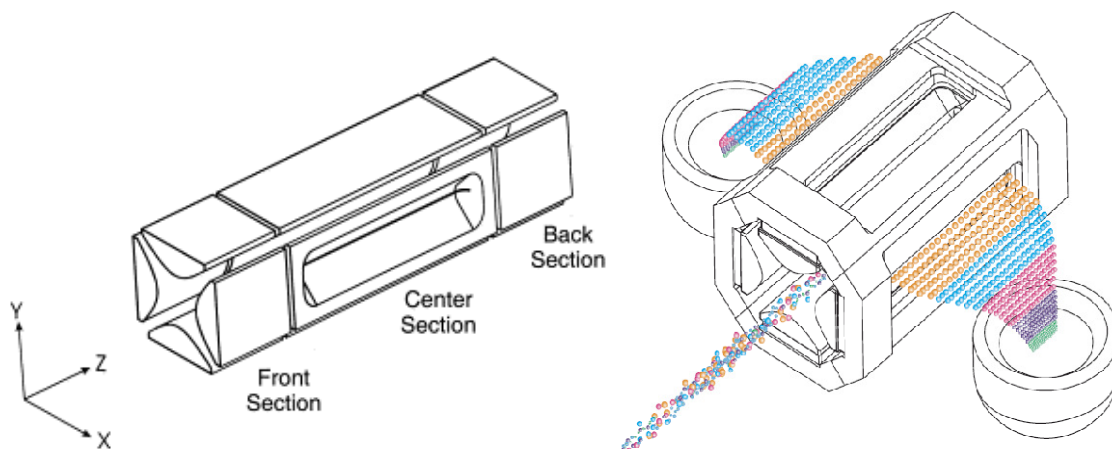


**Figure 3 Basic design of the linear quadrupole ion trap.**

A) Schematic representation of the linear quadrupole ion trap design (adopted from Schwartz et al, 2002). B) Schematic representation of linear quadrupole ion trap during operation. Ions of various masses (represented by different colors) enter the linear ion trap. During scan out the ions are ejected from the trap in order of increasing mass-to-charge ratio. The ions exit the trap through slits in the exit rods. The ions then strike the detection system on either side of the trap (adopted from LTQ XL Hardware Manual, Thermo Electron Corporation, June 2006).

During the operation, DC voltages are applied such that the same voltage is applied to rods facing each other, whereas adjacent rods have identical electrical potential strengths but opposite polarities. Ions are trapped in axial direction by applying different DC voltages to the three sections. Further, the rods end in lenses to which positive potential for positive ions and negative potential for negative ions are applied, thus they also repel the ions into the trap axially. Ions are trapped in radial direction by applying the RF AC voltages (main RF voltage) of the same amplitude but different polarities to the adjacent rods.

In order to store ions in the ion trap, their trajectories should be stable in both radial and axial directions simultaneously. Motion of ions inside a quadrupole trap can be described by the Mathieu equation. Solving the Mathieu equation gives the following relations [41].

$$(1) \quad \frac{m}{z} = \frac{4eV}{q_z \omega^2 r_0^2}$$

$$(2) \quad a_z = \frac{-8zeU}{m\omega^2 r_0^2}$$

$$(3) \quad q_z = \frac{4zeV}{m\omega^2 r_0^2}$$

In the above equations  $m$  is the ion mass;  $z$  is the ion charge.  $U$  and  $V$  are DC and RF potentials applied to the hyperbolic rods, respectively;  $\omega$  is the angular frequency of the RF;  $r_0$  is the radius, i.e. half the distance between the opposite rods;  $a_u$  and  $q_u$  are dimensionless trapping parameters in the Mathieu equation, which establish the relation between coordinates of ion and time;  $\beta_u$  is a additional trapping parameter which is a complex function of  $a_u$ ,  $q_u$  (equation not shown). The values  $\beta_u=0$ ,  $\beta_u=1$  correspond to boundaries of stable regions, i.e. the point at which the trajectory of an ion becomes unstable[41].

The main RF voltage is ramped from low amplitude to high amplitude at constant voltage. Stability of an ion in radial direction depends on the main RF voltage i.e. the trajectory of an ion is stable only up to a certain RF voltage (resonance voltage)[42]. Initially a low RF voltage is applied allowing all the ions above a certain  $m/z$  values to be retained (storage voltage). Then, by ramping the main voltage at constant rate ions can be successively ejected in the order low to high  $m/z$  values. For MS/MS analysis, all the ions except the ion of interest should be ejected before the fragmentation. This is achieved with the help of ion isolation waveform voltages i.e. all resonance voltages except that of the ion of interest are applied[42]. Additionally, a resonance ejection AC voltage, i.e. fixed frequency with increasing amplitude, is applied during the ramping of the main RF voltage. When an ion is about to be ejected from the mass analyzer cavity by the main RF voltage, it approaches resonance with the resonance ejection AC voltage. As a result ions move away from the center into a region where the field produced by the main RF voltage is strong, thus enhancing the ejection of the ion and improving the mass resolution [42].

Linear ion-traps offer many advantages over 3D traps; 15 times higher ion capacity, 3 times faster scan rate, up to 100% detection efficiency, and up to 70% trapping efficiency. However, the mass accuracy of ion traps is in the range of 0.2-2.0 Da and resolution less than 1,000 (at high scanning speed).

### 1.5.2.2 The electrostatic trap or orbitrap

The orbitrap is an electrostatic trap that was developed from a completely new concept, proposed by Makarov [43; 44], and was commercially released by Thermo Electron Corporation in 2005. The orbitrap mass analyzer quickly gained popularity due to its superior mass accuracy (low ppm or ppb) and high resolution (upto 1,00,000) without requiring any powerful magnets. It uses fourier transformation to obtain the mass spectra.

The design of the orbitrap consists of a central spindle shaped electrode (maximum diameter of 8 mm) surrounded by a barrel shaped external electrode. The external electrode is made by two equal half's which are kept at a small distance. DC voltage of several kilovolts is applied to the central electrode, negative for positive ions and positive for negative ions and the external electrode is at ground potential [36]. Ions enter the trap tangentially through this gap with a kinetic energy of few kiloelectronvolts and start oscillating. Ions follow intricate paths inside the trap under the influence of a quadro-logarithmic field, due to the peculiar geometry of the trap. The angular frequency ( $\omega$ ) of an ion inside the trap is given by

$$\omega = \sqrt{\left(\frac{q}{m}\right) k} \quad (k \text{ is field curvature})$$

This equation is of great interest as it implies that the frequency is directly linked to the ratio of  $q/m$  and independent of the initial kinetic energy. As a result, by measuring the frequency of an ion inside the orbitrap, its  $m/z$  value can be calculated.

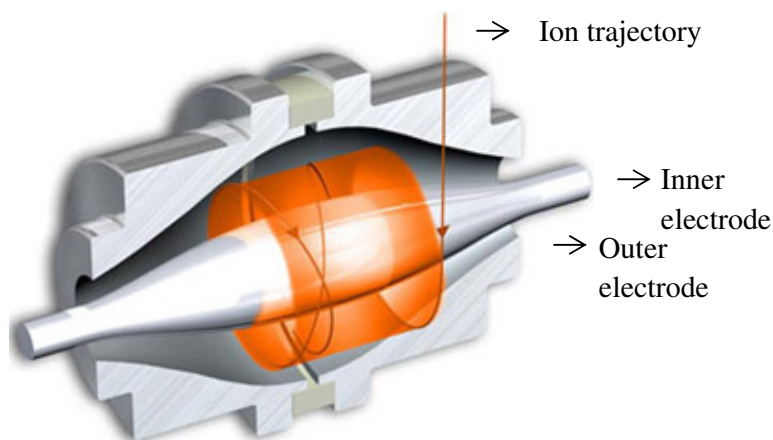


Figure 4. Cross section of orbitrap mass analyzer (courtesy, Thermo Electron Corporation ).

### 1.5.3 Detectors

Detectors generate an electric current proportional to the number of ions reaching them (impact detectors). This electric current is then used to measure the relative intensity. A variety of impact detectors suiting to different mass analyzers are available.

The LTQ MS is equipped with an off-axis detection system (Figure 3). Ions ejected from the ion trap hit two conversion dynodes which are placed perpendicular to the ion exit, producing secondary particles. Positive secondary particles are of interest for negative ions and *vice versa*. The concave shape of the dynode helps in focusing the ions which are channeled through an electron multiplier. The electron multipliers generally operate at a gain of  $10^5$ . The current that is leaving the electron multiplier is converted to voltage by an electrometer and is recorded. Since the detection system is placed off-axis to the mass analyzer, neutral molecules will not reach the conversion dynode thus avoiding noise.

The detectors in Fourier transform ion cyclotron resonance (FTICR) or Orbitrap analyzers are different from impact-type detectors. These detectors measure the broadband current that is generated by the oscillating ions present in the trap. This image current is later resolved in to individual frequencies using the mathematical Fourier transformation.

## 1.6 Methods for quantitation

Mass spectrometry based quantitative methods can be broadly classified as label free and label based methods. Label free methods are simple and inexpensive as they do not involve any additional steps in the experimental design or reagents. Ideally, the intensity value in the mass spectrum should be sufficient to perform relative quantitation. However, ionization of an ion depends on multiple factors including the complexity of the sample. This coupled together with variations in liquid chromatography (LC) profiles leads to large run-to-run variation. Thus, label free methods are less reliable and mostly qualitative (eg. spectral counting). It is important to note that label free methods which make use of identified peptides to correct the variation in LC profiles along with replicates tend to be more accurate [45; 46]. Further, mass accuracy and resolution of the data are very important for any quantitative method. Thus FT instruments are preferred over ion trap instruments.

Label based methods introduce a label into the sample either chemically (iTRAQ, ICAT) or metabolically (SILAC). The label can be either isotopic or isobaric. In case of

isotopic labeling the label introduced into the sample and the control differ by few Daltons. As a result, the peptides show up as doublets in the MS spectrum. Isobaric labeling works slightly differently. The mass of the sample and the control would be the same after labeling. However, when these peptides are fragmented, they release reporter ions of different  $m/z$ , i.e. quantitation is achieved through MS/MS spectra.

Isotopic labeling is exemplified by stable isotope labeling with amino acids in cell culture (SILAC). SILAC is developed mainly for cultured cell lines; however recent studies have shown that it can be successfully extended to popular model systems such as mice (*Mus musculus*), drosophila (*Drosophila melanogaster*), yeast (*Saccharomyces cerevisiae*), etc [47; 48; 49]. In this method, natural amino acids (commonly arginine and lysine) containing C13, N15 and H2 isotopes act as labels [50]. Cells are grown in culture media that are devoid of those amino acids which need to be labeled. Commonly used media are Dulbecco's Modified Eagle's Medium (DMEM) and RPMI-1640 without labeling amino acids. Labeled amino acids are separately added to the medium and are incorporated into the proteins using cells own translation machinery. All 20 amino acids are available in isotopic labeled forms. Arginine and lysine are the preferred choices, because trypsin cleaves after arginine and lysine residues making sure that every peptide will contain at least one arginine or lysine except the peptide containing the protein C-terminus. Further, arginine and lysine are essential amino acids for human cell lines i.e. they cannot be synthesized internally. This ensures complete labeling of the proteome (>97%). For simple quantitative analyses, (e.g., protein quantitation in a simple protein mixture) labeling with one amino acid might be sufficient. However, if all the peptides need to be quantified, such as for PTM analysis, both arginine and lysine should be used for tryptic protein digests. Moreover, normal fetal calf serum (FCS) contains many amino acids, including arginine and lysine. Hence dialyzed FCS is necessary for complete labeling of proteins. SILAC quantitation is more reproducible than the methods using chemical labels. First, as opposed to chemical labeling, SILAC labeling is achieved prior to cell lysis. As a result, cells from sample and control can be mixed and processed together, minimizing variation arising from downstream steps. Second, quantitation is achieved through MS spectra acquired during the peptide elution (which are often more than one) as opposed to MS/MS spectra (which are often one per  $m/z$ ). However, the main limitation of the SILAC method is that it cannot be used to analyze harvested tissue samples.

## 1.7 Phosphoproteomics

Phosphorylation is one of the most common reversible post translational modifications of proteins. In mammals, phosphorylation occurs mainly on serine, threonine and tyrosine residues. Although many proteins are phosphorylated, not all molecules of a given population are phosphorylated. Furthermore, only 1-2 % of peptides are usually phosphorylated, making prior enrichment mandatory for their detection [51]. Many methods were proposed for the enrichment of phosphopeptides. Immobilized metal-ion affinity chromatography (IMAC), which was originally developed for purification of His-tagged proteins, was extended to phosphopeptides [52]. Phospho groups are negatively charged, hence they bind to positively charged metal ions such as  $\text{Fe}^{3+}$ ,  $\text{Ga}^{3+}$ ,  $\text{Al}^{3+}$  or  $\text{Zr}^{4+}$  through electrostatic interactions. As a main drawback, IMAC is highly sensitive to the salt concentration in the sample and prior desalting steps are necessary. On the other hand, metal-oxide chromatography (MOC) using titania, zirconia, and alumina was shown to be tolerant to salts in the sample [53]. Ideally, for comprehensive coverage of the phosphoproteome both methods are incorporated into the workflow [54].

Successful enrichment of phosphopeptides depends on many factors. Non-specific binding of acidic peptides to the metal oxide is a major bottleneck. It was shown that nonspecific binding can be reduced by using low pH and by introducing appropriate aliphatic hydroxy acid (i.e. modifier). At low pH all the carboxyl groups will be protonated and the modified molecules compete with acidic peptides for binding to the metal oxide. Titanium dioxide with lactic acid or glycolic acid as modifiers give good results [55].

Elution of the phosphopeptides from the metal dioxide is a non trivial step. Peptides are eluted by changing the pH of the solution to alkaline. Ammonia solution is the preferred choice for phosphopeptide elution but recent studies suggested that for complete elution of peptides, especially multiply phosphorylated peptides, more than one basic reagent is necessary. Successive elution with ammonia, piperidine and pyrrolidine is shown to be more effective to achieve efficient elution [56].

In addition to IMAC and MOC many other methods have been developed to detect phosphopeptides selectively, including strong cation exchange (SCX) chromatography [57] and MS based methods such as precursor ion scanning in the negative mode [58], neutral loss triggered MS3 [59], and pseudo-MS3 [60].

Once the phosphopeptide is identified by MS, a next important step is to identify the precise location of the phosphorylation site within the peptide. Information about actual phosphorylation sites is biologically more meaningful than information about phosphopeptides. When the peptide sequence contains more than one serine/threonine/tyrosine residue, phosphorylation needs to be assigned to the correct residue, using peptide fragmentation data in the MS/MS spectra. However, gaps in the MS/MS ion series as well as close spacing of the serine/threonine/tyrosine residues often complicate the precise determination of the phosphorylation sites. Hence, for each possible phosphorylation site a probability value is assigned (localization probability) and generally phosphorylation sites with localization probabilities exceeding 75% are considered valid [57].

## **1.8 Bioinformatic tools for the analysis of mass spectrometry data**

Over the past decade, proteomics has undergone a shift from qualitative to quantitative strategies and has emerged as a method-of-choice for analyzing the dynamics of proteomes in different cell types, under various stimuli, or under diverse experimental conditions [61]. As a consequence, the amount of published proteomic data has increased rapidly and in-depth analysis of large-scale proteomic datasets is becoming more and more important as the interest in proper biological interpretation of the data is increasing. Gene ontology, pathway analysis and protein-protein interaction analysis emerged as invaluable tools to convert large datasets into knowledge of biological significance.

### **1.8.1 Gene ontology**

While describing a particular protein or function, researchers often do not use terms consistently. This is now overcome by the use of controlled ontology called Gene Ontology (GO)[62]. Every gene/protein can thus be described by a finite vocabulary at different levels of granularity. Within GO, a limited set of species-independent terms are available, thus strongly reducing ambiguities. Each GO-entry consists of a number (GO-identifier) and a term associated with it. Each term can then belong to one of the three GO-categories, namely 'biological process', 'molecular function' or 'cellular component'. It is important to note that GO is structured in a hierarchical way. Each term constitutes a node in a directed acyclic graph, with one or more parent terms and one or more child nodes.

GO-term analysis often constitutes the most basic step in the bioinformatic characterization of proteomic datasets. A simple way to analyze the data is to annotate the proteins with GO-terms and determine whether they show enrichment for a particular group of biological processes, functions or cellular compartments. Several tools are available to accomplish this task; an extensive list of GO-related tools can be found at <http://www.geneontology.org/GO.tools.microarray.shtml>. Moreover, these tools often serve as meta-tools in that they not only search for GO terms, but also integrate information from pathways, domains and other important biological attributes. DAVID is an example of such a popular meta-tool [63] that helps to detect over- or under-represented GO terms within a dataset.

### **1.8.2 Pathway analysis**

A biological pathway consists of a series of well defined reactions among biomolecules which will result in a specific biological outcome. As pathways focus on physical and functional interactions between proteins rather than merely taking the gene-centric view of GO-based analyses, pathway analyses have the potential to take the analysis of proteomic data one step further. Pathway analysis using proteomic data is extremely useful in areas such as signal transduction, metabolic processes, and cell cycle progression, which involve extensive regulation at the protein level (i.e. by posttranslational modifications) and thus cannot be comprehensively studied by mRNA expression analysis alone. Pathway models are manually curated and are iteratively refined to keep up-to-date with the emerging scientific data. Manual annotation mainly focuses on well-known and well-studied pathways, thus possibly leaving out pathways which may be potentially interesting for other researchers. Metabolic pathways are well established compared to signaling pathways, mostly because they are actively constructed by a number of dedicated groups [64].

Currently, around 300 pathway resources are available. Some of the popular and freely available pathway databases are KEGG[65], Reactome[66], STKE[67], PANTHER[68], Biocompare[69], GenMAPP[70], and PID[71]. Over-representation analysis is often used to annotate the protein lists of interest, in a similar way as mentioned above in the gene ontology section, especially when analyzing data from proteome states measured under different conditions. Meta-tools such as DAVID, PANTHER [68] and Babelomics [72]



provide over-representation analysis of GO terms, domains and pathways. In addition, they cluster similar/relevant annotations in the results in order to reduce the redundancy of terms.

### **1.8.3 Interaction networks**

Proteins work rarely in isolation but rather function in complexes as multi-protein machines. Since their assembly is largely mediated by protein-protein interactions (PPIs), functional modules within a proteome may be revealed by PPI analyses[73]. In general, PPIs comprise both physical and functional interactions, which may be further grouped into experimentally determined and computationally predicted interactions. Functional interactions include sharing a common substrate in a pathway, regulating each other at the transcriptional level, or indirect binding through participation in larger multi-protein assemblies [74]. HPRD [75], IntAct [76], MINT [77], BIND [78], DIP [79], and BioGRID [80] are some of the popular databases covering experimentally obtained PPIs, derived from a combination of automatic extraction and expert curation.

STRING is a powerful meta-database incorporating data from many curated databases (IntAct, BioGRID, HPRD, MINT, DIP and BIND), additional in-silico predicted interactions and additional pathway information with an easy-to-use web interface. STRING thus constitutes a very popular tool for interaction network analysis of proteomic data. It incorporates experimentally derived interactions from the above databases along with interactions obtained from computational predictions and text mining. Importantly, the types of included interactions can be easily specified by the user for any given analysis, thus allowing different levels of stringency. Lists of proteins can directly serve as an input to STRING, so that all known interactions as well as hub-proteins can easily be extracted. However, when interpreting the predicted interactions one has to be very careful to select the right parameters and types of interaction data..

## **2.0 Results (Part 1): Phosphorylation dynamics of protein kinases across mitosis\***

*\*This work is included in a manuscript that has been accepted for publication: Quantitative site-specific phosphorylation dynamics of human protein kinases during different mitotic stages. Kalyan Dulla, Henrik Daub, Renate Hornberger, Erich A. Nigg, Roman Körner. *Molecular & Cellular Proteomics* (2010), in press.*

I would like to state that kinase enrichment from the cell lysates was performed in collaboration with Dr. Henrik Daub and Frau Renate Hornberger (MPIB). All the other upstream and downstream experiments were performed by myself.

### **2.1 Introduction**

Although protein phosphorylation plays a pivotal role in the regulation of cellular networks, many phosphorylation events remain undiscovered mainly due to technical limitations [81]. The advent of mass spectrometry based proteomics along with developments in phosphopeptide enrichment methods has enabled large scale global phosphoproteomic studies [55; 82]. However, the number of phosphorylation sites identified on kinases is limited compared to other proteins due to their frequently low expression levels. In order to overcome this problem, small inhibitor based kinase enrichment strategies were developed resulting in the identification of more than 200 kinases from HeLa cell lysates [83; 84]. This method was also used recently to compare the phospho-kinomes during S-phase and M-phase of the cell cycle resulting in the identification of several hundreds of M-phase specific kinase phosphorylation sites [83]. In the present study, we address the dynamics of the phospho-kinome during mitotic progression using large scale cell synchronization at three distinct mitotic stages, small inhibitor based kinase enrichment and SILAC based quantitative mass spectrometry. Thus we have determined the mitotic phosphorylation dynamics of more than 900 kinase phosphorylation sites, and identified distinctly regulated kinase interaction networks. Our results provide a valuable resource for the dynamics of the kinome during mitotic progression and give insight into the systems properties of kinase interaction networks.

### **2.2 Experimental strategy**

SILAC is amongst the preferred methods for comparative proteomic studies in mammalian cell lines and provides easy and accurate quantitation [50; 85]. In the present

study, we used SILAC triple labeling in combination with small inhibitor based kinase enrichment and large scale cell synchronization methods (Figure 5). In brief, three populations of HeLa cells were grown in large scale under identical conditions using spinner cultures in light, medium and heavy SILAC media containing different isotopic forms of arginine and lysine. Next, cells were synchronized in prometaphase, metaphase and telophase using the drugs nocodazole and MG132 (Figure 5) and the three cell populations were lysed and mixed in equal proportions. From the lysate, cellular protein kinases were enriched using kinase affinity chromatography and fractionated by one dimensional SDS-PAGE followed by tryptic digestion of the proteins. Alternatively, the enriched kinase fraction was in-solution digested by trypsin and fractionated using SCX. All fractions were enriched for phosphopeptides using TiO<sub>2</sub> and measured by nanoLC-MS/MS. Flowthrough fractions remaining after phosphopeptide enrichment were also analyzed for calculating protein ratios. To address the biological reproducibility, experiments were carried out in triplicate.

### **2.3 Large scale synchronization of HeLa cells in different mitotic stages**

HeLa cell lines are popular model systems for mammalian cell cycle research and are often used in large scale proteomics studies [83; 86]. Established protocols for HeLa synchronization at specific mitotic stages, however, are optimized for adherent HeLa cell lines, which are not compatible with the large amounts of cells needed for kinase enrichment. Therefore, we developed mitotic synchronization protocols for HeLa Suspension (HeLa S) cells, which can be grown on a sufficiently large scale in suspension (spinner) cultures. To assure HeLa S undergoes normal cell cycle, growth kinetics were studied and immunofluorescence pictures after DNA and  $\alpha$ -Tubulin staining microscopy pictures were taken across the cell cycle. These results demonstrate that HeLa S cells faithfully mimic the normal cell cycle and can be synchronized with traditional mitotic inhibitors (Figure 6).

Double synchronization with thymidine in S-phase followed by treatment with microtubule destabilizing drugs such as nocodazole is the preferred method to enrich HeLa cells in mitosis. Nocodazole is a reversible inhibitor which efficiently arrests the cells in a prometaphase like state with an active SAC. Generally, drug induced mitotic states mimic natural mitotic stages but may not perfectly represent unperturbed mitosis. However, synchronization with thymidine and nocodazole are accepted methods in biological studies of mitosis and our current knowledge of mitotic progression is to a large extent based on the use of these drugs for synchronization. To reduce possible side effects to a minimum, we used a

single thymidine block instead of the double thymidine arrest. Also for the nocodazole and MG132 synchronization steps, we have carefully determined the minimal concentrations and incubation times of the drugs to reduce possible side effects.

Various nocodazole concentrations were tested and 40-50 ng/ml were found sufficient to block HeLa S cells in mitosis. For adherent nocodazole treated HeLa cell cultures, the purity of the mitotic cell fraction can be strongly increased by shake-off of the rounded mitotic cells. Unfortunately, this shake-off method cannot be applied to cells grown in suspension and we therefore tried other means to increase the purity of mitotic HeLa S cells. Assuming that an increase of the growth stimulus may help cells reaching prometaphase faster and thus more synchronously, nocodazole was applied to media with increased concentrations of FCS. As expected, cells supplemented with higher concentrations of FCS (20%) entered into mitosis more coherently with more than 90% of cells reaching prometaphase within 12 hours of thymidine release (Figure 7B). Next, to enrich cells in metaphase, MG132, a reversible cell permeable proteasome inhibitor, was employed. This drug blocks proteasome mediated degradation of Securin which is required for progression to anaphase. Importantly, cells blocked by MG132 are characterized by an inactivated SAC providing the opportunity to study SAC signaling by comparison with nocodazole blocked cells with an active SAC. Thus approximately 90 % of the MG132 blocked cells were determined to be in metaphase. Finally, to enrich for the telophase state, cells were released from MG132 and the optimal time to harvest telophase cells was determined by immunofluorescence microscopy of DNA stained cell fractions at various time points. Synchronization in telophase turned out to be the most difficult and least reproducible task since this stage is rather short (typically 20-30 minutes) and there are no drugs available to block cells efficiently in telophase. HeLa cells released from MG132 enter telophase after approximately 90-120 minutes (release time from the metaphase block and anaphase). This duration is slightly longer than in unperturbed mitosis as the cells take some time to recover from the MG132 block. After optimization of the release period, 45 %, 60 %, and 70 % telophase cells were counted in experiment 1, experiment 2, and experiment 3, respectively (Figure 7B).

We further benchmarked the samples using western blot analysis of various mitotic markers (Figure 7D). The concentrations of Cyclin B and Securin are known to be low in S-phase, to peak in prometaphase and metaphase, and to be quickly diminished in anaphase after inactivation of the SAC. As shown in Figure 7D, western blot analyses of the synchronized HeLa S cells are fully consistent with the expected expression levels.

Phosphorylation of Ser10 of Histone H3 is a marker for chromosome condensation. Since anti-pSer10 staining is not diminished in the telophase sample (Figure 7D), we conclude that cells did not enter the next G1 cycle yet. Further, BubR1 pSer676 has been shown to be phosphorylated in prometaphase but not in metaphase[87] so the western blots in Figure 7D demonstrate a good separation between prometaphase and metaphase enriched cells. In summary, the western blot results along with the immunofluorescence pictures (Figure 7B) show that the samples faithfully represent the mitotic stages prometaphase, metaphase and telophase.

A) SILAC labeling and Cell synchronization

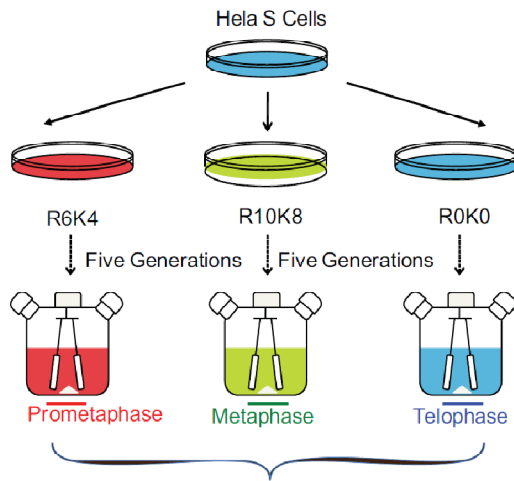
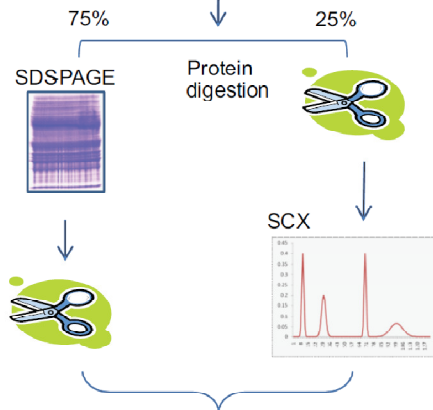


**Figure 5. Schematic overview of the experimental strategy**

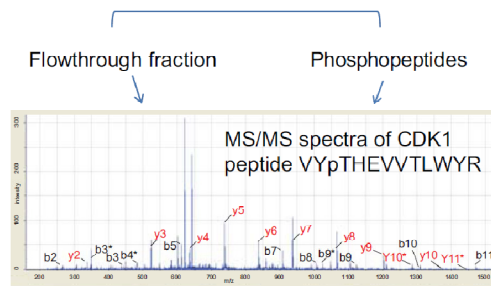
B) Sample pooling and Kinase enrichment



C) Fractionation



D) Phosphopeptide enrichment



E) Nano LC-MS/MS

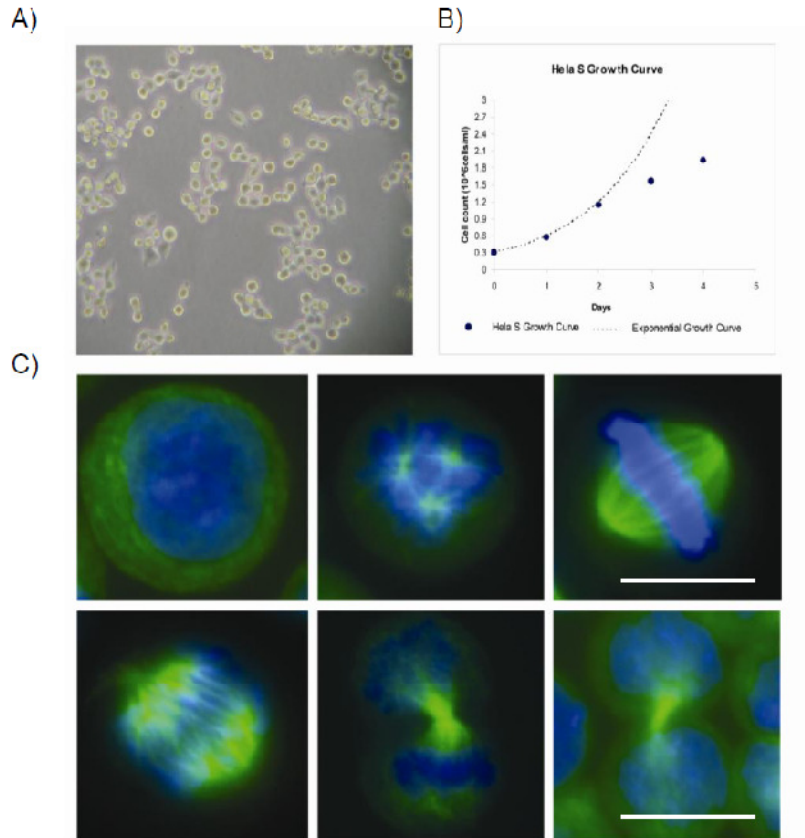


**Figure 6. Characterization of the HeLa S cell line.**

A) Picture of HeLa S cells on cell culture dishes. B) Growth curve of HeLa S cells. C) Representative immunofluorescence pictures of HeLa S cells across different stages of the cell-cycle in the order interphase, prometaphase, metaphase, anaphase, telophase and cytokinesis. DNA and Tubulin are stained in blue and green, respectively. Scale bars represent 10  $\mu\text{m}$ .

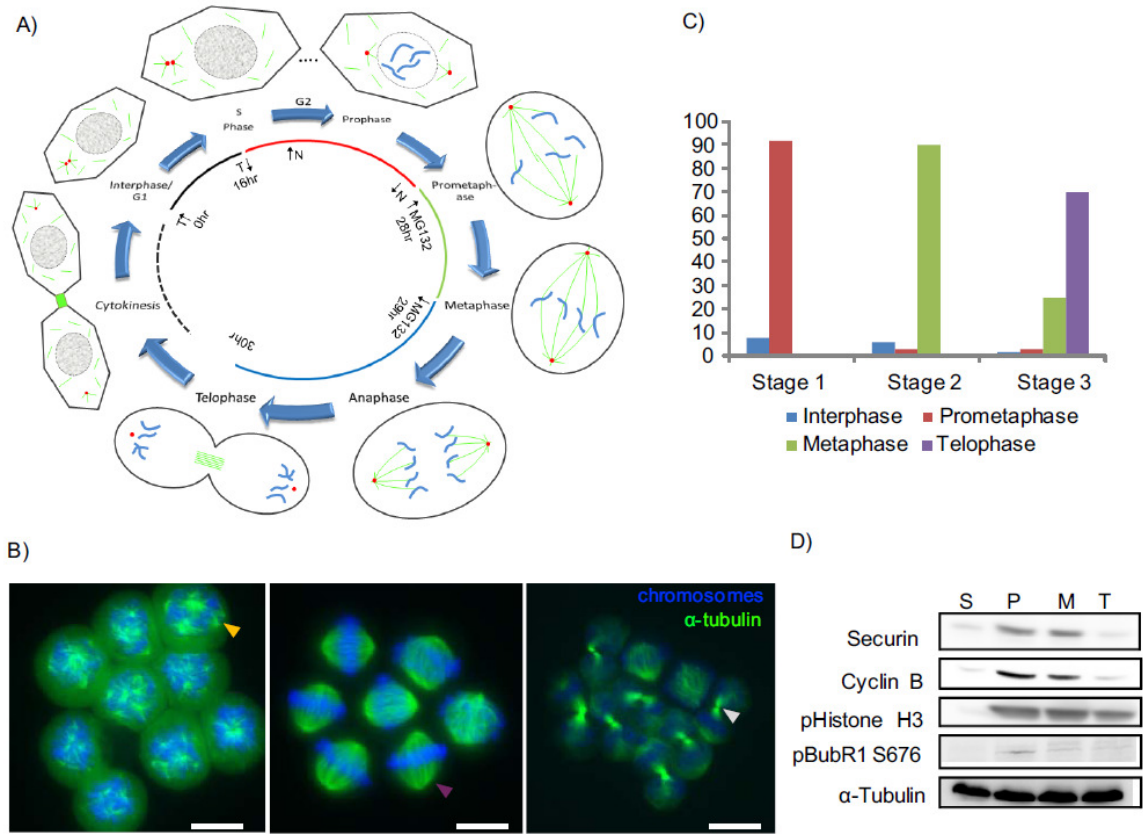


**Figure 7. Outline and quality control of the cell synchronization procedure**

A) Eukaryotic cell cycle with emphasis on mitotic stages. Centrosomes are shown as red dots, chromosomes are depicted in blue, and microtubules are displayed in green. The employed synchronization steps are indicated in the diagram with inward and outward directed arrows marking the addition and release of drugs. T and N refer to thymidine and nocodazole, respectively. B) Representative pictures from prometaphase, metaphase and anaphase cells. The yellow arrow highlights a microtubule cluster; the pink arrow marks a mitotic spindle; and the white arrow points at a midbody, scale bars represent 10  $\mu\text{m}$ . C) Synchronization efficiencies were plotted as counted from the images. D) Western blot analyses of the samples using various mitotic markers. P stands for prometaphase samples obtained from nocodazole block (Stage 1), M represents metaphase samples from a MG132 (Stage 2) block, T marks telophase (Stage 3) samples from MG132 release, and S-stands for thymidine blocked HeLa cells in S-phase. The S-phase stage is not part of the proteomics experiment but was included in the western blot analyses as a reference.

## 2.4 Identification of proteins and phosphorylation sites

The experiments carried out in biological triplicates resulting in 117 raw files with 555,444 MS/MS spectra, making data analysis computationally and technically challenging.



Analysis of SILAC data was done in a fully automated manner using the MaxQuant software suite (version 1.0.12.5)[45] in association with the MASCOT search engine [88]. To ensure the fidelity of protein and phosphorylation site identifications, the decoy database strategy was used to minimize false positive rates (FDR) [89]. Peptide sequences were assigned for one third of the MS/MS spectra at a FDR of 0.01. We used a conservative approach for calculating the number of proteins and phosphopeptides identified in our study. All the peptide isoforms (SILAC and PTM's) matching to a single sequence were counted as one and all the proteins which share common peptides were grouped into one protein group [45]. Distinguishing protein kinases from other proteins turned out to be a complex task, as multiple isoforms and splice variants are annotated for many kinases in the IPI database. Therefore, we strictly adhered to the kinase sequences provided by Manning and coworkers. (KinBase database version 08.02) [15] [90] and kinase peptides were identified by matching identified peptide sequences to kinase sequences. Later, these peptides were assembled into proteins essentially as described for the MaxQuant algorithm. The efficiency of the enrichment for kinases is demonstrated by the large number of kinase identified in this study. From the three biological replicates, 206 protein kinases could be detected of which 163 were phosphorylated (Table I). On average, each kinase was identified by 19 tryptic peptides and at least two un-phosphorylated peptides were identified for 164 kinases. For phosphopeptides with more than one S/T/Y residues, the MaxQuant's PTM scoring algorithm was used to calculate localization probabilities of phosphorylation sites for each of these residues [83]. Regarding the grouping of phosphorylation sites according to the confidence level of phosphorylation site identifications within the phosphopeptide sequences, we adapted the classification scheme of Olsen et al [57]. In total, 944 high-confidence phosphorylation sites on protein kinases were detected (class I sites), whereas 277 phosphorylation sites fell into lower confidence classes (class II and III sites). Kinase phosphopeptides accounted for 68% of the total phosphopeptide ion count, further demonstrating the efficiency of the kinase enrichment strategy. The use of SCX separation after in-solution digestion as an alternative strategy to SDS-PAGE (in combination with in-gel digestion) is beneficial, as only 34% of the total phosphorylation sites were identified by both methods, thus indicating that the two methods are highly complementary. However, we did not detect significant differences between the pools of phosphopeptides detected by the SCX and SDS-PAGE strategies in terms of peptide length and the percentage of multiply phosphorylated peptides. To compare the kinase coverage of this work with the related prior studies of Daub et al.[83] and Dephoure et al. [86], we calculated the numbers and overlaps of the detected kinase

phosphorylation sites. Compared to the Daub et al. dataset we detected about the same number of kinase phosphorylation sites, whereas about 40 % more kinase phosphorylation sites were detected compared to the study by Dephoure et al., thus justifying the use of a kinase enrichment strategy.

Total number of protein kinases (PK)		206
PK Phosphorylation sites	Class I	945
	Class II	169
	Class III	108
False-discovery rate (FDR), peptides		1.0%
Non-PK Phosphorylation sites (Class I)		1374

**Table 1. Summary of the numbers of detected kinases and phosphorylation sites.**

## 2.5 Mitotic dynamics of kinase phosphorylation sites

SILAC triple labeling along with cell synchronization techniques allowed us to compare three specific mitotic stages. Phosphorylation site ratios were normalized to protein ratios in order to eliminate variations resulting from different expression levels at the analyzed stages, unequal sample mixing and labeling efficiency of different isotopic forms of arginine and lysine [45]. If no unphosphorylated peptides were detected to calculate protein ratios (7 % of the detected kinase phosphorylation sites), global correction factors were used [45] (appendix, suppl. Data S3). In order to choose optimal thresholds for identifying regulated phosphorylation sites, we analyzed a 1 to 1 mixture of mitotic lysates (identically prepared but distinctly SILAC labeled samples) in a separate experiment. Less than 95% and 99% of the detected phosphorylation site ratios differed by more than 35% and 50%, respectively (appendix, suppl. Data S4). Based on these values, we decided to accept regulation levels above 1.5 (3/2) for upregulation and below 0.66 (2/3) for downregulation, as significant. Reproducibility of the results between the experiments was found to be high, even though the samples were biological replicates (suppl. Data S3). Less than 11 % and 19 % of the phosphorylation site ratios differed from each other by more than 35% for prometaphase-metaphase and metaphase-telophase transitions, respectively, between experiment 2 and experiment 3 for example. Of the three replicates, experiment 3 was found to be best in terms of synchronization efficiency and number of detected phosphorylation

sites (Figure 8), so results from experiment 3 are shown in all figures unless otherwise mentioned.

During the prometaphase to metaphase transition, phosphorylation site regulation exceeding the above defined threshold was found to be confined to few kinases which comprise important known regulators of the SAC such as TTK (Mps1) and Plk1 (Figure 9A, Figure 10). Notably, even though the percentage of significantly regulated phosphorylation sites did not exceed 10 %, a stronger regulation of phosphorylated peptides compared to non-phosphorylated peptides was observed (Figure 9B), thus demonstrating a small but significant regulation of the phospho-kinome between these mitotic stages. In contrast, a pronounced regulation of the phospho-kinome was observed in telophase with 17% downregulated and 8% upregulated phosphorylation sites (Figure 9C).

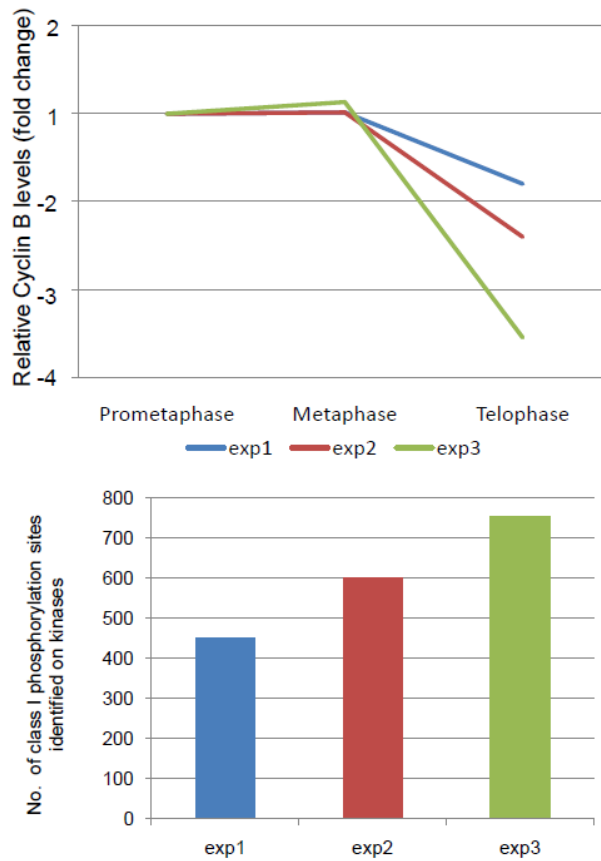


**Figure 8: Comparison of the biological replicate experiments in terms of synchronization efficiency (based on Cyclin B levels) and detected phosphorylation sites.**

A) Cyclin B levels along the analyzed mitotic stages as calculated by MaxQuant were plotted for the three experiments. The levels remained constant during prometaphase-metaphase transition whereas they dropped abruptly between metaphase and telophase, in complete agreement with Cdk1 activity. The extent of Cyclin B degradation is an indication of the synchronization efficiency in telophase. B) Number of class I kinase phosphorylation sites identified in each experiment.

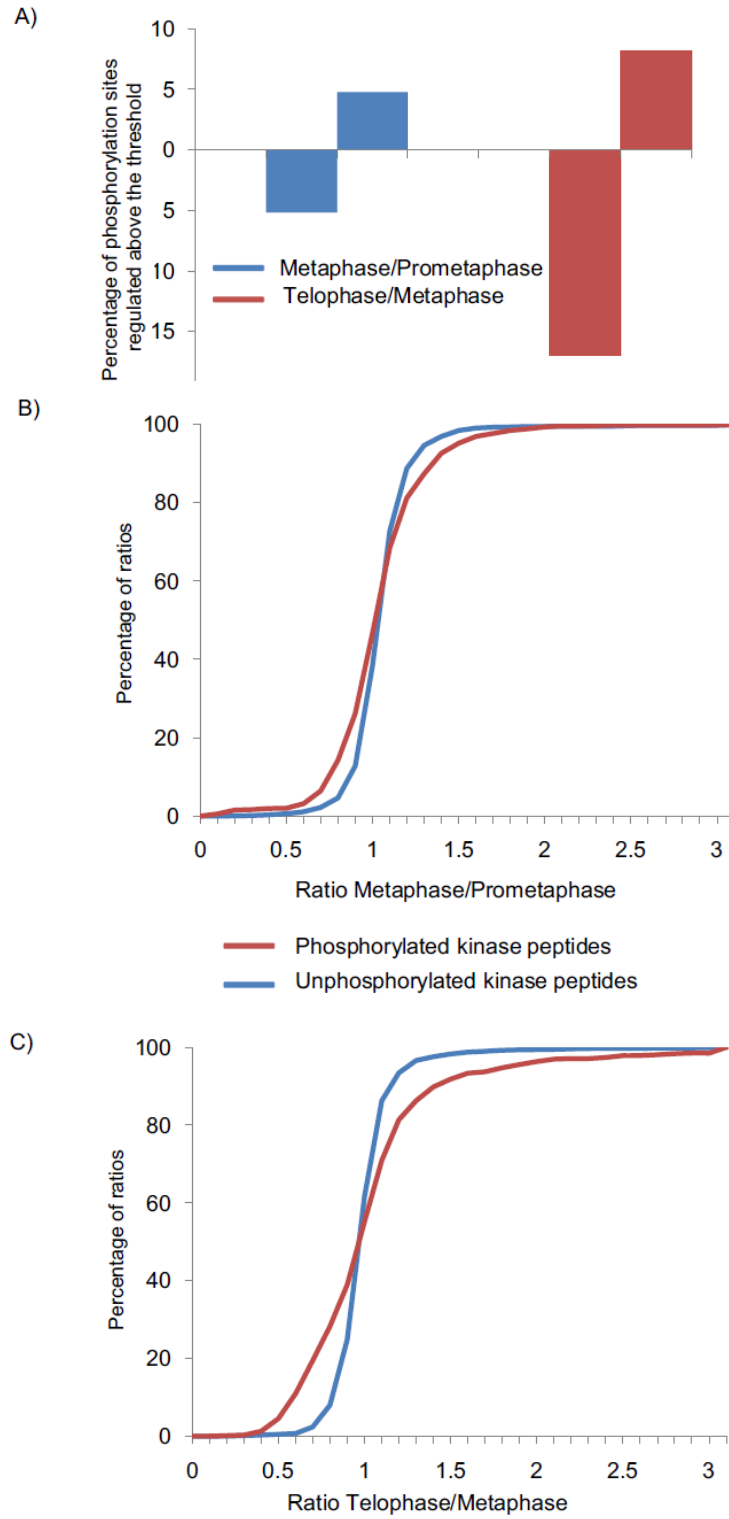


**Figure 9: Quantitative dynamics of the phosphokinome across mitosis.**

A)Percentage of class I phosphorylation sites that are upregulated (upward directed bars) above a ratio of 1.5 or downregulated below a ratio of 0.66 (downward directed bars) between metaphase and prometaphase and telophase and metaphase, respectively. Percentage of the measured ratios between metaphase and Prometaphase B), and between telophase and metaphase C) are depicted separately for phosphorylated kinase peptides (red) and unphosphorylated kinase peptides (blue).

Importantly, the identified phosphoproteins comprise key mitotic kinases, such as Cdk1, Plk1, Aurora A (AURKA), Aurora B (AURKB), and TTK (Mps1), allowing insight into their phosphorylation based regulation during mitosis (Figure 10). The activating phosphorylation site of the key mitotic kinase Cdk1, T161, for example, stayed constant in metaphase whereas the inhibitory phosphorylation site T14 continued to be dephosphorylated (Figure 10). Inactivation of Cdk1, which is required for mitotic exit, is reflected by the down regulation of the activating Cdk1 T-loop phosphorylation site T161 in the telophase sample. Plk1, another crucial mitotic kinase, contains two conserved threonines, T210 and T214, on its activation segment (Figure 10, Table II) which were both phosphorylated in mitosis. T210 has been previously described as the major activating phosphorylation site of Plk1 in mitotic HeLa cells [21] and, in agreement with the essential role of Plk1 in cytokinesis, this site remained phosphorylated throughout mitosis. In contrast, T214 was found to be dephosphorylated after silencing of the spindle checkpoint in metaphase, suggesting that this phosphorylation site may have other functions than regulating Plk1 activity. During mitosis Aurora A is localized at spindle poles and the mitotic spindle, where it regulates the functions of centrosomes and spindles and is required for proper mitotic progression [32]. Aurora A activation segment phosphorylation sites (Figure 10, Table II) as well as 4 other phosphorylation sites of this kinase continued to be phosphorylated during the prometaphase-metaphase transition, indicating that complete activation of Aurora A is not achieved until metaphase. Interestingly, the Aurora A activation segment was dephosphorylated in telophase, whereas phosphorylation of the Aurora B activation segment along with other phosphorylation sites, stayed constant in mitosis, which is in agreement with the reported role of Aurora B in cytokinesis.

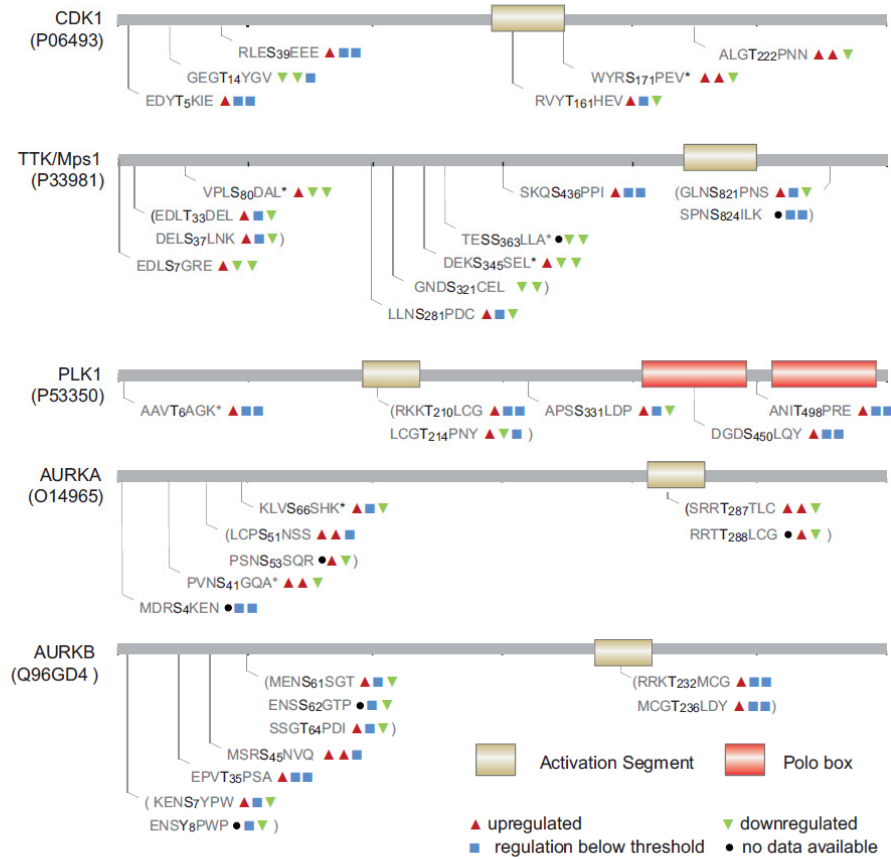


**Figure. 10: Phosphorylation dynamics of key mitotic kinases.**

The regulation of phosphorylation sites (red triangle: upregulated; green triangle: downregulated; blue square: regulation below threshold; black circle: no data available) is shown for the ratios between prometaphase and S-phase (first position, data taken from Daub et al.[83]), between metaphase and prometaphase (second position), and between telophase and metaphase. Data were taken from experiment 3 (best synchronization) if available. Phosphorylation sites marked with a star were only detected in the experiments 1 or 2.

Maternal Embryonic Leucine Zipper Kinase (Melk) inhibits pre-mRNA splicing by binding NIPP1 in a cell-cycle regulated manner. In-vitro studies have shown that phosphorylation of T460, T466 and T478 residues is critical for Melk-Nipp1 binding [91] and pre-mRNA splicing inhibition. Importantly, our in-vivo data confirm these results as the phosphorylated Melk residues are highly dephosphorylated in telophase (suppl. Data S3). Similarly, PKC delta, which was recently shown to be important for meiotic spindle formation, was found to be dephosphorylated on multiple sites in metaphase [92] (suppl. Data

S3), suggesting that these phosphorylation sites may be interesting in the context of potential mitotic roles of this kinase.

Kinase	Uniprot	Mitotic Regulation
AURKA	O14965	T287 ▲▲▼, T288 ●▲▼
AURKB	Q96GD4	T232 ▲■■■, T236 ▲■■■
CDK1	P06493	T161 ▲■▼
CDK10	Q15131	T196 ■■■■
CDK2	P24941	T160 ●■▼
CDK7	P50613	S164 ■■■■, S170 ■■■■
CDK9	P50750	S175 ●■■■, T186 ■■■■
CLK1	P49759	Y331 ■■■■, S337 ■■■■, S341 ■■■■, T342 ■■■■
CRK7	Q9NYV4	S889 ●■■■, T893 ■■■■
EphA2	P29317	Y772 ■■■■, S775 ●■■■
EphB2	P29323	S776* ▲▼■
EphB4	P54760	S769 ■▼■, S770 ●■■■, S777 ●■■■
Erk1	P27361	T202 ▼■▲, Y204 ▼■▲
Erk2	P28482	T181 ▼■▲, T185 ▼■▲, Y187 ▼■▲, T190 ●■▲
FAK	Q05397	Y570 ■■■■
FER	P16591	Y714 ▲■■■
GSK3A	P49840	S278 ■■■■, Y279 ●■■■
STK10	O94804	T185 ■■■■
MAP2K1	Q02750	S231 ▲■■■
MARK2	Q7KZ17	T208 ▲■■■, S212 ▲■■■
NEK2	P51955	S184 ▲■■■
p38a	Q16539	T180 ▼■▲, Y182 ▼■▲
PAK4	O96013	S474 ■■■■
PKACa	P17612	T196 ■■■■, T198 ●■■■
PKCa	P17252	T497 ■■■■
PKCd	Q05655	S503 ■■■■, T511 ■■■■
PKCt	Q04759	T536 ■■■■
PRKD3	O94806	S735 ■■■■
PKN1	Q16512	S773 ■■■■
PKN3	Q6P5Z2	T722 ■■■■
PLK1	P53350	T210 ▲■■■, T214 ▲▼■
PYK2	Q14289	S571 ●■■■
RIPK2	O43353	S176 ▼■■, S178 ▼■■
RSK3	Q15349	Y218 ■■■■, T225 ●■■■
SLK	Q9H2G2	T183 ■■■■, S189 ■■■■
TEC	P42680	Y519* ●▼▼
Wee1	P30291	S472* ▲▲▲



## **Table 2. Dynamics of protein kinase activation segment phosphorylation.**

The regulation of kinase activation segment phosphorylation sites (red triangle: upregulated; green triangle: downregulated; blue square: regulation below threshold; black circle: no data available) is shown for the ratios between prometaphase and S-phase (first position, data taken from Daub et al. [83]), between metaphase and prometaphase (second position), and between telophase and metaphase (third position). Data were taken from experiment 3 (best synchronization) if available. Phosphorylation sites marked with a star were only detected in experiments 1 or 2. Non-Class I sites are underlined.

## **2.6 Network analysis**

Proteins work rarely in isolation but rather function in complexes as multi-protein machines. Importantly, members of protein interaction networks are frequently regulated in a similar fashion thus enhancing the robustness of signaling events [74]. To detect regulatory networks involved in mitotic exit, we therefore asked whether phosphoproteins with similar phosphorylation dynamics in telophase were enriched for members of specific interaction networks. To this end, we extracted a group of proteins containing at least one upregulated phosphorylation site (group U, 59 proteins) and another group, with proteins containing at least one downregulated phosphorylation event (group D, 130 proteins). Importantly, the overlap between the groups was modest (22 proteins), illustrating the specificity of the applied approach. To gain further insight into underlying mitotic phosphorylation networks, interaction network analyses were performed separately for the upregulated and downregulated groups and the results were visualized (appendix, Figure S1, S2). Strikingly, a Cdk1 interaction network was found enriched in group D (Figure 11A), which is in agreement with the de-activation of Cdk1 in late mitosis [93]. To compensate for the unequal number of proteins in each group, average numbers of interactors were computed (number of interactions in a particular group of proteins / total number of proteins in that group). 2.5 fold more Cdk1 interactors were found in D compared to U and 9 fold more, compared to a randomly chosen set of proteins (Figure 11B). Along similar lines, we observed that 54% of the phosphorylation sites matching a stringent Cdk1 motif ((S/T)PXR) were downregulated (suppl. Data S3), compared to the 17% of sites in the total dataset. This demonstrates that

although the overall number of downregulated phosphorylation sites is relatively small, a large number of Cdk1 phosphorylation sites are downregulated nevertheless.

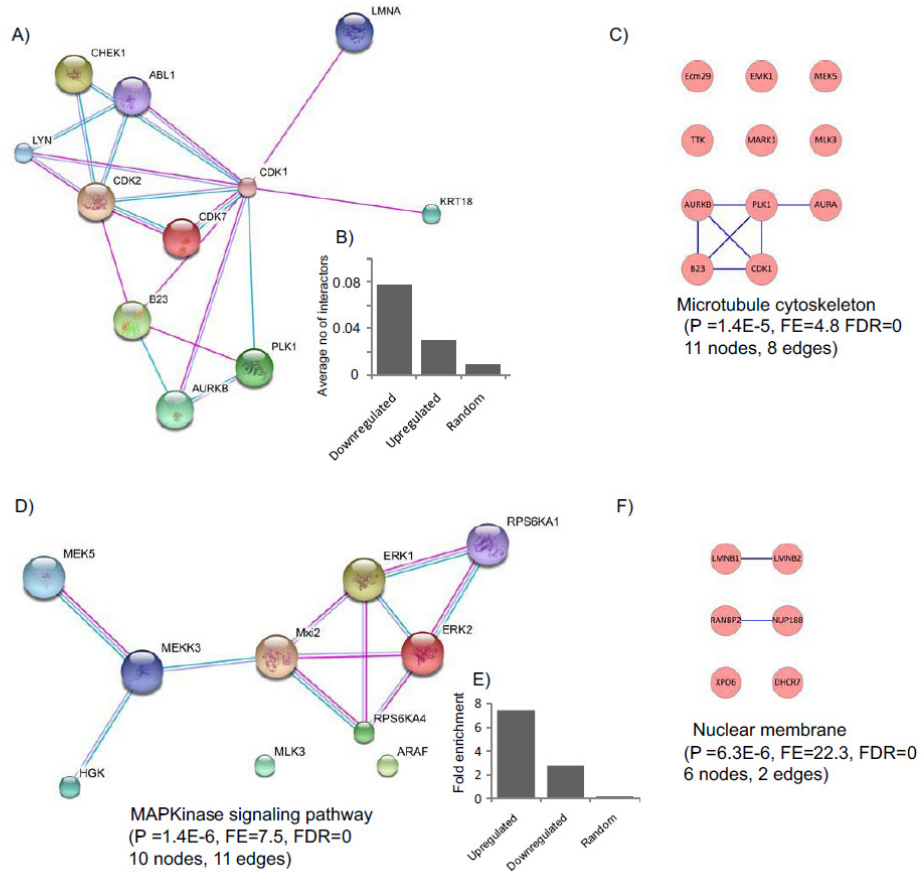


**Figure 11: Interaction networks and enriched functional annotations.**

A) Selected part of an interaction network extracted from a group of proteins with downregulated phosphorylation sites centered on Cdk1; the insert B) shows the enrichment of Cdk1 interactors in the complete interaction network of proteins with downregulated phosphorylation sites (Fig. S5), compared to protein with upregulated phosphorylation sites (Fig. S6), and a random group from the Uniprot dataset. C) Highlights that the functional annotation term “microtubule skeleton” is enriched in this network. D) Selected part of an interaction network extracted from a group of proteins with upregulated phosphorylation sites in telophase, containing many MAP kinases. The insert E) shows the enrichment of MAPK interactors in the complete interaction network of proteins with upregulated phosphorylation sites (Fig. S6), compared to protein with downregulated phosphorylation sites (Fig. S5), and a random group from the Uniprot dataset. The enrichment of the functional annotation “nuclear membrane” in this network is shown in F).

Regarding the group of proteins containing up-regulated phosphorylation sites, MAPK signaling pathway was found to be highly enriched (7.5 folds, p-value 1.4E-6) (Figure 11D). Further, we analyzed the functional annotations of proteins in the D- and U-groups. As may be expected, 'protein kinase' and 'cell cycle' were highly enriched terms in both the groups. Apart from these, the term 'microtubule cytoskeleton' was enriched 4.8 fold (p-value 1.4E-5) in D (Figure 11C). Interestingly, the enrichment of the term 'nuclear membrane part' in U (22.3 folds, P 6.3E-6) (Figure 11F) suggests that phosphorylation may also have a role in nuclear envelope reformation.

In summary, network analysis of sub-groups of proteins with similar phosphorylation dynamics identifies mitotic interaction networks of proteins and is therefore useful for the detection of the pathways targeted by phosphorylation-based signaling.

## **2.7 MAPK pathways are activated during late mitosis**

Although mitotic exit is thought to be mostly driven by dephosphorylation events, some kinases were nevertheless found to be phosphorylated in telophase. As shown above, functional annotation revealed that most of these kinases either belong to the MAPK family or represent components of MAPK pathways (Figure 11D). MAPKs have been studied extensively due to their strong association with many important cellular processes such as cell proliferation, survival, growth and differentiation [94]. As part of key signaling pathways MAPKs are activated in response to various mitogenic signals and stress factors. The role of MAPKs during the G1/S transition is relatively well understood but their function in mitotic progression has been discussed controversially. Initial studies suggested that Erk1 and Erk2 localize to centrosomes and kinetochores and that their activities are required for proper spindle formation and timely metaphase-anaphase transition in mouse fibroblast like 3T3 cells [95]. These finding, however, could not be confirmed by a successive study in normal and transformed human cells [96]. Another member of the MAP kinase family, p38 was observed to localize to centrosomes during HeLa cell mitosis [34] [97] and to be required for the metaphase-anaphase transition in developing retina [98]. However a subsequent study demonstrated that the timing of the metaphase-anaphase transition was not affected in absence of p38 activity [99]. Even though these conflicting results may be partially explained by the use of different model systems and experimental techniques, further elucidation of the

role of MAPK during mitotic progression is clearly needed. Since our study tracked the phosphorylation of kinases during mitosis through a kinome approach, a wide range of MAPK could be analyzed simultaneously (Figure 12A). We found that the MAP kinases Erk1/2 and p38 were phosphorylated on their activation segments and that the relative abundances of these phosphorylation sites peak during late mitosis (telophase). Importantly, these results were found consistently in all three biological replicates (appendix, suppl. Data S3) and were further confirmed using a phosphospecific antibody against the pTXpY motif of p38 and Erk1/2 with additional time points in mitosis (Figure 12B). MG132 treatment of cells is known to activate programmed cell death response that is initiated by Jnk activation, and p38 alpha is one of the prototypical stress-activated kinases. To address the concern that the observed pathway activation was related to drug related side effects, we released cells directly from nocadazole and still observed phosphorylation on p38 and Erk1/2, thus ruling out MG132 treatment as the primary cause of phosphorylation. To rule out nocadazole as the cause of phosphorylation we kept one batch of cells in nocadazole while another batch of cells was released from this drug. We observed phosphorylation on p38 as well as Erk1/2 only in the cells that were released into telophase.

Taken together, we speculate that the detected upregulation of phosphorylation sites on a MAPK interaction network during late mitosis indicates a role of these kinases in late mitotic events, a view which is consistent with a recent report showing that phosphorylation of PKC $\epsilon$  by p38 is required for cytokinesis [26].

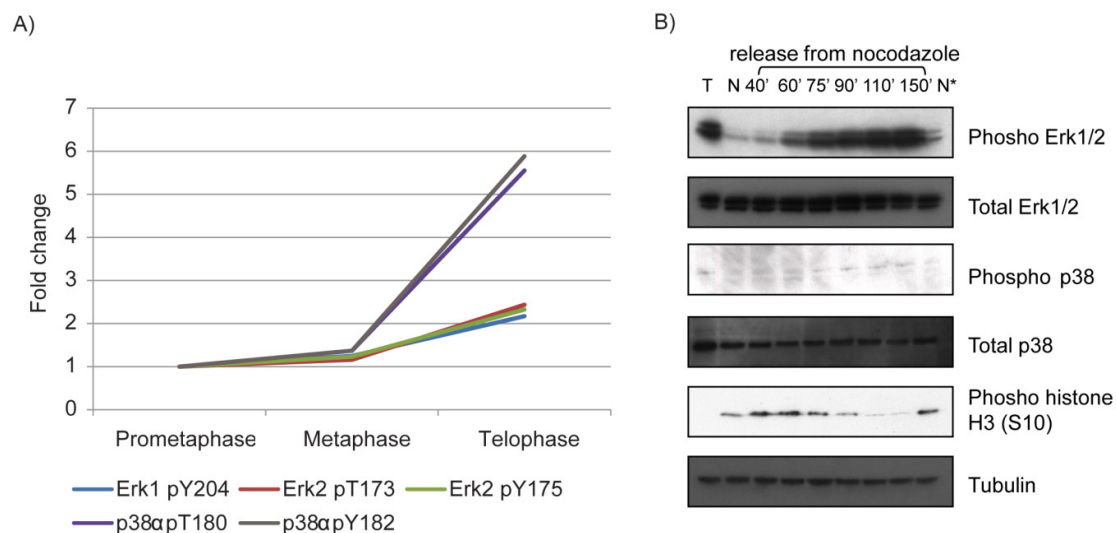


## **Figure 12: Activation segment phosphorylation of MAP kinases in mitosis.**

A) Dynamics of activation segment phosphorylation of different MAP kinases identified in the study.  
B) Western blots depicting the activation segment phosphorylation of p38 & Erk1/2 MAP kinases. T- stands for thymidine blocked HeLa cells in S-phase. N- represents prometaphase sample obtained from nocodazole block. Upon release from nocodazole cells are harvested at 6 different time points. N\* represents the sample for which the nocodazole block was continued for 150 minutes after the initial nocodazole block. Phosphorylation on p38 and Erk1/2 is observed only in the cells that were released into telophase.

## **2.8 Changes made during mitotic entry are restored at the end of mitosis**

Whereas the current study was focused on the dynamics of the phospho-kinome during different phases of mitotic progression, a previous study has quantitatively analyzed the phosphorylation of the kinome during S-phase and prometaphase [83]. Since one common time point (nocodazole block in prometaphase) was used in both experiments, it became possible to combine the results of the two studies to broaden the monitored time window and to analyze the correlation between the observed phospho-kinome dynamics (Figure 13).

Interestingly, phosphorylation sites which were found to be upregulated between S-phase and prometaphase were significantly more downregulated between prometaphase and telophase than phosphorylation sites that either stayed constant during the prometaphase/S-phase transition or were downregulated (Figure 13). This correlation is reminiscent of the cycling behavior of Cdk activities which drive the “cell cycle oscillator” [93; 100]. According to the current perception of mitosis, Cdk1 activity initiates mitosis and mitotic exit requires Cdk1 inactivation, thus restoring the initial state [101]. In line with this view, the observed correlation between upregulation during mitotic entry and downregulation at mitotic exit (and vice versa) can also be interpreted as a partial reconstitution of a “non-mitotic” phosphokinome state towards the end of mitosis.

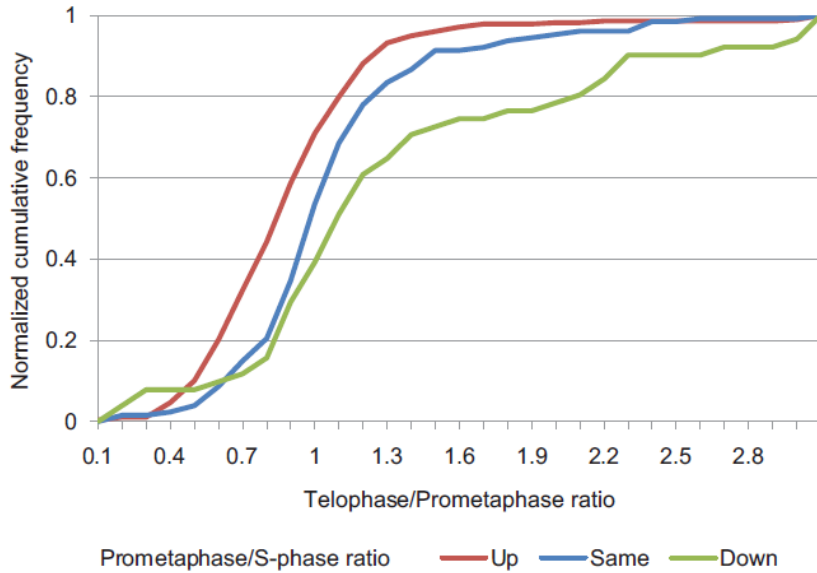


**Figure 13: Correlation between kinase phosphorylation site regulation at mitotic entry and mitotic exit.**

The proportions of the Class I kinase phosphorylation sites which were found upregulated (red), not significantly changed (blue) or downregulated (green) between S-phase and prometaphase (the ratios were taken from Daub et al.(35)) in relation to their regulation in telophase are shown.

## 2.9 Regulation of non-kinases in mitosis

Even though a strong enrichment for kinases could be achieved through our experimental strategy (see above), other ‘contaminating’ proteins were also detected. These ‘non-kinases’ may form stable complexes with kinases, as may be the case for the detected Cyclins, or bind to the kinase affinity columns through undesired selectivities [102]. Thus, a total of 1730 phosphorylation sites (Table I), including 1374 class-I sites could be identified on these proteins in addition to the above discussed kinase phosphorylation sites (suppl. Data S3) Although the detection of these other phosphorylation sites was not the purpose of this study, closer analysis revealed that key mitotic proteins were also covered, thus providing additional information on the regulation of mitotic progression dynamics. For instance, we identified more than 12 phosphorylation sites on Borealin, an important component of the Chromosomal Passenger Complex (CPC). Out of those, three of the conserved pTP sites, located close to the Borealin C-terminus, were consistently downregulated in telophase in all three replicates. During the metaphase to anaphase transition the CPC moves from

centromeres to the spindle midzone, which can be inhibited by constitutively active Cdk1 [103]. Moreover, the C-terminus of Borealin was already previously shown to be important for CPC targeting to centromeres [104]. It is therefore conceivable, that the three downregulated phosphorylation sites at the C-terminus of Borealin may play a role in targeting the CPC to centromeres, so these sites may constitute attractive targets for future mutational analyses. Another detected phosphorylation substrate, Protein Regulator of Cytokinesis (Prc1), is a key protein required for cytokinesis and was found to be phosphorylated on 12 sites during mitosis. Previously, it was already reported that Plk1 phosphorylates Prc1 at the two sites T578 and T602, thus promoting the interaction of Prc1 with several kinesin motor proteins required for cytokinesis [105]. Interestingly, both these reported sites were identified in our study. Since the T602 containing peptide covers the C-terminus of Prc1 and does not contain the SILAC labeled amino acids Lysine and Arginine, this peptide could unfortunately not be quantified. The peptide spanning the other reported phosphorylation site, T578, however, was found to be upregulated once all chromosomes were captured by microtubules (ratio 1.45 metaphase/prometaphase). Interestingly, also the protein level of PCR1 varied during mitosis, peaking in metaphase and decreasing again in telophase (ratios in experiments 1, 2 and 3: 1.3, 1.63, 1.88 metaphase/prometaphase; 1.22, 0.62, 0.67 telophase/metaphase). As previous studies had suggested that the level of Prc1 remains constant throughout mitosis [105], we speculate that the Prc1 level is maintained by an equilibrium between synthesis and degradation, so that MG132 mediated proteasome inhibition as used in this study, would result in elevated protein levels. It is also interesting in this context that, cap-independent protein translation during mitosis was shown to be important for recruiting Plk1 to the central spindle [106]. Since Prc1 plays a crucial role in targeting Plk1 to the central spindle, it may be rewarding to test whether Prc1 is translated through a cap-independent mechanism during mitosis.

In addition to the identification of potentially important regulatory phosphorylation sites, the detection of “non-kinase” proteins also allowed us to further evaluate synchronization efficiencies. The protein level of Cyclin B, the regulatory subunit of Cdk1, stayed constant between prometaphase and metaphase whereas it was found to drop significantly in telophase, a finding which is in agreement with western blot data (Figure 14A) and the dynamics of mitotic Cdk1 activity. In particular, Cyclin B levels were found reduced by more than 3 fold, thus indicating that the synchronization efficiency of telophase cells exceeded 70 %. Further, the levels of  $\alpha$ -Tubulin, a commonly used loading control for

mitotic samples, remained almost constant throughout mitosis (ratios in experiments 1, 2 and 3: 0.98, 0.98, 1.07 metaphase/prometaphase; 0.92, 1.00, 1.00 telophase/metaphase) (Figure 14B), highlighting the accuracy of SILAC based quantitation and downstream data analysis steps.

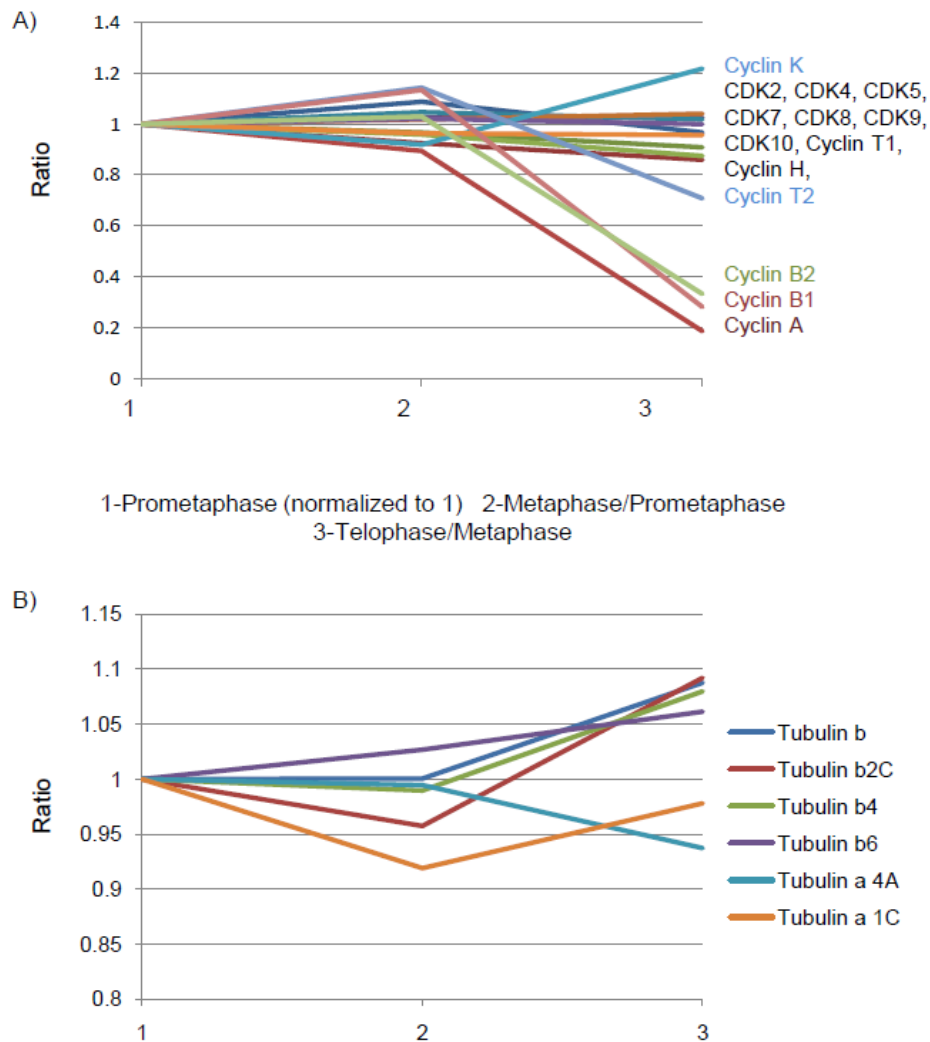


**Figure 14:** Regulation of (A) Cdk's and Cyclin's and (B) Tubulins during mitotic progression were plotted for the three experiments. Except for Cyclin A, Cyclin B1, and Cyclin B2, levels of other Cyclins and Cdk's remained almost constant throughout mitosis. Tubulin levels stayed very close to 1 indicating the analytical accuracy the SILAC based quantitation.



Having demonstrated the value of a comprehensive phosphoproteomic approach for studying the regulation of mitotic progression in part 1 of this thesis, in the following part 2 I will describe my contribution to a collaborative study that focuses on the function of two key components of the mitotic spindle assembly check point, BubR1 and Bub1

### **3.0 Results (Part 2): Characterization of function of BubR1 and Bub1 kinase phosphorylation\***

*\*Part of this work is included in a manuscript that has been accepted for publication: Uncoupling of BubR1 Spindle Checkpoint and Chromosome Congression Functions. Sabine Elowe, Kalyan Dulla, Zhen Dou, Xiuling Li, Erich A. Nigg. *Journal of Cell Science* 123 (2010) 84-94.*

I emphasize that the work presented in this chapter was done in collaboration with Dr. Sabine Elowe (MPIB). The experiments described in 3.3 and 3.4 were performed by Dr. Elowe as well as generation of the Bub1 WT and KD constructs (in 3.6). The results are shown here in order to confer biological relevance to the proteomics analysis that was carried out by me.

### **3.1 Introduction**

Budding uninhibited by benzimidazole 1 homolog beta (BubR1) protein, also known as mitotic-arrest deficient (Mad) 3 in yeast, derived its name from the loss of function study in which it was first identified [107]. Benzimidazole compounds such as nocodazole act as spindle poisons by destabilizing microtubule structures. Contrary to wild type cells, cells depleted of BubR1 fail to arrest in mitosis (metaphase) in presence of spindle poisons, leading to severe chromosomal defects. As described in (section 1.2.1), BubR1 is an essential component of the MCC, which is an integral part of the SAC that monitors spindle defects [2]. In yeast, the SAC is a non essential pathway which becomes important only in presence of spindle poisons or spindle defects. However, in metazoans, components of the SAC such as BubR1 are essential proteins, implying they have additional functions apart from SAC [108]. BubR1 is classified as a protein kinase due to its sequence homology, though substrates are not yet identified *in-vivo* and there is also no evidence for its kinase activity in *in-vitro* kinase assays. It was recently shown by our group that phosphorylation of BubR1 by Plk1 is required for stable kinetochore-microtubule attachments [87; 109]. Nevertheless, Plk1 phosphorylation cannot alone account for the congression defects observed in BubR1-depleted cells [110]. Indeed, in addition to Plk1, Cdk1 is able to efficiently phosphorylate BubR1 *in-vitro* [87]. We therefore sought to identify novel phosphorylation sites on BubR1 that are specifically upregulated in mitosis and studied their functional significance. In addition, we also sought to study a closely related kinase, budding uninhibited by benzimidazole 1 (Bub1), which is also an essential component of SAC signaling. Bub1 is highly phosphorylated in mitosis and localizes to kinetochores. It phosphorylates Cdc20, which regulates the binding of Cdc20 to MCC and thus the activity of the APC/C (see

section 1.2.2) [111]. Similarly, there is also evidence for the involvement of Bub1 in other mitotic functions, though its precise role is poorly understood [2]. Like other kinases, Bub1 is also thought to be regulated by phosphorylation, hence information about the phosphorylation dynamics of Bub1 may provide valuable insight for functional studies.

### **3.2 Identification of BubR1 phosphorylation sites in mitosis**

BubR1 is a low abundant protein, making its identification difficult without prior enrichment. To identify the BubR1 phosphorylation sites that are specifically regulated in mitosis we combined HeLa cell synchronization, antibody based BubR1 purification and SILAC quantitation. We performed two SILAC double labeling experiments (Figure 15). First, we compared phosphorylation and protein levels of BubR1 between S-phase and prometaphase. In a second experiment, comparison is made between prometaphase and metaphase (i.e. SAC active versus SAC inactive) (data not shown). Initial results showed that a large abundance of non-phosphorylated peptides masked the phosphorylated peptides, suggesting the need for a prior phosphopeptide enrichment step. Upon TiO<sub>2</sub> based phosphopeptide enrichment we were able to identify 12 phosphorylation sites (Figure 16a). This is a significant improvement compared to our whole kinome study where only two phosphorylation sites were identified on BubR1 (see part1) justifying the use of a small scale targeted approach. Out of many phosphorylation sites that were identified on BubR1, phospho-Serine-Proline (SP) motifs (S543, S574, S670, S720, and S1043) were of particular interest, as SP motifs are preferentially phosphorylated by Cdk1, the “master-kinase” of mitotic progression (Figure 16b). Using the SILAC approach, we were able to quantify the extent of mitosis-specific phosphorylation at 4 of these sites, and showed that phosphorylation is upregulated in the nocodazole arrested sample (Figure 17a). S574 was identified in a non-tryptic peptide; as it contained neither arginine nor lysine it could not be directly quantified by the SILAC procedure used here. Independently, Huang *et al.* recently reported the identification of S543, S670, and S1043 as mitosis specific phosphorylation sites on BubR1 [112], but S720 and S574 represent novel sites.

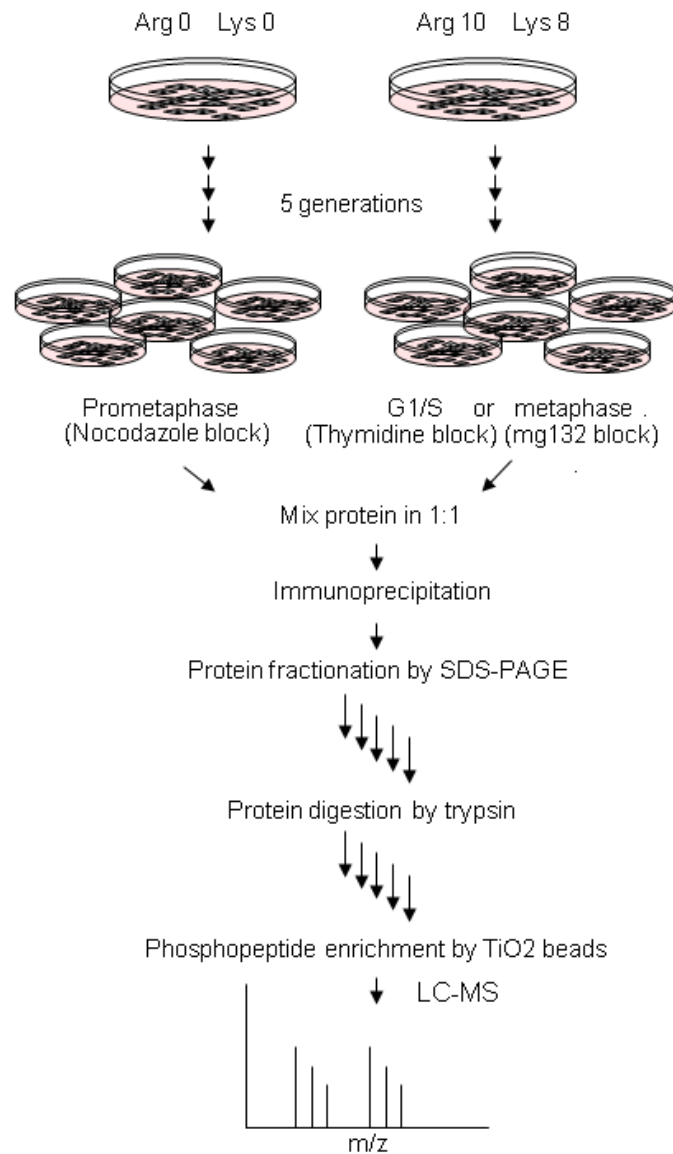


**Figure 15: Schematic representation of the SILAC double labeling procedure**

Two populations of HeLa cells were grown in parallel in different SILAC media under identical conditions. One population of cells was snap frozen after 16 hour of thymidine block where as the second population of cells was washed and released into nocodazole containing media for 12 hours and then snap frozen. In the second experiment i.e. prometaphase vs metaphase, cells were blocked in nocodazole and mg132 respectively. Cells were lysed, mixed in a one to one ratio, and BubR1 pulled down using an anti-BubR1 antibody. BubR1 (along with its interacting partners) was eluted from the antibody, separated on SDS-PAGE and analyzed by MS following trypsin digestion and phosphopeptide enrichment.

A)

Peptide Sequence	Phosphorylation site	Mascot Score	Ratio (M/S)
EGGALSEAMpSLEGDEWELSK	S16	61	3
YISWTEQNYYPQGGK	-	9	-
ESNMpSTLLER	S99	21	-
LQpSQHR	S191	25	5
EAELLp(TS)AEKR	T434 or S435	41	150
pSPPADPPR	S543	37	14
TSESITSNEDVSPDVCDEFTGIEPLESD AII TGFR	-	21	0.5
DLPpSDPER	S633	20	3
KLpSPIIEDSR	S670	62	10
LSPIIEDpSR	S676	35	300
EATHSSGFGSSASVASTSSIK	-	15	7
LELTNETSENPTQpSPWCSQYR	S720	58	24
AEIVHGDLpSPR	S884	51	85
VQLDVFpTLGFR	T926	45	16
VGKLTpSPGALLFQ-	S1043	21	54

B)

S543	KKNKSPADP
S574	NEDVSPDVCD
S670	IKKLSPIEED
S720	NPTQSPWCSQ
S1043	GKLTSPGALL

**Figure 16: List of BubR1 phosphorylation sites identified by mass spectrometry.**

A) The peptides identified in the study are listed along with the position of the phosphorylation site (phosphorylated serine, threonine and tyrosine residues are shown as pS, pT and pY), MASCOT score and the ratio between M-phase and S-phase. In cases where the position of the phosphorylation cannot be determined confidently, only the phosphopeptide sequence is shown. B) Sequence alignment of the five phosphorylation sites which are chosen for further study, indicating the common SP motif between these sites in BubR1.

### 3.3 Cdk1 phosphorylates S543, S670, and S1043 *in-vitro*

To test whether the phosphorylation sites identified here contribute to the characteristic electrophoretic upshift of mitotic BubR1, MYC-tagged constructs for BubR1-WT, -620A (Polo-box domain binding mutant), -5A, and the phospho-mimicking 5D (where all five phosphorylation sites were mutated to aspartate) were expressed in HeLa cells. The S620A mutant was included in this analysis, as we have previously shown that Plk1 phosphorylation regulates the characteristic mitotic upshift in BubR1 [87]. Cells were then harvested after a 16 h release from thymidine arrest into nocodazole, before proteins were analyzed by Western blotting. BubR1-WT exhibited the characteristic double band pattern, whereas BubR1-620A, as predicted, migrated as a single faster migrating species (Figure 17a). Both BubR1-5A and BubR1-5D also exhibited a double band pattern, suggesting that mutation of these 5 residues is not sufficient to eliminate the mitotic BubR1 upshift (Figure 17a).

Interestingly, the 5 sites described here comprise a serine followed by a proline residue, suggesting that a proline-directed kinase such as Cdk1 may phosphorylate these sites, although phosphorylation at several of these has been suggested to be Mps1-dependent [112]. To compare BubR1 phosphorylation by Cdk1 and Mps1, we performed *in-vitro* kinase assays using recombinant full-length BubR1 as a substrate. Whereas Cdk1 was able to efficiently phosphorylate BubR1, there was no detectable phosphorylation on BubR1 by Mps1 kinase representing the same specific activity (Figure 17b), although both Cdk1 and Mps1 efficiently phosphorylated Borealin under the same conditions (Figure 17b). To clarify whether the SP sites identified here are indeed Cdk1 target sites, we generated 12mer peptides centered on each of the 5 serines and used these peptides as *in-vitro* substrates for Cdk1. Corresponding control peptides were synthesized with the serine phospho-acceptor positions changed to alanine to determine signal specificity. The peptides comprising S543, S670, and S1043 became phosphorylated in this assay, whereas the alanine versions of the same peptides were either not detectably phosphorylated or phosphorylated to a significantly reduced extent (Figure 17c). Collectively, these observations suggest that Cdk1 may directly phosphorylate BubR1 *in-vivo*, and that the loss of BubR1 phosphorylation upon Mps1 depletion may reflect an indirect mechanism.

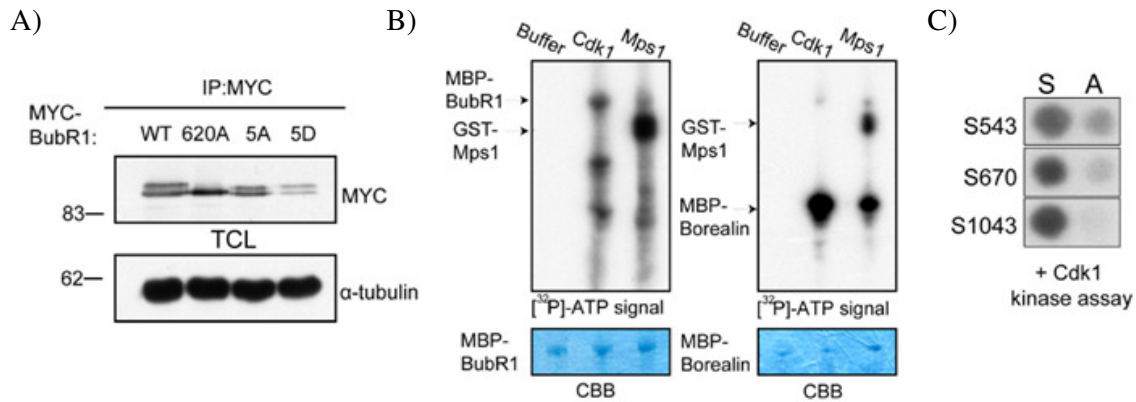


**Figure 17: Cdk1 phosphorylates BubR1 in-vitro on S543, S670, and S1043:**

A) Western blot showing the electrophoretic mobility of MYC-tagged BubR1-WT and the phosphosite mutants BubR1-620A, -5A, and -5D (upper panel). Alpha-tubulin is shown as loading control (lower panel). B) In vitro phosphorylation of recombinant MBP-BubR1 (left panels) or MBP-Borealin (right panels) in either kinase buffer alone, or by Cdk1 or Mps1. BubR1 and Borealin input is illustrated by Coomassie brilliant blue (CBB) staining (lower panels). C) Immobilized peptides synthesized directly on cellulose membranes were used as substrates for Cdk1 in *in-vitro* kinase assays. Peptide phosphorylation was visualized by autoradiography.

### 3.4 BubR1-5A mutant expressing cells exhibit severe congression defects

Initially we sought to determine whether loss of BubR1 phosphorylation at the SP sites identified here results in changes to BubR1 localization or in gross structural defects in the protein. Endogenous BubR1 was depleted using siRNA oligos that target the 3'-UTR region of BubR1 [87], and cells were simultaneously transfected with MYC-tagged BubR1 WT or phosphorylation site mutants. MYC-BubR1 WT localized as expected to the outer-KT, as demonstrated by co-localization with Hec1, as did MYC-BubR1 620A, 5A and 5D (data not shown). In addition BubR1-5A and 5D retained the ability to co-immuno-precipitate Cdc20 and Bub3 (data not shown), confirming that MCC assembly is maintained. These results demonstrate that mutation of the 5 phosphorylation sites on BubR1 did not result in gross conformation or structural defects in the BubR1 protein that would preclude kinetochore localization and MCC formation.

To explore whether the phosphorylation of the 5 identified SP sites on BubR1 contributes to the congression or checkpoint function of BubR1 (or both), we took several independent approaches. Initially, we examined mitotic progression by staining of fixed cells (Figure 18a). After MG132 treatment, BubR1-620A, -5A, and -5D-expressing cells were all

unable to align proper metaphases to the same extent as BubR1-WT expressing cells (Figure 18b). This indicates that lack of phosphorylation on one or several of the 5 sites identified in this study causes congression defects, and that the BubR1-5D phospho-mimicking mutant cannot rescue the BubR1 depletion phenotype. A BubR1-4A/D mutant (which retained the previously described S670) also exhibited aberrant metaphases after MG132 treatment, arguing for a significant contribution from the remaining 4 serine residues to the chromosome alignment function of BubR1.

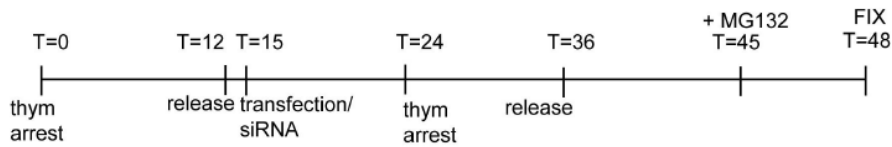
Close examination of cells expressing the various mutants revealed differences with regard to their precise congression defects (Figure 18c). As expected, cells depleted of endogenous BubR1 and rescued with the empty plasmid failed to congress chromosomes efficiently, so that KT's were spread along the length of the pole-to-pole axis (Figure 18c). In contrast, cells expressing BubR1-WT generally formed tight metaphase plates, with KT's efficiently aligned at the spindle equator. Cells expressing BubR1-620A were largely able to align their KT's, although resulting metaphases were considerably broader, whereas both BubR1-5A and -5D expressing cells resembled those depleted of endogenous BubR1, with many KT's remaining unattached and spread along the entire pole-to-pole axis. Quantification of KT misalignment observed with the various BubR1 mutants revealed that the degree of misalignment in cells expressing either BubR1-5A or BubR1-5D was almost as severe as in cells entirely depleted of BubR1 (25% in BubR1-5A and 22% in BubR1-5D compared to 30% of cells transfected with vector control (Figure 18c). These observations suggest that these 5 phosphorylation sites likely make the most significant contribution to the congression function of BubR1. As a second, complementary approach, we examined the function of BubR1 phosphorylation site mutants in real-time by time-lapse video microscopy performed on HeLa cells stably expressing histone H2B-GFP. To track individual cells, we used BubR1 constructs tagged with mCherry, as previously described [87]. Representative stills from each movie, taken at the indicated time points after the onset of chromosome condensation, and quantification of time in mitosis is summarized in Figure 4d. Cells depleted of endogenous BubR1 and expressing the mCherry tag alone exited mitosis very rapidly (90% of the cells within 60 min), without metaphase alignment and often with lagging chromosomes, as expected. This phenotype was rescued by BubR1-WT expression. As previously described, BubR1-620A expressing cells exited mitosis more slowly, with approximately 40% of the cells entering anaphase more than 140 min after chromosome condensation, compared to about 25% of BubR1-WT expressing cells. Cells expressing BubR1-5A or BubR1-5D displayed severe congression defects; they were often unable to reach metaphase and many



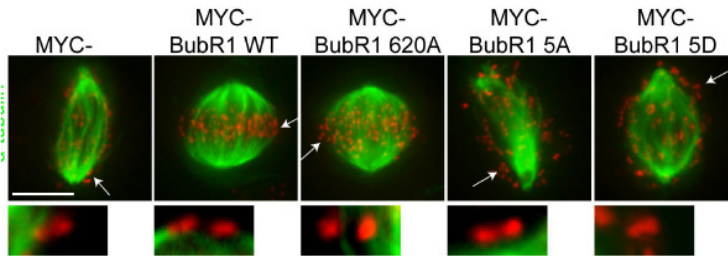
cells were unable to exit mitosis within the imaging period (16 h). As a result, only 25% of BubR1-5A and 42% of BubR1-5D expressing cells reached anaphase within 140 min. Interestingly, amongst the cells expressing BubR1-5A and BubR1-5D that were able to exit mitosis, we were unable to detect any lagging chromosomes in anaphase. This, together with the observation that the many cells unable to align at metaphase did not exit mitosis, suggests that the checkpoint function of BubR1 is maintained in the BubR1-5A mutant.

To more rigorously test this conclusion, we assessed the ability of cells expressing either MYC-BubR1 WT or BubR1 phosphosite mutants to remain mitotically arrested upon microtubule depolymerization. Non-rescued cells were unable to arrest in the presence of nocodazole, whereas cells rescued with BubR1-WT arrested efficiently (Figure 18e). Similarly, cells expressing MYC-BubR1-620A, -5A or -5D all arrested to the same extent as BubR1-WT expressing cells, indicating that the SAC function of BubR1 is functional in these cells. Collectively, our observations indicate that phosphorylation at the 5 sites described here is critical for BubR1 function in KT-MT attachment and chromosome congression, but is not required for mediating the SAC response in either an unperturbed mitosis or after a nocodazole challenge.

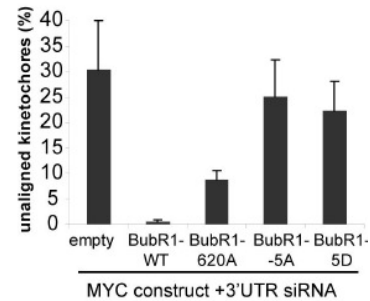
A)



B)



C)



D)

E)

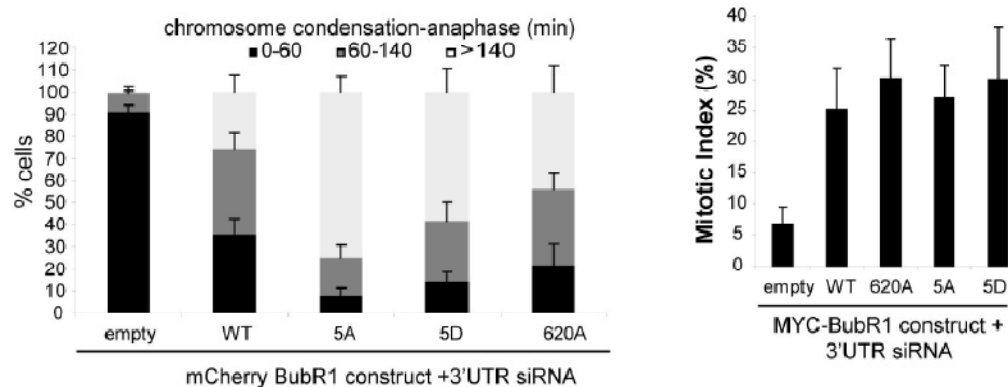


**Figure 18: BubR1-5A mutants cause severe congression defects but retain SAC function.**

(A) Schematic representation of BubR1 rescue protocol for testing mitotic progression and chromosome alignment. B) Representative images of metaphase cells expressing the various BubR1 phosphomutants after 3 h MG132 treatment. Cells were co-stained for alpha-tubulin (Cy2, shown in green), CREST human autoimmune serum (Cy5, shown here in red), and MYC (Cy3, shown in red) to facilitate identification of rescued cells. Representative KT-MT connections (white arrows) were enlarged and are shown below each image. Scale bar represents 10 $\mu$ m. C) Quantitation of the degree of chromosome misalignment in cells expressing BubR1 mutants in (B). KT position was measured as a function of the distance from pole-spindle equator. Bars represent the mean  $\pm$  SE of 5-6 cells, > 60 KTs per cell. E) Bar graph indicating time elapsed between chromosome condensation and anaphase onset. Elapsed time was split into three categories: 0-60 min, 60-140 min, and >140 min, and the percentage of cells fitting into each category was calculated for cells expressing each of the different MYC-BubR1 constructs. Bars are represent the mean  $\pm$  SE of 8 independent experiments (n=100-220 cells). F) Bar graph showing mitotic index (after 14 h nocodazole treatment) in cells depleted of endogenous BubR1, and expressing BubR1 phosphorylation site mutants relative to BubR1-WT expressing cells. Bars indicate mean  $\pm$  SE of 3 independent experiments (160-250 cells per experiment). The mitotic index of non-treated cell analyzed under the same conditions was 27%.

### 3.5 Bub1 phosphorylation in mitosis

With the encouraging results from the functional studies of BubR1 phosphorylation we next sought to also study phospho-regulation of Bub1 kinase. Little is known about the function of Bub1 mitotic phosphorylation. From the whole kinome study we identified four phosphorylation sites on Bub1 (Figure 19). Furthermore, a few additional sites were also reported on Bub1 in the Uniprot database.

Modified Sequence	Phosphorylated Residue	Mascot Score	Ratio (Meta/Prometa)
MGPSVGpSQQLR	S331	25	0.3
VQPSPTVHTK	-	14	1
TLAPSpPK	T593	10	1
SpPGDFTSAAQLASTPFHK	S596	28	0.8
DGKFSpPIQEK	S655	35	1

**Figure 19: Bub1 *in-vivo* phosphorylation sites identified in whole kinome study.**

The Bub1 phosphopeptides identified in the whole kinome study are listed along with the position of the phosphorylation site (phosphorylated serine, threonine and tyrosine residues are shown as pS, pT and pY), MASCOT score and the ratio between metaphase and prometaphase. In cases where the position of the phosphorylation cannot be determined confidently, only the phosphopeptide sequence is shown.

### 3.6 Increasing the sequence coverage of Bub1 by using multiple proteases

In proteomics, trypsin is the protease of choice for generating peptides from proteins. However, digestion by trypsin alone does usually not lead to allow complete sequence coverage of the protein, since many resulting peptides may be too short or too long for sensitive detection by MS. We therefore employed the additional proteases Lys-C, Glu-C (V8) and Elastase in our workflow and found that the use of multiple proteases increased the sequence coverage of Bub1 by two fold (Figure 20).

```

1 MDTPENVLQM LEAHMQSYKG NDPLGEWERY IQWVEENFPE NKEYLITLLE
51 HLMKEFLDKK KYHNDPRFIS YCLKFAEYNS DLHQFFEFY NHGIGTLSSP
101 LYIAWAGHLE AQGELQHASA VLQRGIQQA EPREFLQQQY RLFQTRLTET
151 HLPQAARTSE PLHNVQVLNQ MITSKSNPGN NMACISKNOG SELSGVISSA
201 CDKESNMERR VITISKSEYS VHS SLASKVD VEQVVMYCKE KLIRGESEFS
251 FEELRAQKYN QRRKHEQWVN EDRHYMKRKE ANAFEEQLLK QKMDELHKKL
301 HQVVETSHED LPASQERSEV NPARMGPSVG SQQELRAPCL PVTYQOTPVN
351 MEKNPREAPP VVPPLANAI S AALVSPATSQ SIAPPVPLKA QTVTDSMFAV
401 ASKDAGCVNK STHEFKPQSG AEIKEGCETH KVANTSSFHT TPNTSLGMVQ
451 ATPSKVQPSP TVHTKEALGF IMNMFQAPTL PDISDDKDEW QSLDQNEDEF
501 EAQFQKNVRS SGAWGVNKI I SSLSSAFHVF EDGNKENYGL PQPKNKPTGA
551 RTFGERSVSR LPSKPKEEVP HAEFLDDST VWGIRCNKTL APSPKSPGDF
601 TSAAQLASTP FHKLPVESVH ILEDKENVVA KQCTQATLDS CEENMVVPSR
651 DGKFSPIQEK SPKQALSSHM YSASLLRLSQ PAAGGVLTC EALGVEACRL
701 TDTDAATAED PPDATAGLQA EWMQSS LGT VDAPNFIVGN PWDDKLIFKL
751 LSGLSKPVSS YPNTFEWQCK LPAIKPKTEF QLGSKLVYVH HLLGEGAFQA
801 VYEATQGD LN DAKNKQKFVL KVQK PANPWE FYIGTQLMER LKPSMQHMF
851 KFYSAHLFQN GSVLVGELYS YGTLLNAINL YKNTPEKVMP QGLVISFAMR
901 MLYMIEQVHD CEIIHGDIKP DNFILGNGFL EQDDEDDLSA GLALIDLGQS
951 IDMKLFPGT IFTAKCETSG FQCVEMLSNK PWN YQIDYFG VAATVYCM LF
1001 GTYMKVKN EG GECKPEGLFR RLP HLD MWNE FFHVMLNIPD CHHLPSLDLL
1051 RQKLKKVFOQ HYTNKIRALR NRLIVLLEEC KRSRK

```

**Figure 20: Sequence coverage of Bub1 obtained with multiple proteases.**

Employing multiple proteases increased the sequence coverage of Bub1 from 33% (trypsin alone) to 68% (trypsin, elastase and glu-C). Peptides identified by combination of proteases is shown in bold and red whereas peptides identified with trypsin are underlined.

### 3.7 Identification of auto-phosphorylation sites on Bub1

Bub1 is a multi-tasking kinase required for the SAC and for proper segregation of chromosomes during mitosis. Unlike BubR1, Bub1 was shown to contain active kinase domain *in-vitro* and some *in-vivo* substrates have also been reported [113]. One of the common mechanisms of regulation of kinase activity is through T-loop phosphorylation and/or autophosphorylation. Therefore, identification of Bub1 autophosphorylation sites can throw light on phospho-regulation of Bub1. To identify autophosphorylation sites, we combined SILAC based quantitative Mass spectrometry, antibody based Bub1 purification and *in-vitro* kinase assays.

We expressed Bub1 wild type (WT) and kinase dead (KD) versions in 293T cells (Figure 21). Mitotic cells were lysed and Bub1 was purified by immunoprecipitation. Bub1 WT and KD were subjected to kinase assays separately, allowing autophosphorylation to occur. Next, phosphorylation of Bub1 and its interacting partners was quantitatively compared between WT and KD using SILAC. To address the reproducibility, experiments were carried out in biological triplicates. (Figure 23). We observed around 15

phosphorylation sites which were highly upregulated in kinase assays using the WT enzyme.(Figure 22, Figure 23). Results were consistent between the triplicate experiments.

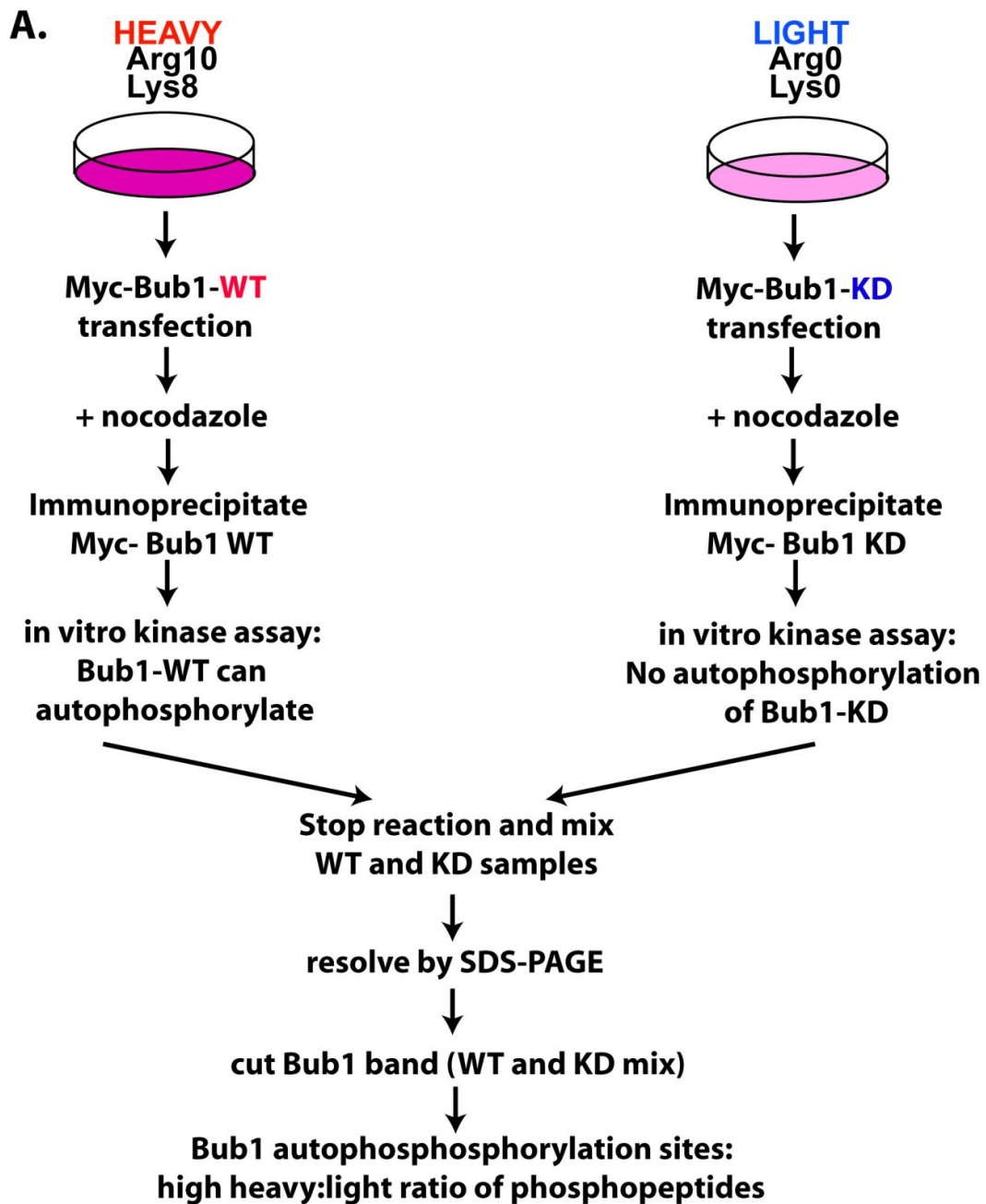


Figure 21: Schematic representation of workflow for the identification of in-vitro Bub1 autophosphorylation sites

Peptide Sequence	Residue	Score	Ratio WT/KD
APCLPVTYQQTPVNMEK	-	7	100
CNKpTLAPSPK	T589	29	66
DGKFpSPIQEK	S655	33	2
EAPPVVPPLANAISAA-LVSPATSQSIAPPVPLK	-	18	4
FpSPIQEKpSPK	S655 & S661	15	2
FSPIQEKpSPK	S661	19	3.4
GESEFSFEELR	S247	46	0.8
GpTIFTAK	T960	38	56
GpTIFpTAK	T960 & T963	12	10
ISSLSSAFHVFEDGNK	-	44	61
LHQVVETSHEDLPpSQER	S314	32	1
LLpSGLSK	S752	14	34
LPpSKPK	S563	17	9
LPVEpSVHILEDK	S618	52	6
LpSQPAAGGVLTCEAELGVEACR	S679	56	11
LpTETHLPAQAR	T148	18	4
MGPSVGpSQEELR	S331	44	1.3
NKPpTGAR	T548	11	100
NQSELSGVIp(SS)ACDK	S198 or S199	67	49
QALSSHMYSASLLR	-	72	28
QCTQATLDSCEENMVVPSR	-	45	1.4
RVITISK	T213	23	100
SEYSVHSSLASK	-	46	8
pSNPGNNMACISK	S176	53	47
pSPGDFTSAAQLASTPFHK	S596	95	2
P(SS)GAWGVNK	S509 or S 510	60	48
TEFQLGSK	-	13	5
pTFGER	T552	22	9
pTLAPSPK	T589	26	49
TSEPLHNVQVLNQMITSK	-	63	43
VANTSSFHTTPNTSLGMVQATPSK	-	30	44

VITISKSEYSVHSSLASK	-	36	10
VQPpSPTVHTK	S459	17	1.4
AQTVTDSMFAVApSK	S402	53	61

**Figure 22: Bub1 auto-phosphorylation analysis.**

List of phosphorylation sites identified on Bub1 upon in-vitro kinase assay. Bub1 sites phosphorylated by kinases other than Bub1 should be of the same abundance between WT and KD samples. Phosphorylation sites that are highly phosphorylated only in the WT (i.e. high WT/KD ratio) are most likely reflecting autophosphorylation.

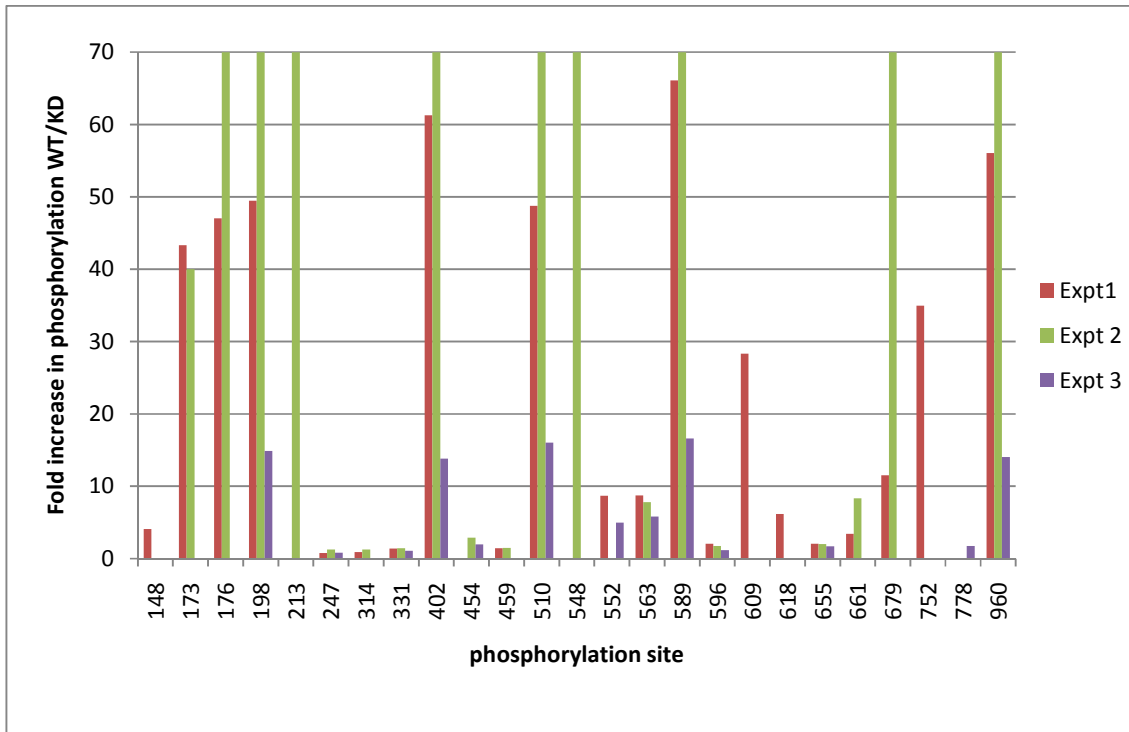


**Figure 23: Results from the three Bub1 auto-phosphorylation experiments were well in agreement with each other**

### 3.8 Identification of phosphorylation sites on Bub1 interaction partners

During the co-immunoprecipitation the Bub1 interaction partners BubR1 and Bub3 were also enriched in the Bub1 preparation. Phosphopeptide analysis showed that both BuR1 and Bub3 contained phosphorylation sites which were upregulated upon Bub1 kinase assay, indicating these sites might be phosphorylated by Bub1 (Figure 24). However, it is important to note that BubR1 and Bub3 phosphorylation sites could be identified only in one experiment each (presumably due to their low abundance in Bub1 immunoprecipitates). Hence further studies would be required to confirm the reality of Bub1 phosphorylation sites on BubR1 and Bub3.

Protein	Peptide	Residue	Score	Ratio Wt/KD
BubR1	DLPpSDPER	S633	15	0.5
BubR1	IEPSINHILSTR	-	18	7.031
BubR1	LQpSQHR	S191	17	18.544
BubR1	VQpSHQQASEEK	S384	23	21.339
BubR1	STLAELKpSK	S232	15	35.493
Bub3	VAVEYLDpSPEVQK	S211	28	1.26
Bub3	TGSNEFK	-	8	1.34

**Figure 24: BubR1 and Bub3 phosphorylation upon Bub1 kinase assay.**

List of phosphorylation sites identified on BubR1 and Bub3 upon Bub1 *in-vitro* kinase assay. BubR1 and Bub3 sites phosphorylated by kinases other than Bub1 should be of similar abundance between WT and KD samples; hence, the phosphorylation sites that are highly phosphorylated only in WT enzyme (i.e. high WT/KD ratio) are most likely phosphorylated by Bub1.



## 4.0 Discussion

### 4.1 Small-molecule kinase inhibitor based enrichment of the kinome

By using large amounts of starting material and a combination of approaches, we have identified more than 900 unique phosphorylation sites on protein kinases, including novel sites, illustrating the complexity of the mitotic kinome signalling network. Prior enrichment of the kinases using inhibitor based affinity chromatography was found to be the key to increase the coverage of the kinome. The strategies presented here for studying phosphokinome are not specific to mitosis and in principle can be applied to any comparative proteomic study focused on the regulation of the kinome. For instance, Schreiber *et al.* studied Lysophosphatidic acid (LPA) induced signaling events in A498 kidney carcinoma cells using both total cell lysates and protein kinase-enriched fractions. This integrated workflow allowed extensive coverage of LPA signaling by capturing both kinases and their substrates[114]. Similarly, Sharma *et al* were able to identify and quantify cellular target protein interactions with externally introduced ligands using a kinase inhibitors based enrichment strategy [115].

To get a good coverage of the mitotic phosphokinome, we used 60mg of protein from each cell cycle stage. However, for many applications obtaining such a large amount of starting material would be a difficult task. Moreover, in many cases quantitating the kinome itself, across different cell types or physiological states, can provide valuable insights. Such small scale studies or the studies focusing on protein levels, can still benefit from using just one inhibitor (VI16832) alone as immobilized kinase capturing ligand (our study used four additional capturing ligands along with VI16832). This simplified workflow provides enrichment for more than 150 kinases from 1 mg of starting material [102].

Although we identified more than 200 kinases in our present study, these represent only 40% of the human kinome. However this can be explained considering that not all kinases are ubiquitously expressed; many kinases are specific to a particular tissue or physiological state. This is exemplified in the recent study by Oppermann *et al* who compared kinomes of three different cell lines and observed that expressed kinome greatly vary among different cell types [102]. Moreover many members of the kinase superfamily share high sequence homology. In bottom up proteomics, proteins are digested into peptides and the peptides capable of discriminating the isoforms (unique peptides) may not be suitable

for analysis in MS due to their size, sequence or PTMs. This problem is even more pronounced in shotgun proteomics where frequently only few peptides are identified for the proteins. For instance, the peptides indentified in our study map to 292 kinases but only 190 of them contained unique peptides.

## **4.2 HeLa cell synchronization**

Interestingly, in spite of the complex nature of events involved, eukaryotic mitosis lasts less than one hour. Quantitation of phosphorylation/protein levels across mitosis poses a challenge as mitotic stages are difficult to synchronize due to their close spacing in time. Efficiency of cell synchronization is a critical factor that decides the minimum measurable change in phosphorylation/protein levels. For instance, in a hypothetical scenario where a phosphorylation site is regulated fourfold between two stages, when studied in a sample of 50% purity, only 2 fold regulation is observed. Hence, we addressed this situation by optimizing the cell synchronization methods to improve purity of the sample and conducting the experiments in biological triplicates.

Cell permeable inhibitors targeting various proteins involved in cell cycle progression serve as valuable tools for basic research. Although thymidine and nocodazole blocks do not exactly mimic physiological stages of the cell cycle, both have been shown to fairly reproduce cell cycle events and help in understanding cell cycle regulation. This is exemplified by the vast amount of scientific literature citing these reagents. However, some concerns still remain- for example, it cannot be ruled out that some of the observed changes may be the result of mild activation of the DNA damage and/or response apoptosis induced by thymidine and nocodazole blocks, respectively. In the event of DNA damage, key mitotic kinases such as Cdk1 and Plk1 are inactivated, preventing cell entry into mitosis. In our synchronization procedure more than 90% of the cells entered mitosis, arguing against DNA damage response activation. Further, in case of MAP kinase phosphorylation, which is examined using additional experiments (Figure 12), similar results were obtained even in the absence of MG132 or during prolonged nocodazole block. So it is more probable that the observed phospho-regulation is specific to each mitotic stage and not related to drug induced side effects.

Growing HeLa cells in suspension cultures has many advantages over growing them on plates. Studies requiring large amounts of material would be laborious and costly if done on cell culture plates. Suspension cultures achieve high cell densities ( $1.2\text{-}1.8 \times 10^6$  cells/ml), minimizing the usage of cell culture medium usage and other reagents. This would be an important consideration if the medium is supplemented with expensive reagents such as isotopic amino acids, inhibitors etc. Typical HeLa S3 cells form cell aggregates after few generations in suspension cultures. To overcome this problem we used a non adherent variant of the HeLa S3 cell line, known as HeLa S. Additionally, comparisons of results with Daub *et al* [83] and Dephoure *et al* [86] as well as further studies carried out in our laboratory shown that the results obtained in these two cell lines are similar (data not shown).

The protocols for large scale synchronization of cells in mitosis are useful in isolating many other sub-proteomes such as the mitotic spindle. As an example, isolation of mitotic spindles also requires large amounts of starting material and spinner cultures are found unsuitable due to high percentage of interphase cells, making their purification laborious [116]. Since in our method we were able to minimize the interphase cells in the mitotic preparation, we tried isolating the spindles from spinner cultures and obtained good results. These strategies thus respond to a growing contemporary need for comparative studies of different sub proteomes.

#### **4.3 Identification of protein kinases**

After extensive analysis of the human genome and EST databases, Manning *et al* narrowed down the human kinome to 518 putative members and provided their sequences [15]. However sequence databases such as IPI, NCBI, Swissprot etc. contained several additional sequences (redundant entries, splice variants) with different names. As mentioned in the above section, in bottom-up proteomic studies proteins are digested prior to measurement by MS and thus protein sequences are inferred by matching the peptide sequences to the protein sequence database. This is a non trivial step as the peptide sequence may match to multiple protein sequences, especially to different splice variants [89]. Whenever the set of identified peptides in one protein was equal to or completely contained in the set of identified peptides of another protein, these two proteins were joined in a single protein group and the protein with maximum number of peptides is shown as the leading protein for that protein group. However, most of the 944 protein kinase phosphorylation sites identified in our study matched to more than one protein sequence in the IPI database (suppl.

Data S3). Furthermore, in some cases identified peptides in both proteins were identical, meaning that leading protein assignment was arbitrary. This created a problem for counting the number of protein kinases, comparison of phosphorylation sites between different studies and also while using bioinformatic tools such as DAVID. We dealt with this problem by stripping off the protein information from the phosphopeptide sequence and using this sequence for comparing with kinase sequences provided by Manning *et al* and also for comparisons with datasets from Daub *et al* [83] and Dephoure *et al* [86]. This approach has the advantages that we were able to match the peptide/phosphorylation sites between different datasets even if they corresponded to different names of a same protein. However, the caveat remains that in some minority cases two different proteins (with different functions) may generate an identical peptide sequence and assigning the peptide to the wrong protein can give rise to artifacts in comparison between different datasets as well as in the downstream GO, pathway and PPI analysis.

#### **4.4 Global view of mitotic kinome**

Traditionally, the study of protein phosphorylation was a difficult task; new phosphorylation sites were indentified using mutational analyses and their regulation studied using phospho-specific antibodies. As a result, protein phosphorylation was often studies in isolation or using few controls. However, the situation changed with the introduction of MS and the advances in phosphoproteomics. MS based phosphorylation analysis allows the study of multiple proteins simultaneously, thus generating a global view of the system that is being studied. The main advantage of our data is that we were able to quantitatively measure the dynamics of site-specific phosphorylation as well as protein levels from a single sample. Kinases and their substrates form complex signaling networks where the status of each node depends on the status of other nodes in that network. As an example, the activity of the mitotic master kinase Cdk1 is controlled in a coordinated manner. Phosphorylation on the T-loop activates the kinase, whereas phosphorylation in the N-terminus inactivates it. Cdk1 inactivating kinases (Wee1, Myt1) as well as activating(Cdc25) phosphatases are also controlled by Cdk1 by feedback loops. The activity of Cdk1 is further modulated by its cyclin binding partner, which stabilizes T-loop phosphorylation and confers substrate specificity. In such a complex network, looking for a particular phosphorylation state or protein will not give the real picture. Especially while studying a disease state, such as tumor cells which have undergone adoption in response to their environment, comprehensive coverage of the

system is essential. As a result the ability to measure the regulation of a particular protein in comparison to the status of other proteins is of utmost importance. The large number of identified kinase phosphorylation sites (and also their interacting partners) enables an unbiased and quantitative view of the regulation of kinase networks, and thus constitutes a valuable tool to study the systems properties of the kinome during mitosis. It is a well established fact that Cdk1 is made inactive at the end of mitosis. We could see this phenomenon in our data at multiple levels. The levels of the Cdk1 subunit cyclin B went down in telophase samples, together with T-loop dephosphorylation on Cdk1. Further network analysis of jointly regulated protein groups suggested that the Cdk1 centered interaction network is downregulated in late mitosis (Figure 11 a,b). Similarly we found that Erk1/2, p38 MAP kinases are activated late in mitosis (Figure 11 d,e). This novel finding is further strengthened by the observation that members of MAP kinase pathways are enriched in proteins with upregulated phosphorylation sites in telophase.

The above discussion clearly illustrates the power of a comprehensive kinome analysis. As described in the first part of this thesis, the analysis of phosphorylation sites on a protein population enriched for protein kinases has provided a wealth of information on the regulation of mitotic progression. However it would be unrealistic to expect that a comprehensive analysis of the type discussed above could provide complete coverage or detailed information on the phosphorylation events on any particular mitotic kinase. Hence, it is indispensable to complement comprehensive approaches with focused approaches, as detailed in part 2 of this thesis and discussed below with regard to our results on BubR1 and Bub1

#### **4.5 Regulation of BubR1 function by phosphorylation**

We reported here the identification of 5 proline-directed phosphorylation sites on BubR1 and shown that at least 3 of the 5 sites are direct targets of Cdk1 *in-vitro*. Further we have showed that loss of BubR1 phosphorylation results in faulty KT-MT attachments and poor chromosome congression. In contrast, phosphorylation, at least at the sites described here, appears to be largely dispensable for the SAC functions of BubR1. Huang et al. recently suggested that Mps1 may be a major kinase for BubR1 *in-vivo* [112]. Although we also observe loss of BubR1 phosphorylation upon Mps1 inhibition (data not shown), we have been unable to directly phosphorylate BubR1 by Mps1 and thus favor the view that the

reported result may represent an indirect effect, perhaps reflecting mislocalization of BubR1. Indeed, a mislocalization of endogenous BubR1 upon Mps1 inhibition (our unpublished results), and the lack of any detectable phosphorylation on the mislocalized BubR1-E413K mutant support the conclusion that KT localization of BubR1 is required for its phosphorylation. Importantly, the finding that phosphorylation on BubR1 at one of these SP sites, S670, is significantly enhanced at unattached KTs but not at KTs lacking tension (appendix), is in excellent agreement with the above study [112]. Recent studies indicate that Cdk1-cyclin B1 localizes to KTs during prometaphase, where it contributes to the correct attachment of MTs to KTs and efficient chromosome alignment through phosphorylation of local substrates [117; 118]. Moreover, KT recruitment of Cdk1 is increased in nocodazole but not taxol treated cells [117], in agreement with the increase in S670 phosphorylation observed here upon nocodazole but not taxol treatment.

#### **4.6 Regulation of SAC and chromosome congression by different motifs of BubR1**

BubR1 is a checkpoint protein which performs multiple functions in mitosis. In our present study, we carried out functional analysis of conserved motifs of human BubR1 and demonstrated that SAC and chromosome attachment functions can be uncoupled from each other. Mutation of five proline-directed serine phosphorylation sites identified *in vivo* by mass spectrometry abolished chromosome-spindle attachments but had no effect on SAC functionality. In contrast, mutation of the two conserved KEN boxes required for SAC function did not impact on chromosome congression [119]. Interestingly, the contribution of the two KEN box motifs was found to be not equal. Cdc20 associated with the N-terminal but not the C-terminal KEN-box, and mutation of the N-terminal KEN motif resulted in more severe acceleration of mitotic timing. Moreover, the two KEN motifs were not sufficient for maximal binding of Cdc20 and APC/C, which also requires sequences in the BubR1 C-terminus. Finally, mutation of the GLEBS motif caused loss of Bub3 interaction and mislocalization of BubR1 from the kinetochore; concomitantly, BubR1 phosphorylation as well as SAC activity and chromosome congression were impaired, indicating that the GLEBS motif is strictly required for both major functions of human BubR1[119].

#### **4.7 Autophosphorylation and substrates of Bub1 kinase**

We have combined quantitative mass spectrometry and phosphopeptide enrichment with traditional *in-vitro* kinase assays to identify site-specific autophosphorylation on Bub1 and its substrates. Contrary to BubR1, Bub1 kinase activity is well established and required for multiple mitotic functions. Kawashima *et al* shown that phosphorylation of yeast histone 2A by Bub1 prevents chromosomal instability by insuring centromeric localization of shugoshin [113]. Similarly, Gao *et al* reported that Bub1 phosphorylates p53 (at serine 37) upon SAC activation. This delays p53 mediated cell death and provides time for cells reach chromosome biorientation [120]. In spite of these efforts many substrates of Bub1 still remain elusive. Eukaryotic cells have high kinase activity; as a result, differentiating phosphorylation sites by a kinase of interest against a huge pool of phosphorylation sites targeted by other kinase poses a big challenge. Further, the coverage of the phospho-proteome obtained in typical proteomic studies is far from complete and mostly confined to abundant proteins. In our experience, many of the important mitotic proteins (including the known interactors of Bub1) are difficult to identify in MS without prior enrichment. To counteract some of these problems we devised an Affinity purification MS (AP-MS) method. In these experiments, Bub1 was pulled down from cell lysates along with its interacting partners, using a Bub1-derived monoclonal antibody. Then, *in-vitro* kinase assays were performed using the same endogenous Bub1 kinase. This setup allowed us to identify both autophosphorylation on Bub1 and Bub1 phosphorylation sites on its interacting partners.

We identified more than 24 phosphorylation sites on Bub1. Out of those sites 15 were phosphorylated more than two fold compared to a Bub1 kinase dead mutant meaning that these sites are most likely phosphorylated by Bub1 (autophosphorylation). Moreover we achieved 67% of Bub1 sequence coverage compared to 16% in the large scale kinome study. We also identified 3 sites on BubR1 which are highly phosphorylated in presence of Bub1. Taken together this shows that our strategy was successful in identifying Bub1 autophosphorylation sites.

Interesting, we could also identify phosphorylation sites on BubR1 (a Bub1 interactor) that were highly phosphorylated Bub1 kinase assays, suggesting that they are likely to be phosphorylated by Bub1 *in-vivo* also. In contrast, the phosphorylation sites identified on Bub3 within the Bub1 immunoprecipitates stayed constant, indicating that they are most likely phosphorylated another kinase. Interestingly, of the two phosphorylation sites identified in Bub3, S211 is highly conserved among different species (data not shown).

Since little is known about Bub3 phosphorylation I might be rewarding to explore the function of S211.

#### **4.8 Advances in MS instrumentation and data analysis tools make large scale proteomic studies possible**

In the current report we presented results from three sets of experiments aimed at understanding the phospho-regulation of kinases. First, a large scale whole kinome study which captured known key mitotic kinases such as Plk1, TTK (Mps1), Aurora A, and Aurora B as well as many kinases which have not previously been implied in mitotic functions. Thus, the results of this study recapitulate many of the previously known mitotic events but also identify attractive candidates for future studies of phosphorylation-based mitotic signaling. Second, a small scale targeted study showed that the chromosome congression function of BubR1 is mediated through five proline-directed phosphorylation sites. And third, a further small scale targeted study investigated regulation of Bub1 by autophosphorylation and in addition identified candidate Bub1 phosphorylation sites on its interactors. In all these studies, we combined advances in mass spectrometry with biochemistry and cell biology techniques. The orbitrap MS, which became commercially available around the time this project was initiated, helped immensely in both identifying the phosphorylation sites and quantifying their regulation across different states. Phosphopeptides often have low signal-to-noise ratio and do not fragment well in MS/MS. However, the high mass accuracy and resolution of orbitraps (<7 ppm, 60,000 FWHM) reduce false positive identifications allowing identification of peptides with low Mascot scores. Further, this also helped during SILAC based quantitation; high mass accuracy and resolution helps to precisely locate the SILAC pair and distinguishes true signal from noise[121]. Reduced false positive rates also benefit quantitation accuracy as SILAC ratios of wrongly identified peptides may differ from the ratios of true peptides, thus shifting the mean ratio.

On an concluding note, as the proteomic studies are becoming larger and larger, with multiple replicates and thousands of protein/peptide identifications, data analysis is becoming the major bottleneck. For instance, we used two different software suits; MSQuant (BubR1 and Bub1 studies) and MaxQuant (whole kinome study) for SILAC data analysis. Although, MSQuant, one the popular open source programs, offered flexibility and supported multiple workflows, became very difficult to scale up when the number of identifications and raw files



increased.. In contrast, MaxQuant, a recently introduced freely available program, is fully automated with minimal user intervention. It cuts down the analysis time for of around 150 raw files and half a million MS/MS spectra to just a few days. Thus programs such as MaxQuant are indispensable for large scale proteomic studies.

## **5.0 Experimental procedures:**

### **5.1 Antibodies**

Anti-pSer676 BubR1 was raised in-house [87], anti-pThr180/Tyr182 p38 (#9211); anti-p38 (#9212); anti-pThr173/Tyr175 Erk1/2 (#4376); anti-Erk1/2 (#9102) were from Cell Signaling Technologies, anti-pSer10 HistoneH3 (#06570) and anti-Cyclin-B (#05373) were from Upstate, anti-Securin (#ab3305) was from Abcam, and anti- $\alpha$ -Tubulin (#T9026), anti- $\alpha$ -Tubulin-FITC (#F2168) were from Sigma-Aldrich, anti-MYC (9E10, ATCC), anti-Bub1 (Chemicon), CREST anti-human auto-immune serum (Immunovision).

### **5.2 Cell Culture, SILAC labeling and synchronization**

For SILAC, HeLa S cells were grown in DMEM containing 10% dialyzed FCS (PAA), 50 U/ml penicillin, 50  $\mu$ g/ml streptomycin and unlabeled L-arginine (R0) and L-lysine (K0) (Sigma) (SILAC light) or L-[U-13C6,14N4]arginine (R6) and L-[2H4]lysine (K4) (SILAC medium) or L-[U-13C6,15N4]arginine (R10) and L-[U-13C6,15N2]lysine (K8) (SILAC heavy) (Cambridge Isotope Laboratories). Cells were grown at 37 °C in a humidified incubator with 5% CO<sub>2</sub> atmosphere. After five cell doublings on culture dishes, cell cultures were expanded in spinner flasks (INTEGRA Biosciences). Spinner flasks were operated at 45 rpm and were kept inside the cell culture incubator. Prior to synchronization, cells were transferred to 400 ml fresh medium with 20% FCS and the cell density was adjusted to 0.6 x 10<sup>6</sup> cells/ml. HeLa S cells were first synchronized at the G1/S phase boundary by treatment with 4 mM thymidine (Sigma) for 16 h. They were then released for 12 h into fresh medium. After 4 h of release, 40 ng/ml nocodazole (Sigma) was added to arrest the cells in prometaphase. One population of the prometaphase arrested cells was harvested by centrifugation, whereas the two other populations were washed once, centrifuged at 300 x g in PBS, and released in fresh medium containing 20  $\mu$ M of MG132 (Calbiochem) to induce metaphase arrest. The population of metaphase arrested cells was then harvested by centrifugation, whereas the last population of cells was washed and released in fresh medium for 90 min, when most of them had reached telophase. Harvested cells were snap-frozen by liquid nitrogen and stored at -80°C until cell lysis. For BubR1 and Bub1 studies, cells were grown essentially as described above but only using SILAC light and heavy media. These experiments were performed using 15-25 million cells per each stage.

### **5.3 Immunofluorescence staining of cells**

Before harvesting the cells at different mitotic stages, a small aliquot of around 0.5 ml of cell suspension was taken into a 1.5 ml tube and incubated with fixing solution (1% paraformaldehyde and 3% sucrose). Approximately 10% of the fixed cells were transferred to a fresh 1.5 ml tube, treated with Triton X-100 (final concentration 0.1%) at room temperature for 15 min with constant shaking. Cells were then centrifuged at 300 g and the supernatant was discarded. The cell pellet was resuspended in 100  $\mu$ l of PBS with 2% BSA. DAPI and anti- $\alpha$ -Tubulin-FITC antibody were added. After 60 min of incubation, unbound DAPI and antibody were removed and cells were washed once with PBS to reduce background staining. Cells were kept at 4 °C and the mitotic stages of fixed cells were examined by immunofluorescence microscopy.

### **5.4 Kinase enrichment**

Affinity chromatography with the immobilized kinase inhibitors V16832 [83], bisindolylmaleimide X (Alexis Biochemicals), AX14596 [122] SU6668 [123] and purvalanol B (Tocris) was done on an ÄKTA explorer system (GE Healthcare) as described except that 2 volumes of 1.5 mM and 5 mM inhibitor solutions were reacted with 1 volume of epoxy-activated Sepharose beads to generate the V16832 and bisindolylmaleimide X affinity resins, respectively [83; 124]. Cell lysate was prepared as reported previously [124] and equal protein amounts of prometaphase, metaphase and telophase HeLa S cell extracts were combined prior to multi-resin affinity chromatography. Combined total cell extracts were loaded on the 5 different inhibitor resins filled into three consecutive columns at a flow rate of 70  $\mu$ l/min. The first and third column contained 0.5 ml of the V16832 and purvalanol B affinity resins, whereas the second column was packed with 0.33 ml of the SU6668, AX14596, and bisindolylmaleimide X matrices on top of each other. After sample loading and column washing, resin-bound proteins were eluted and concentrated as described previously [83]. (Kinase enrichment was done in association with Henrik Daub and Renate Hornberger).

### **5.5 In-gel protein digestion**

Around 700  $\mu\text{g}$  of the kinase-enriched fraction was dissolved in LDS loading buffer and separated by SDS-PAGE using NuPAGE Novex Bis-Tris gels (Invitrogen) according to the manufacturer's instructions. The gel was stained with Coomassie blue and protein bands were visualized. The resulting lane was cut into around 15 slices which were then subjected to in-gel digestion, essentially as described previously [125]. Gel slices were cut into small cubes of  $1\text{ mm}^3$  and washed with 50 mM ammonium bicarbonate (ABC) and 30% acetonitrile (ACN) until the cubes were fully destained. Gel cubes were dehydrated with 100% acetonitrile and rehydrated with 50 mM ABC containing 10 mM DTT. Proteins were reduced for 1 h at 56 °C. Resulting free thiol groups were then alkylated by adding 55 mM iodoacetamide in 50 mM ABC for 30 min at 25 °C in the dark. Gel pieces were washed twice with a 50 mM ABC solution, dehydrated with 100% acetonitrile, and dried in a vacuum concentrator. Each gel fraction was rehydrated in 50 mM ABC solution containing 15 ng/ $\mu\text{l}$  of trypsin, and samples were incubated at 37 °C overnight. Supernatants were transferred to new tubes, and residual peptides were extracted out of the gel pieces by double incubation with 30% ACN in 5% TFA and double incubation with 100% ACN. All extracts were combined, and ACN was evaporated in a vacuum concentrator. In case of experiment 3, peptides were analyzed twice (technical replicate).

## **5.6 In-solution protein digestion**

One third of the precipitated kinase-enriched fraction was directly dissolved in 20 mM HEPES buffer (pH 7.5) containing 7 M urea, and 2 M thiourea. Proteins were reduced by adding 2 mM DTT (final concentration) for 45 min at 25 °C, and thiols were carboxymethylated with 5.5 mM iodoacetamide for 30 min at room temperature. Endoproteinase Lys-C (Wako) was added in an enzyme/substrate ratio of 1:50 (5–6  $\mu\text{g}$  of Lys-C), and the proteins were digested for 4 h at room temperature. The resulting peptide mixtures were diluted with water (1:4) to reduce the final urea concentration below 2 M. For double digestion, modified trypsin (sequencing grade, Roche) was added in an enzyme/substrate ratio of 1:50 (5–6  $\mu\text{g}$  of trypsin), and the digest was incubated at 30 °C overnight. Trypsin activity was quenched by adding TFA to a final concentration of 1%.

### **5.7 Strong-cation exchange (SCX)**

The in-solution digests were loaded onto a strong-cation exchange (SCX) column (Polysulfoethyl, 1 x 150 mm, 5  $\mu\text{m}$  particles, 200 Å pore size, PolyLC Inc.) using a Jasco 2000-series HPLC system (Jasco Corporation). Peptides were separated by a linear 30 minutes gradient between 100% buffer A (5 mM  $\text{KH}_2\text{PO}_4$ , pH 2.7, 33% ACN) and 30% buffer B (350 mM KCl, 5 mM  $\text{KH}_2\text{PO}_4$ , pH 2.7, 33% ACN) with a flow rate of 120  $\mu\text{L}/\text{min}$ . 60 seconds fractions were collected using an automated fraction collector.

### **5.8 Phosphopeptide enrichment and desalting**

Titanium dioxide beads were used to selectively enrich for phosphorylated peptides with glycolic acid as a modifier [55]. About 3 mg of titanium dioxide beads were transferred to a GELoader tip (plugged at the constricted end by a small piece of C8 material) and washed with 40  $\mu\text{L}$  of 80  $\mu\text{g}/\mu\text{L}$  glycolic acid in a mixture of 80% ACN and 0.2% TFA. Digested peptides were dissolved in 20  $\mu\text{L}$  of 80  $\mu\text{g}/\mu\text{L}$  glycolic acid in a mixture of 80% ACN and 2% TFA and applied to microcolumns allowing phosphopeptides to bind to the titanium dioxide phase. Microcolumns were then washed with 40  $\mu\text{L}$  of 80  $\mu\text{g}/\mu\text{L}$  glycolic acid in a mixture of 80% ACN and 0.2% TFA and 40  $\mu\text{L}$  of a mixture of 80% ACN and 0.2% TFA (collected as flow-through). Finally, phosphorylated peptides were eluted slowly with 40  $\mu\text{L}$  of 0.6%  $\text{NH}_4\text{OH}$  and subsequently 40  $\mu\text{L}$  of 60% ACN. Flow-through fractions were desalted with C18 reversed-phase material prior to LC-MS/MS analysis essentially as described [126].

### **5.9 Nano-LC-MS/MS Analysis**

All peptide samples were separated by online reverse phase nano-LC and analyzed by electrospray MS/MS. Using a nanoACQUITY ultra performance liquid chromatography system (Waters), samples were injected onto a 14-cm fused silica capillary column with an inner diameter of 75  $\mu\text{m}$  and a tip of 8  $\mu\text{m}$  (New Objective) packed in-house with 3- $\mu\text{m}$  ReproSil-Pur C18-AQ (Dr. Maisch GmbH). The LC setup was connected to a LTQ-Orbitrap MS (Thermo Fisher Scientific) equipped with a nanoelectrospray ion source (Proxeon Biosystems). Peptides were separated and eluted by a stepwise 180 min gradient of 0–100% between buffer A (0.2% formic acid in water) and buffer B (0.2% formic acid in acetonitrile). Data-dependent acquisition was performed on the LTQ-Orbitrap using Xcalibur 2.0 software in the positive ion mode. Survey full scan MS spectra (from  $m/z$  300 to 2000) were acquired

in the FT-Orbitrap with a resolution of 60 000 at  $m/z$  400. A maximum of five peptides were sequentially isolated for fragmentation in the linear ion trap using collision induced dissociation (CID). The Orbitrap lock mass feature was applied to improve mass accuracy as described [59]. To improve phosphopeptide analysis, the multistage activation option in the software was enabled, and the neutral loss species at 97.97, 48.99, or 32.66  $m/z$  below the precursor ion were activated for 30 ms during fragmentation (pseudo-MS<sup>3</sup>) [60].

### **5.10 Data processing and analysis**

Raw data files were processed using the MaxQuant software suite (version 1.0.12.5) which performs, amongst other tasks, peak list generation, mass re-calibration, SILAC based quantitation, estimation of false discovery rates based on Mascot search results, and assembling peptides to protein groups[45]. Generation of peak lists was performed with the following MaxQuant parameters; top 12 MS/MS peaks for 100 Da, 3 data points for centroid, Gaussian centroid determination, slice peaks at local minima. During the peak list generation MaxQuant identified potential SILAC pairs based on mass differences of specified labeled amino acids, intensity correlation over elution time etc. Mascot (version 2.2.0, Matrix Science) was used for peptide identifications[88]. The initial precursor mass tolerance was set to  $\pm 7$  ppm, whereas an accuracy of  $\pm 0.5$  Da was used for MS/MS fragmentation spectra. Carbamidomethylation was set as fixed modification and methionine oxidation, protein N-terminal acetylation, and phosphorylation (STY) were considered as variable modifications. Putative SILAC pairs are searched with their respective labeled amino acids as fixed modification whereas peaks which were not assigned to any of the SILAC pairs were searched using R6, R10, K4 and K8 as variable modifications. Enzyme specificity was set to Trypsin/P i.e. allowing cleavage N-terminal to proline in the context of [KR]P. Up to two missed cleavages were allowed. The minimum required peptide length was set to 6 amino acids. Searches were performed against IPI human (version 3.48; 71,400 protein entries) that was concatenated with reverse database sequences (142,800 protein entries in total) [127]. Further, MaxQuant filtered Mascot results using additional parameters, such as the number of labeled amino acids (max of 3) in the identified peptide sequence and the measured mass accuracy as a function of intensity [45]. As an additional quality measure to increase identification stringencies, we only accepted phosphorylation site identifications with Mascot scores of at least 12 or PTM scores of at least 30. Quantitation of SILAC pairs was performed with the following parameters; re-quantify, for protein quantitation discard unmodified

counterpart peptides except for oxidation and acetyl protein N-terminal, use razor and unique peptides, minimum ratio count of 1, minimum score 0, minimum peptides 1[45]. The initial maximum false-discovery rates (FDR) were set to 0.02, and 0.05 for peptides and proteins, respectively, and further reduced by Mascot score filtering as described above. FDR's were calculated as (number of hits in the reversed database/number of hits in the forward database)  $\times$  100% [128]. Whenever the set of identified peptides in one protein was equal to or completely contained in the set of identified peptides of another protein these two proteins were joined in a single protein group. Shared peptides are most parsimoniously associated with the group with the highest number of identified peptides ('razor' peptides [89]) but remain in all groups where they occur [45]. In cases where the peptides have more than one phosphorylation site, some of these phosphorylation sites are identified as multiply phosphorylated peptides whereas others are identified on multiple singly phosphorylated peptides. Different ratios of phosphorylation sites within the same peptide can only be determined if the different singly phosphorylated peptides eluted at different time points. In general, singly phosphorylated peptides are preferred for quantitation purposes compared to multiply phosphorylated peptides, since the individual contributions of multiple phosphorylation sites on the observed ratio of the phosphopeptide cannot be determined. SILAC data from BubR1 and Bub1 studies is analyzed using MSQuant [129]

### **5.11 Interaction networks and functional clustering**

Protein interaction networks were obtained from the STRING database version 8[74] using the web interface available at string.embl.de with the following parameters: required confidence, medium; network depth of 1; experiments and databases as prediction methods. Interaction data obtained from string database were loaded to Cytoscape [130] for drawing the images. Functional annotation clustering was done using DAVID Bioinformatics Resources [131]. Default parameters with medium classification stringency were used.

### **5.12 Cell lysis and co-immunoprecipitation**

Cells were mixed with lysis buffer consisting of 50 mM Tris pH 7.4, 150 mM NaCl, 1% NP-40 (igepal), 0.1% deoxycholate, phosphatase inhibitor cocktails I and II (sigma), 30 ug/ml DNase, 30 ug/ml RNase and protease inhibitors (roche), to give a final protein concentration

of about 2 ug /ul. Cells were left on ice for 10-20 minutes to lyse and then centrifuged at 14,000 rpm to remove the cell debris.

For co-immunoprecipitation, protein concentration of extract was measured and approximately 1 ug of antibody bound to protein G beads per 1 mg of protein extract is added. Co-immunoprecipitation was carried out in the cold room for about 2 hours under constant mixing. Later beads are spun down and washed three times in the lysis buffer. Laemmli buffer was added to the beads and separated on SDS-PAGE.

### **5.13 Kinase assay**

In vitro phosphorylation of recombinant BubR1 was carried out in 30  $\mu$ l of kinase reaction buffer as previously described [87]. Recombinant active Cdk1 was purchased from Upstate Biotechnology, and GST-Mps1 from invitrogen. For Cdk1 assays on peptides immobilized cellulose membranes, dried membranes were first washed in ethanol and then hydrated in kinase buffer (50mM Tris-HCl pH7.5, 10 mM MgCl<sub>2</sub>, 1 mM DTT, 100  $\mu$ M NaF, 10 $\mu$ M Sodium Vanadate) for 1 h, followed by overnight blocking in kinase buffer with 100mM NaCl and 0.5 mg/ml BSA. The next day, the membrane was blocked again with kinase buffer containing 1mg/ml BSA, 100 mM NaCl, and 50  $\mu$ M cold ATP at 30°C for 45 min. The block was subsequently replaced with kinase reaction buffer containing 0.2 mg/ml BSA, 50  $\mu$ Ci/ml [ $\gamma$ -<sup>32</sup>P]ATP [3000 Ci/mmol, 10 mCi/ml], 2  $\mu$ g/ml recombinant Cdk1, and 50  $\mu$ M ATP for 3 h on a shaker at 30°C. The membranes were then washed extensively: 10x 15 min in 1M NaCl, 3 x 5 min in H<sub>2</sub>O, 3 x 5 min 5% H<sub>3</sub>PO<sub>4</sub>, 3 x 5 min in H<sub>2</sub>O, and then sonicated overnight in 8M urea, 1% SDS (w/v), and 0.5% (v/v)  $\beta$ -mercaptoethanol to remove residual nonspecific radioactivity. Phosphorylation was visualized by autoradiography.

For *in-vitro* Bub1 IP and kinase assay six 15 cm cell culture plates were transfected with myc-Bub1-WT and myc-Bub1-KD constructs, after 24 hrs nocodazole was added, and 16hr later cells are harvested. Co-immunoprecipitation and kinase assays were performed separately, essentially as described above. After the co-immunoprecipitation beads were washed with lysis buffer with 300 mM NaCl followed by wash with 1X kinase reaction buffer without ATP. Then beads were incubated with 200  $\mu$ l kinase reaction buffers with at 30 °C for 60 minutes. Later beads were washed once with kinase reaction buffer without ATP, and beads from both the myc-Bub1-WT and myc-Bub1-KD were combined together. Laemmli buffer was added to the beads and separated on SDS-PAGE.



#### **5.14 Peptide array synthesis and spots blotting**

Peptide arrays were constructed according to the Spots-synthesis method according to the manufacturer's directions (Intavis). For Cdc20 binding experiments, purified GST-Cdc20 fusion protein generated in SF9 insect cells was added at 5 µg/ml in TBST and incubated together with the membrane overnight at 4 °C. Membranes were washed three times in TBST and bound protein was visualized with anti-Cdc20 antibodies. Sequences of peptides synthesized are as follows: KEN30: DEWELSKENVQPLRQ, KEN304: PPMPRAKENELQAGP, S543: SEKKNKSPPADP, S574: TSNEVDSPDVCD, S670: LSIKKLSPIIED, S720: SENPTQSPWCSQ, S1043: KVGKLTSPGALL.

## 6.0 Appendix

### 6.1 PPI network for proteins with upregulated phosphorylation sites

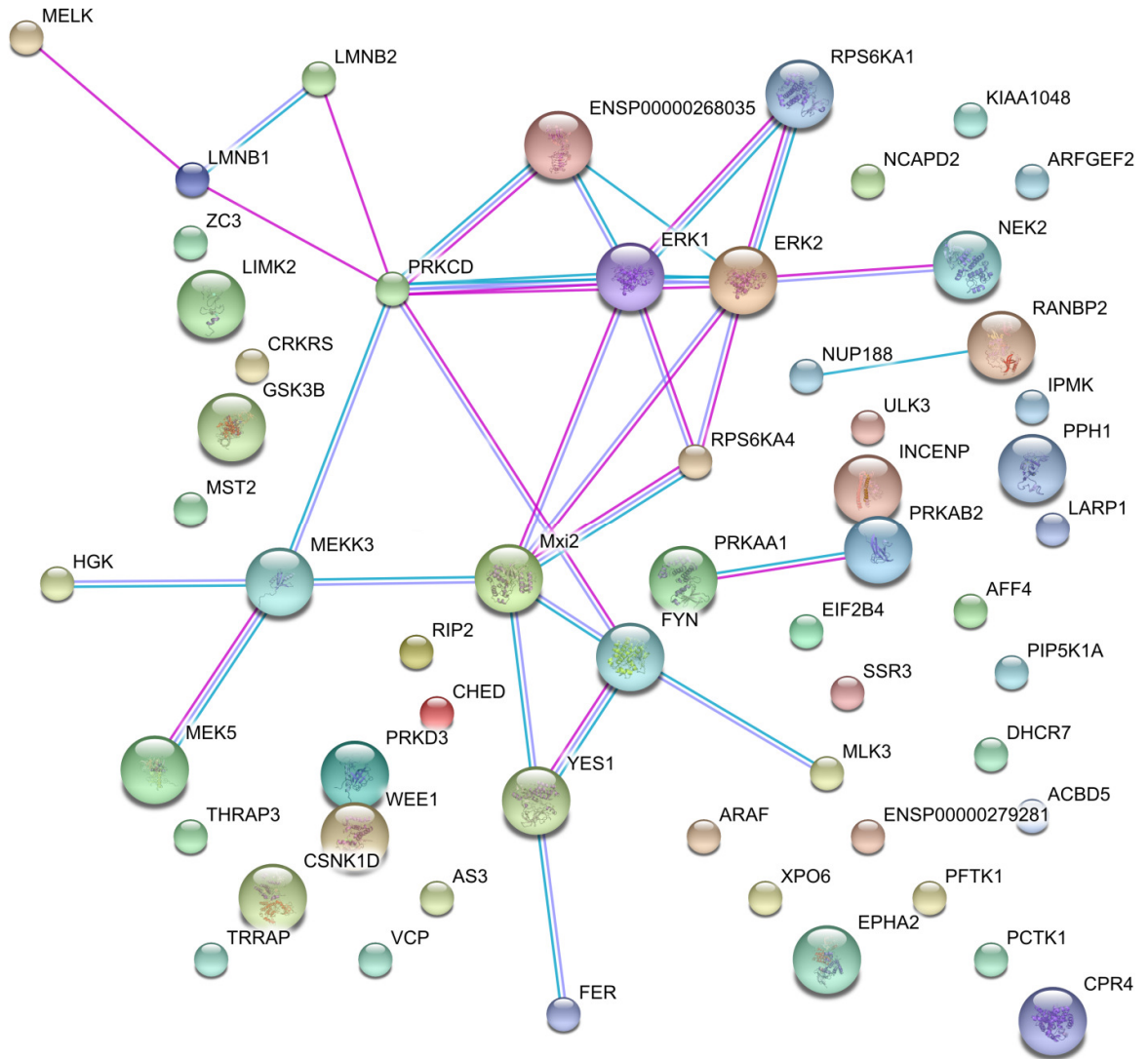


**Figure S1:** Picture depicting interactions between proteins with upregulated phosphorylation sites. The picture is generated using the STRING interaction database.



### 6.3 Supporting data available at tranche

The following supporting data is saved at tranche: <https://proteomecommons.org/tranche/>.

They can be accessed using their corresponding hash:

**Suppl. Data S3:** SILAC ratios for proteins and phosphorylation sites

IFQ3DPx0drMMnDH7TO8yLW3sDkGPm7GzCUNt9SqNUMdkTr7uRB21btU9inx173mgR  
+xYJMHZreG+9nB/0ZDQ7YWqXp8AAAAAAACbw==

**Suppl. Data S4:** Reproducibility between the biological replicates

yZ4uG0EdwwuNvYMH+DqJ6jSnxTw2VsB6Mdq+jhd2iS4dv3hwI/jOeL8VQp1vT0swEGn  
HIVRoqGmxSCJDZA9Pocf2GM4AAAAAAACaA==

**Suppl. Data S5:** Raw Files

L4TzF0GZAYPyYmI+3GL6/WJ5JEyHg4uxtGNefDjSBIW9q211zxEVq1ZPkOj8wK9qvE0d  
LcrqawRw3yVmqqGuXx/KLRYAAAAAAABYPA==

**Suppl. Data S6:** MS/MS peak lists of the 117 raw data

filesXZXixrydqHkFY0t6jDa25U0LuTQJ4E+7jnZK18O69QHLOWjoSdQitT04IGvBwOunW  
PB5upvnLq8Ha6kl+MK2OZ02NWIAAAAAAAACOA==

**Suppl. Data S7:** Annotated MS/MS spectra (based on full resolution profile data) of all phosphopeptides exported from MaxQuant

r1SCPFUElrBZO0/8UnYyvIgOrIQA1LneEOdcWX4QpIp6yPA6VILahGA3WH0ctK8RFA  
CLd1ZOeVeR9vhCHoLMr5QokDoAAAAAAAmLhA==

## Abbreviations

APC/C	Anaphase promoting complex/cyclosome
ATP	Adenosine 5'-triphosphate
BSA	Bovine serum albumin
Bub1	Budding uninhibited by benzimidazole 1
BubR1	Budding uninhibited by benzimidazole 1 homolog beta
CDK1	Cyclin-dependent kinase 1
CID	Collision induced dissociation
C-terminus	Carboxyl terminus
DAPI	4',6-diamidino-2-phenylindole
DMEM	Dulbecco's modified eagle's medium
DNA	Deoxyribonucleic Acid
DTT	Dithiothreitol
ECD	Electron capture dissociation
ESI	Electrospray ionization
ETD	Electron transfer dissociation
FCS	Fetal calf serum
FDR	False positive rates
GO	Gene ontology
HeLa S	HeLa suspension cell line
ICAT	Isotope coded affinity tag
IMAC	Immobilized metal-ion affinity chromatography
IP	Immunoprecipitation
iTRAQ	Isobaric tag for relative and absolute quantitation
kDa	kilo Daltons
MALDI	Matrix-assisted laser desorption/ionization

MCC	Mitotic checkpoint complex
MOC	Metal-oxide chromatography
mRNA	Messenger ribonucleic acid
MS	Mass spectrometry
N-terminus	Amino terminus
PBS	Phosphate-buffered saline
PMSF	phenylmethylsulfonyl fluoride
PPI	Protein-protein interaction
PRC1	Protein regulator of cytokinesis
PTM	Posttranslational modification
RF	Radio frequency
SAC	Spindle assembly checkpoint
SCX	Strong cation exchange
SDS-PAGE	Sodium dodecylsulfate polyacrylamide gelelectrophoresis
SILAC	Stable isotope labeling with amino acids in cell culture
siRNA	Small interference ribonucleic acid
Tris	Tris(hydroxymethyl)-aminomethane
WT	Wild-type

## References

- [1]E.A. Nigg, Mitotic kinases as regulators of cell division and its checkpoints. *Nat Rev Mol Cell Biol* 2 (2001) 21-32.
- [2]A. Musacchio, E.D. Salmon, The spindle-assembly checkpoint in space and time. *Nat Rev Mol Cell Biol* 8 (2007) 379-393.
- [3]C.L. Rieder, R.W. Cole, A. Khodjakov, G. Sluder, The checkpoint delaying anaphase in response to chromosome monoorientation is mediated by an inhibitory signal produced by unattached kinetochores. *J Cell Biol* 130 (1995) 941-948.
- [4]D. Cimini, F. Degrossi, Aneuploidy: a matter of bad connections. *Trends Cell Biol* 15 (2005) 442-451.
- [5]D. Morgan, *The Cell Cycle: Principles of Control* 1st edition ed., New Science Press Ltd, 2007.
- [6]L.H. Hwang, L.F. Lau, D.L. Smith, C.A. Mistrot, K.G. Hardwick, E.S. Hwang, A. Amon, A.W. Murray, Budding yeast Cdc20: a target of the spindle checkpoint. *Science* 279 (1998) 1041-1044.
- [7]S.H. Kim, D.P. Lin, S. Matsumoto, A. Kitazono, T. Matsumoto, Fission yeast Slp1: an effector of the Mad2-dependent spindle checkpoint. *Science* 279 (1998) 1045-1047.
- [8]D.W. Cleveland, Y. Mao, K.F. Sullivan, Centromeres and kinetochores: from epigenetics to mitotic checkpoint signaling. *Cell* 112 (2003) 407-421.
- [9]K.G. Hardwick, R.C. Johnston, D.L. Smith, A.W. Murray, MAD3 encodes a novel component of the spindle checkpoint which interacts with Bub3p, Cdc20p, and Mad2p. *J Cell Biol* 148 (2000) 871-882.

- [10]R. Fraschini, A. Beretta, L. Sironi, A. Musacchio, G. Lucchini, S. Piatti, Bub3 interaction with Mad2, Mad3 and Cdc20 is mediated by WD40 repeats and does not require intact kinetochores. *EMBO J* 20 (2001) 6648-6659.
- [11]V. Sudakin, G.K. Chan, T.J. Yen, Checkpoint inhibition of the APC/C in HeLa cells is mediated by a complex of BUBR1, BUB3, CDC20, and MAD2. *J Cell Biol* 154 (2001) 925-936.
- [12]P. Cohen, The origins of protein phosphorylation. *Nat Cell Biol* 4 (2002) E127-130.
- [13]J.D. Graves, E.G. Krebs, Protein phosphorylation and signal transduction. *Pharmacol Ther* 82 (1999) 111-121.
- [14]T. Pawson, J.D. Scott, Protein phosphorylation in signaling--50 years and counting. *Trends Biochem Sci* 30 (2005) 286-290.
- [15]G. Manning, D.B. Whyte, R. Martinez, T. Hunter, S. Sudarsanam, The protein kinase complement of the human genome. *Science* 298 (2002) 1912-1934.
- [16]V.M. Draviam, S. Orrechia, M. Lowe, R. Pardi, J. Pines, The localization of human cyclins B1 and B2 determines CDK1 substrate specificity and neither enzyme requires MEK to disassemble the Golgi apparatus. *J Cell Biol* 152 (2001) 945-958.
- [17]J.R. Bischoff, L. Anderson, Y. Zhu, K. Mossie, L. Ng, B. Souza, B. Schryver, P. Flanagan, F. Clairvoyant, C. Ginther, C.S. Chan, M. Novotny, D.J. Slamon, G.D. Plowman, A homologue of *Drosophila* aurora kinase is oncogenic and amplified in human colorectal cancers. *EMBO J* 17 (1998) 3052-3065.
- [18]K.E. Mundt, R.M. Golsteyn, H.A. Lane, E.A. Nigg, On the regulation and function of human polo-like kinase 1 (PLK1): effects of overexpression on cell cycle progression. *Biochem Biophys Res Commun* 239 (1997) 377-385.
- [19]J.A. Ubersax, J.E. Ferrell, Jr., Mechanisms of specificity in protein phosphorylation. *Nat Rev Mol Cell Biol* 8 (2007) 530-541.



- [20]B. Nolen, S. Taylor, G. Ghosh, Regulation of protein kinases; controlling activity through activation segment conformation. *Mol Cell* 15 (2004) 661-675.
- [21]Y.J. Jang, S. Ma, Y. Terada, R.L. Erikson, Phosphorylation of threonine 210 and the role of serine 137 in the regulation of mammalian polo-like kinase. *J Biol Chem* 277 (2002) 44115-44120.
- [22]W. Krek, E.A. Nigg, Cell cycle regulation of vertebrate p34cdc2 activity: identification of Thr161 as an essential in vivo phosphorylation site. *New Biol* 4 (1992) 323-329.
- [23]W. Krek, E.A. Nigg, Differential phosphorylation of vertebrate p34cdc2 kinase at the G1/S and G2/M transitions of the cell cycle: identification of major phosphorylation sites. *EMBO J* 10 (1991) 305-316.
- [24]A.E. Elia, L.C. Cantley, M.B. Yaffe, Proteomic screen finds pSer/pThr-binding domain localizing Plk1 to mitotic substrates. *Science* 299 (2003) 1228-1231.
- [25]W. Qi, Z. Tang, H. Yu, Phosphorylation- and polo-box-dependent binding of Plk1 to Bub1 is required for the kinetochore localization of Plk1. *Mol Biol Cell* 17 (2006) 3705-3716.
- [26]A.T. Saurin, J. Durgan, A.J. Cameron, A. Faisal, M.S. Marber, P.J. Parker, The regulated assembly of a PKCepsilon complex controls the completion of cytokinesis. *Nat Cell Biol* 10 (2008) 891-901.
- [27]R.M. Biondi, D. Komander, C.C. Thomas, J.M. Lizcano, M. Deak, D.R. Alessi, D.M. van Aalten, High resolution crystal structure of the human PDK1 catalytic domain defines the regulatory phosphopeptide docking site. *EMBO J* 21 (2002) 4219-4228.
- [28]N. Watanabe, H. Arai, Y. Nishihara, M. Taniguchi, T. Hunter, H. Osada, M-phase kinases induce phospho-dependent ubiquitination of somatic Wee1 by SCFbeta-TrCP. *Proc Natl Acad Sci U S A* 101 (2004) 4419-4424.
- [29]T. Hunter, The age of crosstalk: phosphorylation, ubiquitination, and beyond. *Mol Cell* 28 (2007) 730-738.

- [30]J.J. Li, S.A. Li, Mitotic kinases: the key to duplication, segregation, and cytokinesis errors, chromosomal instability, and oncogenesis. *Pharmacol Ther* 111 (2006) 974-984.
- [31]F.A. Barr, H.H. Sillje, E.A. Nigg, Polo-like kinases and the orchestration of cell division. *Nat Rev Mol Cell Biol* 5 (2004) 429-440.
- [32]T. Marumoto, D. Zhang, H. Saya, Aurora-A - a guardian of poles. *Nat Rev Cancer* 5 (2005) 42-50.
- [33]P. Meraldi, R. Honda, E.A. Nigg, Aurora kinases link chromosome segregation and cell division to cancer susceptibility. *Curr Opin Genet Dev* 14 (2004) 29-36.
- [34]J. Tang, X. Yang, X. Liu, Phosphorylation of Plk1 at Ser326 regulates its functions during mitotic progression. *Oncogene* 27 (2008) 6635-6645.
- [35]R. Kittler, L. Pelletier, A.K. Heninger, M. Slabicki, M. Theis, L. Mirosław, I. Poser, S. Lawo, H. Grabner, K. Kozak, J. Wagner, V. Surendranath, C. Richter, W. Bowen, A.L. Jackson, B. Habermann, A.A. Hyman, F. Buchholz, Genome-scale RNAi profiling of cell division in human tissue culture cells. *Nat Cell Biol* 9 (2007) 1401-1412.
- [36]V.S. Edmond de Hoffmann, *Mass Spectrometry: Principles and Applications* 3 edition ed., Wiley-Interscience 2007.
- [37]M. Karas, D. Bachmann, F. Hillenkamp, Influence of the wavelength in high-irradiance ultraviolet laser desorption mass spectrometry of organic molecules. *Analytical Chemistry* 57 (1985) 2935-2939.
- [38]M. Karas, D. Bachmann, U. Bahr, F. Hillenkamp, Matrix-assisted ultraviolet laser desorption of non-volatile compounds. *International Journal of Mass Spectrometry and Ion Processes* 78 (1987) 53-68.
- [39]J.B. Fenn, M. Mann, C.K. Meng, S.F. Wong, C.M. Whitehouse, Electrospray ionization for mass spectrometry of large biomolecules. *Science* 246 (1989) 64-71.

- [40]S.H. Paul W., Ein neues Massenspektrometer ohne Magnetfeld. RZeitschrift für Naturforschung 8 (1953) 3.
- [41]R. March, An Introduction to Quadrupole Ion Trap Mass Spectrometry. JOURNAL OF MASS SPECTROMETRY 32 (1997) 19.
- [42]Thermo Electron Corporation. Finnigan™ LTQ™ Hardware Manual.
- [43]A. Makarov, Electrostatic axially harmonic orbital trapping: a high-performance technique of mass analysis. Anal Chem 72 (2000) 1156-1162.
- [44]Q. Hu, R.J. Noll, H. Li, A. Makarov, M. Hardman, R. Graham Cooks, The Orbitrap: a new mass spectrometer. J Mass Spectrom 40 (2005) 430-443.
- [45]J. Cox, M. Mann, MaxQuant enables high peptide identification rates, individualized p.p.b.-range mass accuracies and proteome-wide protein quantification. Nat Biotechnol 26 (2008) 1367-1372.
- [46]L.N. Mueller, O. Rinner, A. Schmidt, S. Letarte, B. Bodenmiller, M.Y. Brusniak, O. Vitek, R. Aebersold, M. Muller, SuperHirn - a novel tool for high resolution LC-MS-based peptide/protein profiling. Proteomics 7 (2007) 3470-3480.
- [47]L.M. de Godoy, J.V. Olsen, J. Cox, M.L. Nielsen, N.C. Hubner, F. Frohlich, T.C. Walther, M. Mann, Comprehensive mass-spectrometry-based proteome quantification of haploid versus diploid yeast. Nature 455 (2008) 1251-1254.
- [48]M. Kruger, M. Moser, S. Ussar, I. Thievensen, C.A. Luber, F. Forner, S. Schmidt, S. Zanivan, R. Fassler, M. Mann, SILAC mouse for quantitative proteomics uncovers kindlin-3 as an essential factor for red blood cell function. Cell 134 (2008) 353-364.
- [49]T. Bonaldi, T. Straub, J. Cox, C. Kumar, P.B. Becker, M. Mann, Combined use of RNAi and quantitative proteomics to study gene function in Drosophila. Mol Cell 31 (2008) 762-772.

- [50]S.E. Ong, B. Blagoev, I. Kratchmarova, D.B. Kristensen, H. Steen, A. Pandey, M. Mann, Stable isotope labeling by amino acids in cell culture, SILAC, as a simple and accurate approach to expression proteomics. *Mol Cell Proteomics* 1 (2002) 376-386.
- [51]J. Reinders, A. Sickmann, State-of-the-art in phosphoproteomics. *Proteomics* 5 (2005) 4052-4061.
- [52]J. Porath, J. Carlsson, I. Olsson, G. Belfrage, Metal chelate affinity chromatography, a new approach to protein fractionation. *Nature* 258 (1975) 598-599.
- [53]S.S. Jensen, M.R. Larsen, Evaluation of the impact of some experimental procedures on different phosphopeptide enrichment techniques. *Rapid Commun Mass Spectrom* 21 (2007) 3635-3645.
- [54]T.E. Thingholm, O.N. Jensen, P.J. Robinson, M.R. Larsen, SIMAC (sequential elution from IMAC), a phosphoproteomics strategy for the rapid separation of monophosphorylated from multiply phosphorylated peptides. *Mol Cell Proteomics* 7 (2008) 661-671.
- [55]N. Sugiyama, T. Masuda, K. Shinoda, A. Nakamura, M. Tomita, Y. Ishihama, Phosphopeptide enrichment by aliphatic hydroxy acid-modified metal oxide chromatography for nano-LC-MS/MS in proteomics applications. *Mol Cell Proteomics* 6 (2007) 1103-1109.
- [56]Y. Kyono, N. Sugiyama, K. Imami, M. Tomita, Y. Ishihama, Successive and selective release of phosphorylated peptides captured by hydroxy acid-modified metal oxide chromatography. *J Proteome Res* 7 (2008) 4585-4593.
- [57]J.V. Olsen, B. Blagoev, F. Gnad, B. Macek, C. Kumar, P. Mortensen, M. Mann, Global, in vivo, and site-specific phosphorylation dynamics in signaling networks. *Cell* 127 (2006) 635-648.
- [58]R.S. Annan, M.J. Huddleston, R. Verma, R.J. Deshaies, S.A. Carr, A multidimensional electrospray MS-based approach to phosphopeptide mapping. *Anal Chem* 73 (2001) 393-404.

- [59]A. Gruhler, J.V. Olsen, S. Mohammed, P. Mortensen, N.J. Faergeman, M. Mann, O.N. Jensen, Quantitative phosphoproteomics applied to the yeast pheromone signaling pathway. *Mol Cell Proteomics* 4 (2005) 310-327.
- [60]M.J. Schroeder, J. Shabanowitz, J.C. Schwartz, D.F. Hunt, J.J. Coon, A neutral loss activation method for improved phosphopeptide sequence analysis by quadrupole ion trap mass spectrometry. *Anal Chem* 76 (2004) 3590-3598.
- [61]J. Cox, M. Mann, Is proteomics the new genomics? *Cell* 130 (2007) 395-398.
- [62]M. Ashburner, C. Ball, J. Blake, D. Botstein, H. Butler, J. Cherry, A. Davis, K. Dolinski, S. Dwight, J. Eppig, M. Harris, D. Hill, L. Issel-Tarver, A. Kasarskis, S. Lewis, J. Matese, J. Richardson, M. Ringwald, G. Rubin, G. Sherlock, Gene ontology: tool for the unification of biology. The Gene Ontology Consortium. *Nat Genet* 25 (2000) 25-29.
- [63]G.J. Dennis, B. Sherman, D. Hosack, J. Yang, W. Gao, H. Lane, R. Lempicki, DAVID: Database for Annotation, Visualization, and Integrated Discovery. *Genome Biol* 4 (2003) P3.
- [64]M. Cary, G. Bader, C. Sander, Pathway information for systems biology. *FEBS Lett* 579 (2005) 1815-1820.
- [65]M. Kanehisa, M. Araki, S. Goto, M. Hattori, M. Hirakawa, M. Itoh, T. Katayama, S. Kawashima, S. Okuda, T. Tokimatsu, Y. Yamanishi, KEGG for linking genomes to life and the environment. *Nucleic Acids Res* 36 (2008) D480-484.
- [66]I. Vastrik, P. D'Eustachio, E. Schmidt, G. Joshi-Tope, G. Gopinath, D. Croft, B. de Bono, M. Gillespie, B. Jassal, S. Lewis, L. Matthews, G. Wu, E. Birney, L. Stein, Reactome: a knowledge base of biologic pathways and processes. *Genome Biol* 8 (2007) R39.
- [67]N. Gough, Science's signal transduction knowledge environment: the connections maps database. *Ann N Y Acad Sci* 971 (2002) 585-587.

- [68]P. Thomas, A. Kejariwal, M. Campbell, H. Mi, K. Diemer, N. Guo, I. Ladunga, B. Ulitsky-Lazareva, A. Muruganujan, S. Rabkin, J. Vandergriff, O. Doremieux, PANTHER: a browsable database of gene products organized by biological function, using curated protein family and subfamily classification. *Nucleic Acids Res* 31 (2003) 334-341.
- [69]N. Le Novère, B. Bornstein, A. Broicher, M. Courtot, M. Donizelli, H. Dharuri, L. Li, H. Sauro, M. Schilstra, B. Shapiro, J. Snoep, M. Hucka, BioModels Database: a free, centralized database of curated, published, quantitative kinetic models of biochemical and cellular systems. *Nucleic Acids Res* 34 (2006) D689-691.
- [70]N. Salomonis, K. Hanspers, A. Zambon, K. Vranizan, S. Lawlor, K. Dahlquist, S. Doniger, J. Stuart, B. Conklin, A. Pico, GenMAPP 2: new features and resources for pathway analysis. *BMC Bioinformatics* 8 (2007) 217.
- [71]C. Schaefer, K. Anthony, S. Krupa, J. Buchoff, M. Day, T. Hannay, K. Buetow, PID: the Pathway Interaction Database. *Nucleic Acids Res* 37 (2009) D674-679.
- [72]F. Al-Shahrour, P. Minguez, J. Tárraga, D. Montaner, E. Alloza, J. Vaquerizas, L. Conde, C. Blaschke, J. Vera, J. Dopazo, BABELOMICS: a systems biology perspective in the functional annotation of genome-scale experiments. *Nucleic Acids Res* 34 (2006) W472-476.
- [73]R. Zaidel-Bar, S. Itzkovitz, A. Ma'ayan, R. Iyengar, B. Geiger, Functional atlas of the integrin adhesome. *Nat Cell Biol* 9 (2007) 858-867.
- [74]L. Jensen, M. Kuhn, M. Stark, S. Chaffron, C. Creevey, J. Muller, T. Doerks, P. Julien, A. Roth, M. Simonovic, P. Bork, C. von Mering, STRING 8--a global view on proteins and their functional interactions in 630 organisms. *Nucleic Acids Res* 37 (2009) D412-416.
- [75]T. Prasad, K. Kandasamy, A. Pandey, Human Protein Reference Database and Human Proteinpedia as discovery tools for systems biology. *Methods Mol Biol* 577 (2009) 67-79.

- [76]S. Kerrien, Y. Alam-Faruque, B. Aranda, I. Bancarz, A. Bridge, C. Derow, E. Dimmer, M. Feuermann, A. Friedrichsen, R. Huntley, C. Kohler, J. Khadake, C. Leroy, A. Liban, C. Liefstink, L. Montecchi-Palazzi, S. Orchard, J. Risse, K. Robbe, B. Roechert, D. Thorneycroft, Y. Zhang, R. Apweiler, H. Hermjakob, IntAct--open source resource for molecular interaction data. *Nucleic Acids Res* 35 (2007) D561-565.
- [77]M. Persico, A. Ceol, C. Gavrilu, R. Hoffmann, A. Florio, G. Cesareni, HomoMINT: an inferred human network based on orthology mapping of protein interactions discovered in model organisms. *BMC Bioinformatics* 6 Suppl 4 (2005) S21.
- [78]C. Alfarano, C. Andrade, K. Anthony, N. Bahroos, M. Bajec, K. Bantoft, D. Betel, B. Bobechko, K. Boutilier, E. Burgess, K. Buzadzija, R. Cavero, C. D'Abreo, I. Donaldson, D. Dorairajoo, M. Dumontier, M. Dumontier, V. Earles, R. Farrall, H. Feldman, E. Garderman, Y. Gong, R. Gonzaga, V. Grytsan, E. Gryz, V. Gu, E. Haldorsen, A. Halupa, R. Haw, A. Hrvojic, L. Hurrell, R. Isserlin, F. Jack, F. Juma, A. Khan, T. Kon, S. Konopinsky, V. Le, E. Lee, S. Ling, M. Magidin, J. Moniakis, J. Montojo, S. Moore, B. Muskat, I. Ng, J. Paraiso, B. Parker, G. Pintilie, R. Pirone, J. Salama, S. Sgro, T. Shan, Y. Shu, J. Siew, D. Skinner, K. Snyder, R. Stasiuk, D. Strumpf, B. Tuekam, S. Tao, Z. Wang, M. White, R. Willis, C. Wolting, S. Wong, A. Wrong, C. Xin, R. Yao, B. Yates, S. Zhang, K. Zheng, T. Pawson, B. Ouellette, C. Hogue, The Biomolecular Interaction Network Database and related tools 2005 update. *Nucleic Acids Res* 33 (2005) D418-424.
- [79]L. Salwinski, C. Miller, A. Smith, F. Pettit, J. Bowie, D. Eisenberg, The Database of Interacting Proteins: 2004 update. *Nucleic Acids Res* 32 (2004) D449-451.
- [80]B. Breitkreutz, C. Stark, T. Reguly, L. Boucher, A. Breitkreutz, M. Livstone, R. Oughtred, D. Lackner, J. Bähler, V. Wood, K. Dolinski, M. Tyers, The BioGRID Interaction Database: 2008 update. *Nucleic Acids Res* 36 (2008) D637-640.
- [81]S.A. Johnson, T. Hunter, Kinomics: methods for deciphering the kinome. *Nat Methods* 2 (2005) 17-25.

- [82]T.B. Schreiber, N. Mausbacher, S.B. Breitkopf, K. Grundner-Culemann, H. Daub, Quantitative phosphoproteomics--an emerging key technology in signal-transduction research. *Proteomics* 8 (2008) 4416-4432.
- [83]H. Daub, J.V. Olsen, M. Bairlein, F. Gnad, F.S. Oppermann, R. Korner, Z. Greff, G. Keri, O. Stemmann, M. Mann, Kinase-selective enrichment enables quantitative phosphoproteomics of the kinome across the cell cycle. *Mol Cell* 31 (2008) 438-448.
- [84]M. Bantscheff, D. Eberhard, Y. Abraham, S. Bastuck, M. Boesche, S. Hobson, T. Mathieson, J. Perrin, M. Raida, C. Rau, V. Reader, G. Sweetman, A. Bauer, T. Bouwmeester, C. Hopf, U. Kruse, G. Neubauer, N. Ramsden, J. Rick, B. Kuster, G. Drewes, Quantitative chemical proteomics reveals mechanisms of action of clinical ABL kinase inhibitors. *Nat Biotechnol* 25 (2007) 1035-1044.
- [85]M. Mann, Functional and quantitative proteomics using SILAC. *Nat Rev Mol Cell Biol* 7 (2006) 952-958.
- [86]N. Dephoure, C. Zhou, J. Villén, S. Beausoleil, C. Bakalarski, S. Elledge, S. Gygi, A quantitative atlas of mitotic phosphorylation. *Proc Natl Acad Sci U S A* 105 (2008) 10762-10767.
- [87]S. Elowe, S. Hummer, A. Uldschmid, X. Li, E.A. Nigg, Tension-sensitive Plk1 phosphorylation on BubR1 regulates the stability of kinetochore microtubule interactions. *Genes Dev* 21 (2007) 2205-2219.
- [88]D.N. Perkins, D.J. Pappin, D.M. Creasy, J.S. Cottrell, Probability-based protein identification by searching sequence databases using mass spectrometry data. *Electrophoresis* 20 (1999) 3551-3567.
- [89]A.I. Nesvizhskii, R. Aebersold, Interpretation of shotgun proteomic data: the protein inference problem. *Mol Cell Proteomics* 4 (2005) 1419-1440.
- [90]<http://kinase.com/>, in.



- [91]V. Vulsteke, M. Beullens, A. Boudrez, S. Keppens, A. Van Eynde, M.H. Rider, W. Stalmans, M. Bollen, Inhibition of spliceosome assembly by the cell cycle-regulated protein kinase MELK and involvement of splicing factor NIPP1. *J Biol Chem* 279 (2004) 8642-8647.
- [92]W. Ma, J.A. Koch, M.M. Viveiros, Protein kinase C delta (PKCdelta) interacts with microtubule organizing center (MTOC)-associated proteins and participates in meiotic spindle organization. *Dev Biol* 320 (2008) 414-425.
- [93]D. Morgan, *The Cell Cycle: Principles of Control (Primers in Biology)*. , New Science Press Ltd, 2007.
- [94]T.W. Sturgill, MAP kinase: it's been longer than fifteen minutes. *Biochem Biophys Res Commun* 371 (2008) 1-4.
- [95]F.S. Willard, M.F. Crouch, MEK, ERK, and p90RSK are present on mitotic tubulin in Swiss 3T3 cells: a role for the MAP kinase pathway in regulating mitotic exit. *Cell Signal* 13 (2001) 653-664.
- [96]M. Shinohara, A.V. Mikhailov, J.A. Aguirre-Ghiso, C.L. Rieder, Extracellular signal-regulated kinase 1/2 activity is not required in mammalian cells during late G2 for timely entry into or exit from mitosis. *Mol Biol Cell* 17 (2006) 5227-5240.
- [97]H. Cha, X. Wang, H. Li, A.J. Fornace, Jr., A functional role for p38 MAPK in modulating mitotic transit in the absence of stress. *J Biol Chem* 282 (2007) 22984-22992.
- [98]C.B. Campos, P.A. Bedard, R. Linden, Activation of p38 mitogen-activated protein kinase during normal mitosis in the developing retina. *Neuroscience* 112 (2002) 583-591.
- [99]A. Mikhailov, M. Shinohara, C.L. Rieder, Topoisomerase II and histone deacetylase inhibitors delay the G2/M transition by triggering the p38 MAPK checkpoint pathway. *J Cell Biol* 166 (2004) 517-526.

- [100]S. Kauffman, J.J. Wille, The mitotic oscillator in *Physarum polycephalum*. *J Theor Biol* 55 (1975) 47-93.
- [101]A.W. Murray, M.J. Solomon, M.W. Kirschner, The role of cyclin synthesis and degradation in the control of maturation promoting factor activity. *Nature* 339 (1989) 280-286.
- [102]F.S. Oppermann, F. Gnad, J.V. Olsen, R. Hornberger, Z. Greff, G. Keri, M. Mann, H. Daub, Large-scale proteomics analysis of the human kinome. *Mol Cell Proteomics* 8 (2009) 1751-1764.
- [103]M. Murata-Hori, M. Tatsuka, Y.L. Wang, Probing the dynamics and functions of aurora B kinase in living cells during mitosis and cytokinesis. *Mol Biol Cell* 13 (2002) 1099-1108.
- [104]R. Gassmann, A. Carvalho, A.J. Henzing, S. Ruchaud, D.F. Hudson, R. Honda, E.A. Nigg, D.L. Gerloff, W.C. Earnshaw, Borealin: a novel chromosomal passenger required for stability of the bipolar mitotic spindle. *J Cell Biol* 166 (2004) 179-191.
- [105]R. Neef, U. Gruneberg, R. Kopajtich, X. Li, E.A. Nigg, H. Sillje, F.A. Barr, Choice of Plk1 docking partners during mitosis and cytokinesis is controlled by the activation state of Cdk1. *Nat Cell Biol* 9 (2007) 436-444.
- [106]E.W. Wilker, M.A. van Vugt, S.A. Artim, P.H. Huang, C.P. Petersen, H.C. Reinhardt, Y. Feng, P.A. Sharp, N. Sonenberg, F.M. White, M.B. Yaffe, 14-3-3sigma controls mitotic translation to facilitate cytokinesis. *Nature* 446 (2007) 329-332.
- [107]M.A. Hoyt, L. Totis, B.T. Roberts, *S. cerevisiae* genes required for cell cycle arrest in response to loss of microtubule function. *Cell* 66 (1991) 507-517.
- [108]G.J. Kops, B.A. Weaver, D.W. Cleveland, On the road to cancer: aneuploidy and the mitotic checkpoint. *Nat Rev Cancer* 5 (2005) 773-785.

- [109]S. Matsumura, F. Toyoshima, E. Nishida, Polo-like kinase 1 facilitates chromosome alignment during prometaphase through BubR1. *J Biol Chem* 282 (2007) 15217-15227.
- [110]M.A. Lampson, T.M. Kapoor, The human mitotic checkpoint protein BubR1 regulates chromosome-spindle attachments. *Nat Cell Biol* 7 (2005) 93-98.
- [111]Z. Tang, H. Shu, D. Oncel, S. Chen, H. Yu, Phosphorylation of Cdc20 by Bub1 provides a catalytic mechanism for APC/C inhibition by the spindle checkpoint. *Mol Cell* 16 (2004) 387-397.
- [112]H. Huang, T.J. Yen, BubR1 is an effector of multiple mitotic kinases that specifies kinetochore: microtubule attachments and checkpoint. *Cell Cycle* 8 (2009) 1164-1167.
- [113]S.A. Kawashima, Y. Yamagishi, T. Honda, K. Ishiguro, Y. Watanabe, Phosphorylation of H2A by Bub1 prevents chromosomal instability through localizing shugoshin. *Science* 327 (2010) 172-177.
- [114]T.B. Schreiber, N. Mausbacher, G. Keri, J. Cox, H. Daub, An integrated phosphoproteomics workflow reveals extensive network regulation in early lysophosphatidic acid signaling. *Mol Cell Proteomics* (2010).
- [115]K. Sharma, C. Weber, M. Bairlein, Z. Greff, G. Keri, J. Cox, J.V. Olsen, H. Daub, Proteomics strategy for quantitative protein interaction profiling in cell extracts. *Nat Methods* 6 (2009) 741-744.
- [116]H.H. Sillje, E.A. Nigg, Purification of mitotic spindles from cultured human cells. *Methods* 38 (2006) 25-28.
- [117]A.M. Bentley, G. Normand, J. Hoyt, R.W. King, Distinct sequence elements of cyclin B1 promote localization to chromatin, centrosomes, and kinetochores during mitosis. *Mol Biol Cell* 18 (2007) 4847-4858.

- [118]Q. Chen, X. Zhang, Q. Jiang, P.R. Clarke, C. Zhang, Cyclin B1 is localized to unattached kinetochores and contributes to efficient microtubule attachment and proper chromosome alignment during mitosis. *Cell Res* 18 (2008) 268-280.
- [119]S. Elowe, K. Dulla, A. Uldschmid, X. Li, Z. Dou, E.A. Nigg, Uncoupling of the spindle-checkpoint and chromosome-congression functions of BubR1. *J Cell Sci* 123 (2010) 84-94.
- [120]F. Gao, J.F. Ponte, M. Levy, P. Papageorgis, N.M. Cook, S. Ozturk, A.W. Lambert, A. Thiagalingam, H.M. Abdolmaleky, B.A. Sullivan, S. Thiagalingam, hBub1 negatively regulates p53 mediated early cell death upon mitotic checkpoint activation. *Cancer Biol Ther* 8 (2009) 548-556.
- [121]C.E. Bakalarski, J.E. Elias, J. Villen, W. Haas, S.A. Gerber, P.A. Everley, S.P. Gygi, The impact of peptide abundance and dynamic range on stable-isotope-based quantitative proteomic analyses. *J Proteome Res* 7 (2008) 4756-4765.
- [122]D. Brehmer, Z. Greff, K. Godl, S. Blencke, A. Kurtenbach, M. Weber, S. Muller, B. Klebl, M. Cotten, G. Keri, J. Wissing, H. Daub, Cellular targets of gefitinib. *Cancer Res* 65 (2005) 379-382.
- [123]K. Godl, O.J. Gruss, J. Eickhoff, J. Wissing, S. Blencke, M. Weber, H. Degen, D. Brehmer, L. Orfi, Z. Horvath, G. Keri, S. Muller, M. Cotten, A. Ullrich, H. Daub, Proteomic characterization of the angiogenesis inhibitor SU6668 reveals multiple impacts on cellular kinase signaling. *Cancer Res* 65 (2005) 6919-6926.
- [124]J. Wissing, L. Jansch, M. Nimtz, G. Dieterich, R. Hornberger, G. Keri, J. Wehland, H. Daub, Proteomics analysis of protein kinases by target class-selective prefractionation and tandem mass spectrometry. *Mol Cell Proteomics* 6 (2007) 537-547.
- [125]A. Shevchenko, M. Wilm, O. Vorm, M. Mann, Mass spectrometric sequencing of proteins silver-stained polyacrylamide gels. *Anal Chem* 68 (1996) 850-858.

- [126]J. Rappsilber, Y. Ishihama, M. Mann, Stop and go extraction tips for matrix-assisted laser desorption/ionization, nanoelectrospray, and LC/MS sample pretreatment in proteomics. *Anal Chem* 75 (2003) 663-670.
- [127]J.E. Elias, S.P. Gygi, Target-decoy search strategy for increased confidence in large-scale protein identifications by mass spectrometry. *Nat Methods* 4 (2007) 207-214.
- [128]H. Choi, A.I. Nesvizhskii, False discovery rates and related statistical concepts in mass spectrometry-based proteomics. *J Proteome Res* 7 (2008) 47-50.
- [129]P. Mortensen, J.W. Gouw, J.V. Olsen, S.E. Ong, K.T. Rigbolt, J. Bunkenborg, J. Cox, L.J. Foster, A.J. Heck, B. Blagoev, J.S. Andersen, M. Mann, MSQuant, an open source platform for mass spectrometry-based quantitative proteomics. *J Proteome Res* 9 (2010) 393-403.
- [130]P. Shannon, A. Markiel, O. Ozier, N. Baliga, J. Wang, D. Ramage, N. Amin, B. Schwikowski, T. Ideker, Cytoscape: a software environment for integrated models of biomolecular interaction networks. *Genome Res* 13 (2003) 2498-2504.
- [131]W. Huang da, B.T. Sherman, R.A. Lempicki, Systematic and integrative analysis of large gene lists using DAVID bioinformatics resources. *Nat Protoc* 4 (2009) 44-57.

## **Acknowledgements**

It gives me immense pleasure to introduce the people who are pivotal in the successful completion of this thesis.

First and foremost I would like to thank Prof. Dr. Erich A. Nigg for giving me opportunity to work in highly interdisciplinary, motivating and international scientific environment. His supervision, inputs and support helped me immensely in shaping up the project and also to finish it in a timely manner.

I also thank Erich and Elena Nigg for the kind invitation to their family at the beginning of my stay in Germany and also the support in times of difficulty. I really appreciate that.

Further, I am highly indebted to Dr. Roman Koerner, our group leader, for his constant guidance, scientific freedom and support in professional and personal matters which made the time I spent at MPIB a very pleasant and fruitful learning experience. He is undoubtedly the best supervisors one could ever ask for.

I thank Dr. Anna Santamaria for her guidance and support throughout my time at MPIB. I treasure her friendship.

I grateful to Albert Ries for helping me on numerous occasions in day to day lab matters.

A special thanks to the members of our mass spectrometry group viz Dr. Rainer Malik, Bin Wang, and Dr. Rene Lenobel for all the discussions and help.

I am thankful to Ms. Alison Dalfovo for her assistance with my paperwork. I also thank her for all the help and kind suggestions she gave.

I would like to thank my collaborators Dr. Henrik Daub, Renate Hornberger for kinase project and Dr. Sabine Elowe for BubR1, Bub1 project. I also thank her for helping in the preparation of this thesis.

I thank Prof. Dr. Matthias Mann and Dr. Jürgen Cox for early access to the MaxQuant software package.

I want to thank all the members of Erich Nigg's department members for creating such an inspiring and pleasant atmosphere in the lab.

Lastly, I would like to thank all my friends and family members. Without you it wouldn't have been possible.

## **Publications**

Parts of this work are published in:

**K. Dulla**, H. Daub, R. Hornberger, E.A. Nigg, R. Korner, Quantitative site-specific phosphorylation dynamics of human protein kinases during mitotic progression. ( in press Mol Cell Proteomics 2010).

S. Elowe, **K. Dulla**, A. Uldschmid, X. Li, Z. Dou, E.A. Nigg, Uncoupling of the spindle-checkpoint and chromosome-congression functions of BubR1. J Cell Sci 123 (2010) 84-94.

R. Malik, **K. Dulla**, E.A. Nigg, R. Korner, From proteome lists to biological impact- tools and strategies for the analysis of large MS data sets. (Review article, in press Proteomics 2010).

## Curriculum Vitae

Kalyana Dulla

Date and place of birth: 11.11.1982, Vijayawada

## Education

- 11.06 - 01.10 DEPARTMENT OF CELL BIOLOGY, MAX PLANCK INSTITUTE OF BIOCHEMISTRY, MARTINSRIED, GERMANY  
PhD thesis with Prof. Dr. Erich A. Nigg: Analysis of mitotic phosphoproteomes using SILAC based mass spectrometry.
- 08.05 - 11.06 CENTER FOR CELLULAR AND MOLECULAR BIOLOGY, HYDERABAD, INDIA  
Research Fellow with Dr. Ravi Sirdeshmukh. Proteomics group.
- 08.03 - 06.05 INDIAN INSTITUTE OF TECHNOLOGY ROORKEE (IIT ROORKEE), INDIA  
Masters in Biotechnology (grade point 7.94/10)
- 07.00 - 06.03 PB SIDHARDHA COLLEGE, NAGARJUNA UNIVERSITY, INDIA  
Bachelors in Science with the subjects Genetics, Chemistry and Botany (grade 86.00 %)
- 06.98 - 05.00 INTERMEDIATE BOARD, ANDHRA PRADESH , INDIA  
Botany, Zoology, Chemistry, Physics 88.00 %
- 06.88 - 05.98 Secondary School Certificate, Board of Secondary Education, Andhra Pradesh, INDIA  
84.00 %



## **Awards**

- 02.10 – Marie Curie Fellowship
- 11.06 - 01.10: Receiver of Max Planck Society Fellowship, Germany
- 08.05 - 11.06: Receiver of CSIR Research Fellowship, India.
- 08.03 - 06.05: Receiver of Merit Scholarship from Department of Biotechnology, under the Ministry of Education, Government of India.

## **Conferences and workshops**

- Phospho-Proteomics Seminar with Practical Workshop, Vienna 2008, 13 -14 October.  
**Oral Presentation**
- HUPO 7th Annual World Congress, Amsterdam 2008, 16 - 20 August. **Poster Presentation**
- ENFIN Annual General Meeting. Rome 2008, 5-6 March. **Poster Presentation**
- Summer school on "Advanced Statistics and Data Mining". Madrid 2009, 13-17 July.